POLYVINYL ALCOHOL (PVA) BASED GEL ELECTROLYTES: CHARACTERISATION AND APPLICATIONS IN DYE-SENSITIZED SOLAR CELLS

MOHD FAREEZUAN BIN ABDUL AZIZ

FACULTY OF SCIENCE
UNIVERSITY OF MALAYA
KUALA LUMPUR

2017

POLYVINYL ALCOHOL (PVA) BASED GEL ELECTROLYTES: CHARACTERISATION AND APPLICATIONS IN DYE-SENSITIZED SOLAR CELLS

MOHD FAREEZUAN BIN ABDUL AZIZ

THESIS SUBMITTED IN FULFILLMENT OF THE REQUIREMENTS FOR THE DEGREE OF DOCTOR OF PHILOSOPHY

DEPARTMENT OF PHYSICS
FACULTY OF SCIENCE
UNIVERSITY OF MALAYA
KUALA LUMPUR

2017

UNIVERSITY OF MALAYA

ORIGINAL LITERARY WORK DECLARATION

Name of Candidate: **Mohd Fareezuan Bin Abdul Aziz**

Matric No: **SHC130023**

Name of Degree: **Doctor of Philosophy**

Title of Project Paper/Research Report/Dissertation/Thesis ("this Work"): **POLYVINYL ALCOHOL (PVA) BASED GEL ELECTROLYTES: CHARACTERISATION AND APPLICATIONS IN DYE-SENSITIZED SOLAR CELLS**

Field of Study: **Experimental Physics**

I do solemnly and sincerely declare that:

(1) I am the sole author/writer of this Work;
(2) This Work is original;
(3) Any use of any work in which copyright exists was done by way of fair dealing and for permitted purposes and any excerpt or extract from, or reference to or reproduction of any copyright work has been disclosed expressly and sufficiently and the title of the Work and its authorship have been acknowledged in this Work;
(4) I do not have any actual knowledge nor do I ought reasonably to know that the making of this work constitutes an infringement of any copyright work;
(5) I hereby assign all and every rights in the copyright to this Work to the University of Malaya ("UM"), who henceforth shall be owner of the copyright in this Work and that any reproduction or use in any form or by any means whatsoever is prohibited without the written consent of UM having been first had and obtained;
(6) I am fully aware that if in the course of making this Work I have infringed any copyright whether intentionally or otherwise, I may be subject to legal action or any other action as may be determined by UM.

Candidate's Signature Date:

Subscribed and solemnly declared before,

Witness's Signature Date:

Name:

Designation:

POLYVINYL ALCOHOL (PVA) BASED GEL ELECTROLYTES: CHARACTERISATION AND APPLICATIONS IN DYE-SENSITIZED SOLAR CELLS

ABSTRACT

Three systems of gel polymer electrolytes have been prepared in this work. First system was PVA-DMSO-EC-PC-KI-I_2 gel polymer electrolytes. In the first system, various amount of KI salt were added. The highest conductivity of gel polymer electrolyte for the first system was 12.50 mS cm^{-1} for the gel polymer electrolyte with the composition of 5.58 wt. % of PVA - 8.37 wt. % of EC - 11.16 wt. % of PC - 61.37 wt. % of DMSO - 11.72 wt. % of KI - 1.80 wt. % of I_2. To this composition, part of KI was replaced with the quaternary ammonium iodide salt which is TMAI, TPAI and TBAI for the second system. The conductivity of the gel polymer electrolyte decreased with the increasing amount of quaternary ammonium iodide salts. The best electrolyte in systems 2 which gave the highest efficiency of 5.51 % and 5.80 %, respectively have been chosen for incorporation with diethyl carbonate (DEC) plasticizer (systems 3). With the addition of DEC plasticizer, the conductivity of the gel polymer electrolyte and efficiency of DSSC were enhanced. The highest efficiency of 7.5 % was obtained for the DSSC having 5.47 wt. % of PVA - 8.21 wt. % of EC - 10.95 wt. % of PC - 60.22 wt. % of DMSO - 3.45 wt. % of KI - 8.05 wt. % of TBAI - 1.08 wt. % of I_2 - 2.57 wt. % of DEC. The interaction of gel polymer electrolytes have been studied via fourier transform infrared (FTIR) spectroscopy. The peak shifting observed for S=O, O-H, C-O-C and C=O bands indicates that the interaction has occurred. X-ray diffraction (XRD) pattern reveals that all gel polymer electrolytes are amorphous.

Keyword: Conductivity, Gel polymer electrolyte, Dye-sensitized solar cells, Polyvinyl alcohol

GEL ELEKTROLIT-POLYVINYL ALCOHOL (PVA) : CIRI-CIRI DAN APLIKASI DALAM PEWARNA-PEMEKA SEL SOLAR

ABSTRAK

Dalam pembelajaran ini, tiga sistem gel polimer elektrolit telah disediakan Sistem pertama adalah PVA-DMSO-EC-PC-KI-I_2 gel polimer elektrolit. Sistem pertama, berlainan jumlah garam KI telah ditambah. Dalam sistem yang pertama, kekonduksian tertinggi 12.50 mS cm^{-1} ditunjukkan oleh gel elektrolit yang mempunyai komposisi 5.58 berat % PVA – 8.37 berat % EC – 11.16 berat % PC – 61.37 berat % DMSO – 11.72 berat % KI – 1.80 berat % I_2. Dengan komposisi ini, sebahagian jumlah garam KI telah diganti dengan garam quat-ammonium iodida iaitu TMAI, TPAI dan TBAI untuk system kedua. Bagi sistem kedua, garam quat-ammonium iodida telah mengurangkan nilai kekonduksian. Elektrolit terbaik dalam sistem kedua yang memberikan nilai kecekapan 5.51 % dan 5.80 % telah digunakan dengan tambahan diethyl karbonat (DEC) untuk sistem ketiga. Kekonduksian gel polimer elektrolit dan kecekapan DSSC meningkat adalah disebabkan penambahan DEC. Kecekapan paling tinggi iaitu 7.5 % diperolehi daripada gel elektrolit yang mengandungi 5.47 wt. % of PVA - 8.21 wt. % of EC - 10.95 wt. % of PC - 60.22 wt. % of DMSO - 3.45 wt. % of KI - 8.05 wt. % of TBAI - 1.08 wt. % of I2 - 2.57 wt. % of DEC. Melalui fourier transform infrared (FTIR), interaksi dalam gel electrolyte telah dipelajari. Perubahan puncak untuk S=O, O-H, C-O-C and C=O telah diperhatikan. X-ray diffraction (XRD) bagi gel elektrolit menunjukan keamorfusannya.

Kata kunci: Kekonduksian, Gel polimer elektrolit, Pewarna-pemeka sel solar, Polyvinyl alcohol

ACKNOWLEDGEMENT

بِسْمِ ٱللَّهِ ٱلرَّحْمَٰنِ ٱلرَّحِيمِ

In the name of Allah, Most Gracious, Most Merciful. Salawat and salaam to the beloved Prophet Muhammad S.A.W. Alhamdulillah, I am very thankful to Allah for giving me strength, patience and health in completing this work.

I would like to express my infinite appreciation and gratitude to my supervisor, Professor Dr. Abdul Kariem bin Mohd Arof for his guidance and encouragement in completing this work. He was my mentor who is full with knowledge and never stingy in sharing knowledge. He guides me to be a good researcher and shed a light towards research field. I would like to extend my thanks to my another supervisor, Dr. Mohd Hamdi Bin Ali @ Buraidah for his guidance and support in making sure I kept an interest in these research studies.

I would like to thank my parents, Abdul Aziz Bin Kasdi and Siti Haliah Bt. Selamat for their nonstop prayers and encouragement until this thesis is complete. I am very grateful to have parents who always supported me in finishing my PhD degree. I am thankful also to my sister, Arina Amira for her support.

To my beloved wife, Shuhaida Binti Khalid, I am very grateful for your support and prayer in achieving my ambition and also I dedicate my PhD degree to my lovely daughter, Airiss Zulaikha. To all my lab mates in Centre for Ionics University of Malaya (C.I.U.M), thank you for the help, support and encouragement in completing this research study.

Last but not list, I would like to thanks to Ministry of High Education Malaysia for the financial support under MyBrain 15 (MyPhD) Programme during my studies.

TABLE OF CONTENTS

LIST OF FIGURES

LIST OF TABLES

LIST OF SYMBOLS AND ABBREVIATIONS

$[TiO_6]^{2-}$	:	Titanium oxide tetrahedra
D	:	Diffusion coefficient
d	:	Sample thickness
DEC	:	Diethyl carbonates
DMSO	:	Dimethyl sulfoxide
DSSC	:	Dye-sensitized solar cell
EC	:	Ethylene carbonate
EIS	:	Electrochemical impedance spectroscopy
FF	:	Fill factor
FTIR	:	Fourier transform infrared spectroscopy
FTO	:	Fluorine-doped tin oxide
GPE	:	Gel polymer electrolyte
I	:	Iodide
I_3	:	Triiodide
ITO	:	Indium-tin oxide
J_{sc}	:	Short circuit current density
KI	:	Potassium Iodide
LCD	:	Liquid crystal displays
n	:	Number density of ions
N3	:	*cis*-Ru(II) bis (2,2'-bipyridyl-4,4'-dicarboxylate)-$(NCS)_2$
N719	:	*cis*-diisothiocyanato-bis(2,2'-bipyridyl-4,4'-dicaboxylato)Ru(II)bis (tetrabutylammonium)
N749	:	Ru (II) tri(cyanato)-2,2',2"-terpyridyl-4,4',4"-tricarboxylate
PAN	:	Poly (acrylonitrile)
PC	:	Propylene carbonate

PEG	:	Polyethylene glycol
PEO	:	Poly (ethylene oxide)
PMMA	:	Poly (methyl methacrylate)
PVA	:	Poly(vinyl alcohol)
PVDF-HFP	:	Poly (vinylidenefluoride-co-hexafluoropropylene)
PVP	:	Polyvinyl pyrrolidone
QAI	:	Quaternary ammonium iodide
TBAI	:	Tetrabutyl ammonium iodide
TBP	:	Tert-butylpyridine
TCO	:	Transparent conducting
TiO_2	:	Titanium dioxide
TMAI	:	Tetramethyl ammonium iodide
TPAI	:	Tetrapropyl ammonium iodide
V_{oc}	:	Open circuit voltage
XRD	:	X-ray diffraction
Z_i	:	Imaginary Impedance
Z_r	:	Real Impedance
γ-BL	:	γ-butyrolactone
ε_i	:	Imaginary part of complex permittivity
ε_o	:	Vacuum permittivity
ε_r	:	Real part of complex permittivity
μ	:	Ionic mobility
σ	:	Conductivity

CHAPTER 1: INTRODUCTION TO THE THESIS

1.1. Introduction

Generally, there are two types of energy resources which are non-renewable energy and renewable energy. Non-renewable energy resources such as coal, oil and natural gas are mainly come from fossil fuel. Biomass is the resource that does not renew itself at a necessary rate for sustainable economic extraction in expressive human time-frames. These kinds of energy resources give global atmospheric contaminants and also create a greenhouse gases. In contrast, renewable energy is defined as energy that comes from natural resources and quickly restocks them such as solar, wind, tidal and wave. These types of renewable energy resources are potentially infinite energy supply and has long term sustainable source.

In 2016, world population which is the number of humans living on earth is recorded more than 7.5 billion. This estimation has been declared by the United States Census Bureau. They also predicted that the world population will be increased up to 11.20 billion at year 2100 (Hollmann *et al*., 1999). Furthermore, with the high number of population the consumption for energy also increases wisely. Currently, in Malaysia the largest energy sources are mainly come from coal, oil and natural gas production (Mekhilef *et al*., 2014). The depletion of fossil fuel, climate change and rapid urbanization are the reasons for high demand on green renewable energy. Thus, solar energy is one example of green energy which is the most promising energy sources in Malaysia. Total radiation energy of the sun received from outer atmosphere of the earth is 1368 W m^{-2} (Ahmad *et al*., 2011). Malaysia, being a tropical country with an average daily solar emission of 5.5 kW m^{-2} (equivalent to 15 MJ m^{-2}) is very suitable for the generation of solar energy (Oh *et al*., 2010). Ahmad *et al*. (2011) reported that the

present production of electricity from the solar energy in Malaysia is around 1 MW only.

Generally, solar cell technologies are classified into three generations. First generation solar cells (also known as conventional or wafer cell) are usually made of crystalline silicon (c-Si). This silicon-based solar cell follows the *p-n* junction concept. The second generation of solar cells is based on thin-film solar cells which include of amourphous silicon, cadmium telluride (CdTe) and copper indium gallium selenide (CIGS). These thin-film solar cells have improved by years and dominantly used in most solar PV systems. The third generation solar cells usually use organic materials in the solar cells. This third generation solar cells include organic solar cells, dye-sensitized solar cells, quantum dot solar cells, polymer solar cells and perovskite solar cells.

Dye-sensitized solar cells (DSSCs) were invented by Michael Grätzel and Brian O'Regan. This type of solar cells is well known as "Grätzel cells" and has been designed in 1991. The DSSCs are capable to produce electricity under visible spectrum. DSSCs are cheap and easy to fabricate. Currently, highest efficiency achieved for DSSC is nearly 14 % (Mathew *et al*., 2014).

1.2. Objectives of the thesis

Poly (vinyl alcohol) (PVA) has been used in this work as polymer host. The objectives of this work are:

- To prepare the PVA based gel polymer electrolytes containing different amount of potassium iodide salts.

- To study the effect of various quarternary iodide salts such as tetrametyhl ammonium iodide, tetrapropyl ammonium iodide and tetrabutyl ammonium iodide on the conductivity of the gel polymer electrolytes.
- To improve the ionic conductivity by adding diethyl carbonate in the gel polymer electrolyte system.
- To fabricate dye-sensitized solar cell (DSSC) and investigate its performance.

1.3. Scope of the thesis

In this thesis, there are nine chapters including the introductory chapter. Chapter 2 focuses on the literature review about the working principle of DSSC and its components. Chapter 3 presents the details of the sample preparation and basic characterization such as x-ray diffraction (XRD), fourier transform infrared (FTIR) spectroscopy and electrochemical impedance spectroscopy (EIS). The fabrication of DSSC has also been summarized in this chapter.

The results have been presented in Chapters 4 to 7. FTIR results showing the interactions between solvent, salts, polymer and also plasticizer have been properly arranged in Chapter 4. Chapter 5 is on the X-ray diffraction (XRD) characteristic of gel polymer electrolytes. The impedance properties of the gel polymer electrolytes are shown in Chapter 6 whereas the DSSC's performance is presented in Chapter 7. Discussion part has been compiled in Chapter 8 and the conclusion of the thesis with further future work is presented in Chapter 9.

CHAPTER 2: LITERATURE REVIEW

2.1. Introduction

Dye-sensitized solar cell (DSSC) is considered as low-cost production and promises attractive features (Grätzel, 2004). DSSC have more advantages compared to thin film and silicon-wafer based solar cells (Bagher *et al.*, 2015). This generation of solar cell is more flexible and easy to prepare. The DSSC generally consist of three main components:

(1) Sensitized nanoparticles of titanium dioxide (TiO_2) layer coated on the active side of transparent conducting oxide (TCO) glass
(2) Electrolyte consist of redox mediator and
(3) Platinum layer coated on TCO glass as counter electrode (CE).

DSSC structure is illustrated in Figure 2.1. Each of these components plays an important role in the performance of DSSC.

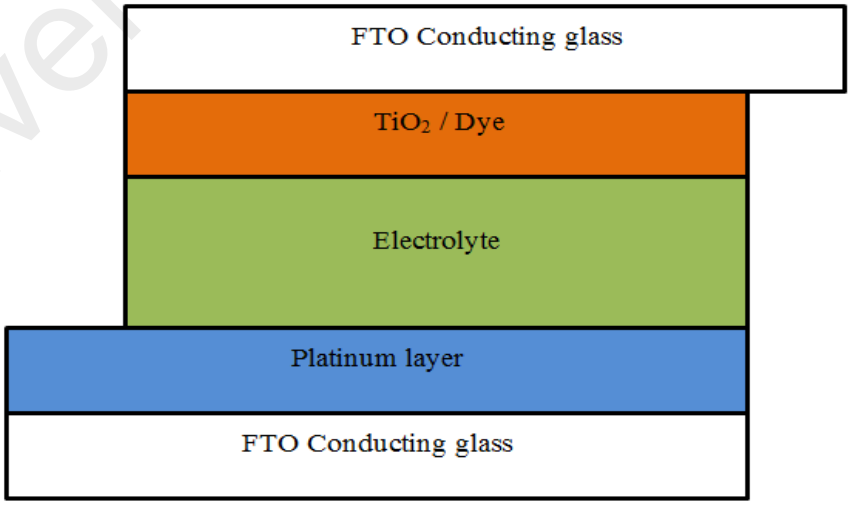

Figure 2.1: Schematic diagram of the DSSC structure

2.2. Working Principle

In dye-sensitized solar cells (DSSC), the working process is not same as the conventional *p-n* junction solar cells where the absorption of photons and charges transportation in DSSC, occurred in the same material. Photons are absorbed by dye molecules and generate electrons. The electrons then transported through TiO_2 nanoparticles network and electrolyte. The basic operation of a DSSC is summarized in the schematic diagram in Figure 2.2.

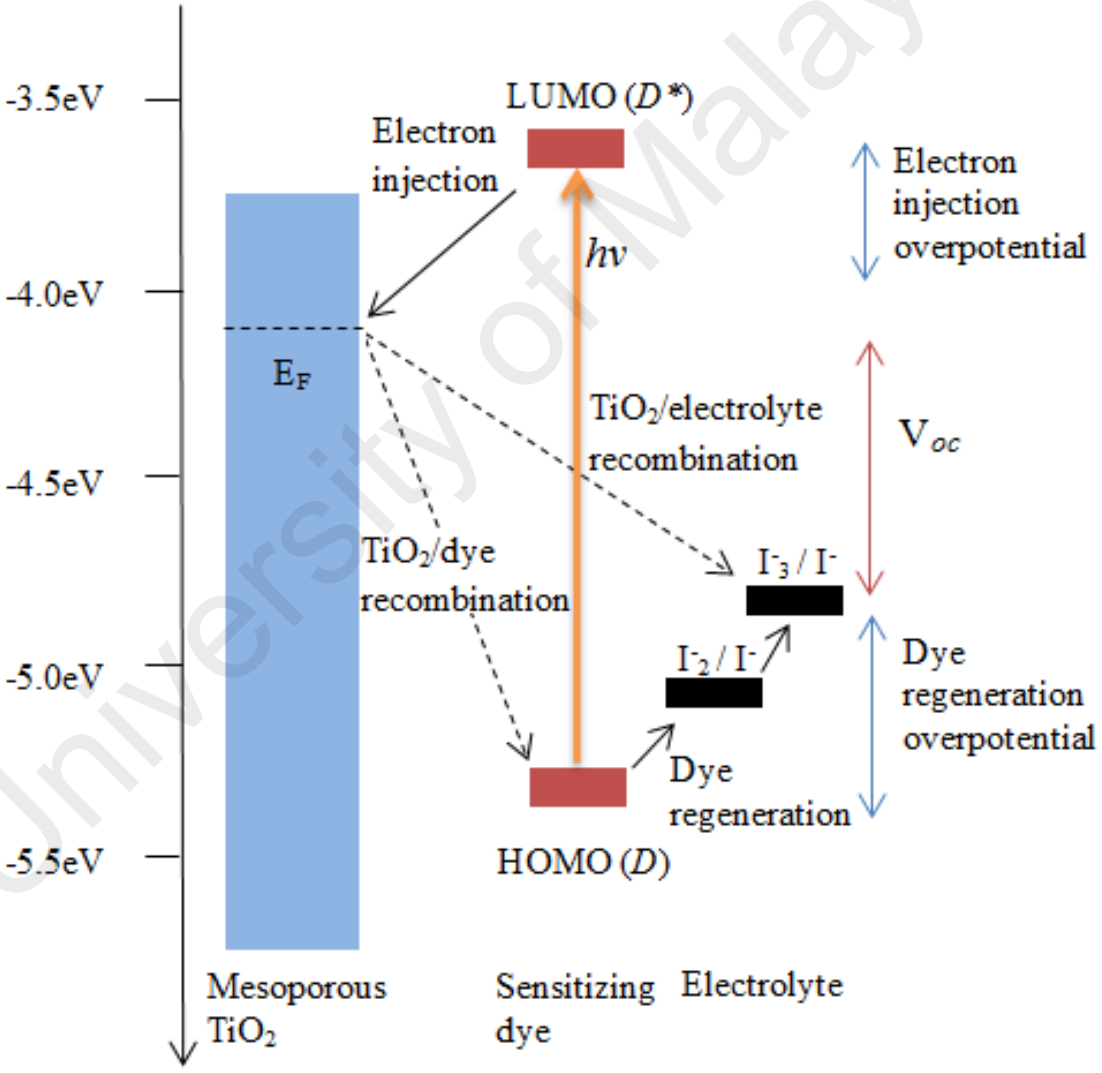

Figure 2.2: Illustration of the DSSC principle (Hardin *et al*., 2012)

The working principle of DSSC can be roughly summarized in a stepwise manner in the following equations:

$$hv + D \rightarrow D^{*} \quad \text{(photoanode)} \quad (2.1)$$

$$D^{*} + TiO_2 \rightarrow D^{+} + e_{cb}^{-}\left(TiO_2\right) \quad \text{(photoanode)} \quad (2.2)$$

$$2D^{+} + 3I^{-} \rightarrow I_3^{-} + 2D \quad \text{(photoanode / electrolyte)} \quad (2.3)$$

$$I_3^{-} + 2e^{-}\left(CE\right) \rightarrow 3I^{-} \quad (2.4)$$

DSSC is exposed under illumination of light that consists of energy particles which are photons (*hv*). Photons will be absorbed by dye molecules. With enough energy, electrons in the dye will be excited, D* (Equation 2.1). These excited electrons will be injected into the conduction band of TiO_2 nanoparticles. The process occurs within ~50 *fs* (Grätzel, 1999) and the dyes become oxidized (D^{+}) (Equation 2.2). The oxidized dye molecules will be reduced or regenerated by iodide ions which then turn to triiodide ions (Equation 2.3). The triiodide ions will be diffused to the counter electrode. Meanwhile, the electrons in the conduction band of TiO_2 will be transported to the counter electrode through the TiO_2 network and external circuit which then reducing triiodide ions to iodide ions (Equation 2.4). This cycle will be continuous as long as the DSSC is exposed under the light source.

2.3. Photoanode

2.3.1. Fluorine-doped tin oxide (FTO) coated glass

TCO glasses such as fluorine-doped tin oxide (FTO) and indium-tin oxide (ITO) were widely used in DSSC. ITO glass has transmittance more than 80 % with sheet resistance 18 Ω cm^{-2}, while FTO glass displays a transmittance of about 75 % in the visible region with sheet resistance of 8.5 Ω cm^{-2} (Umer *et al*., 2014). Choosing between ITO and FTO are highly dependent on the glass usage (Sima *et al*., 2010). ITO

glass mostly used as transparent electrode in opto-electronics devices such as liquid crystal displays (LCD) and plasma panels (Kawashima *et al*., 2004). However, ITO has some disadvantages which include expensive, unstable resistance at high temperature and the indium present can easily diffuse into the emissive polymer layer (Andersson *et al*., 1998; Hollars, 2005). FTO glass is a better option for DSSC since it is cheaper than ITO and thermally stable.

The comparison between ITO and FTO glass in DSSC also shows that the usage of FTO glass is promising with high efficiency (Qiao *et al*., 2006). The cell using ITO glass has gain high resistivity after thermal treatment at high temperature compare to the FTO glass with initial low resistivity remains unchanged. Thus the current density of the cell is high due to the low resistivity of the glass. Sima *et al.* (2010) have reported that the efficiency of DSSC using ITO glass is 2.24 % while solar cells with FTO glass gave the efficiency of 9.6 %.

2.3.2. Nanocrystalline Titanium dioxide (TiO_2) photoelectrode

Nanocrystalline titania (TiO_2) has been developed as potential material with good physical, chemical and electrical properties. Other than DSSC, it can be also used in lithium-ion batteries (Wang *et al*., 2014) and as photo-catalyst (Miao *et al*., 2016).

TiO_2 nanoparticles have some good properties such as (Nakata & Fujishima, 2012; Lin *et al*., 2015):

- Inexpensive
- Stable structure
- Long life cycle
- Harmless with transparency in the visible light region

TiO_2 nanoparticles have been categorized into different types of structure such as rutile and anatase although both are tetragonal structure. These two are categorized depending on the arrangement of $[TiO_6]^{2-}$ octahedra where it is connected by edges in rutile and sharing vertices in anatase (Hu *et al*., 2003).

Rutile has less energy band gap (~3 eV) compared with anatase (3.2 eV). The mobility of electron transport in rutile-based TiO_2 is slow due to the high packing density. Due to the smaller surface area per unit volume, this rutile is difficult for dye adsorption and shows less efficient performance. In DSSC, anatase structure is favoured over the rutile structure. Anatase structure exhibits high electron mobility, lower dielectric constant, less density and lower deposition temperature (Carp *et al*., 2004). Futhermore, short circuit photo current of an anatase-based DSSC show 30 % higher than the rutile-based DSSC with same film thickness (Park *et al*., 2000). The comparison between two types of TiO_2 nanoparticles has been shown in Table 2.1.

Table 2.1: Comparison between two types of categories TiO_2 nanoparticles

TiO_2 nanoparticles	**Comparison**
Rutile	-Electron transport process is slow due to the high packing density. -Less energy band gap (~3 eV) -Owing to smaller surface area per unit volume -Less absorbs dye
Anatase	-Electron transport process is fast due to low density -High energy band gap (3.2 eV) -Chemically stable -Lower dielectric constant

Another variants form of TiO_2 is brookite which is occurs in four natural polymorphic forms. Brookite has larger cell volume compared to anatase and rutile, where brookite contains eight TiO_2 groups per unit cell while anatase has four and rutile has two.

Usually, the preparation of TiO_2 layer for DSSC is made up by two layers; the first layer (small particle size) and the second layer (large particle size). The significance of double layers result a higher efficiency which is influenced by improvement of light harvesting (Im *et al.,* 2011).

2.3.3. Dye

Dye is one of the main component in DSSC which acting as a molecular pump. It starts from absorbing visible light, injection of electrons into the conduction band of TiO_2 and receiving electrons from the redox couple in the electrolyte (Meyer, 1997). The excellent properties of dye-sensitizer for DSSC are listed in Table 2.2 (Longo & De Paoli, 2003; Grätzel, 2004):

Table 2.2: List of good dye-sensitizer properties

Properties of good dye-sensitizer
• A strong absorption in the visible light range. • Good interfacial properties with the TiO_2 surface. • Long lifetime consistent with device life. • Highly stable to sustain about 20 years of light exposure.

Generally, the dye sensitizer can be divided into two groups which are natural dye and synthetic dye. Natural dyes can be obtained from simple procedures of extraction of flowers, leaves and fruits. This kind of low-cost production dyes has been chosen as the subject in DSSC research due to the non-toxicity and complete biodegradation properties (Zhou *et al*., 2011). Some example of natural dyes that use as sensitizer in DSSC is cyanin (Sirimanne *et al*., 2006), carotene (Yamazaki *et al*., 2007) and chlorophyll (Kumara *et al*., 2006). Table 2.3 shows some examples of natural dyes used in DSSC.

Table 2.3: List of example for natural dye-sensitizer used for DSSC

Dye-sensitizer	**Contain**	**Efficiency (%)**
Purple corn extract	Anthocyanin	1.06 (Phinjaturus *et al*., 2016)
Male flowers *Luffa cylindrica* L extract	Anthocyanin	0.13 (Maurya *et al*., 2016)
Rosella extract	Anthocyanin	0.37 (Wongcharee *et al*., 2007)
Callindra haematocephata flower	Anthocyanin	0.06 (Maurya *et al*., 2016)
Peltophorum pterocarpum flower	*β*-carotene	0.04 (Maurya *et al*., 2016)
Amaranthus caudatus flower	Anthocyanin	0.61 (Godibo *et al*., 2015)
Pawpaw Leaf	Chlorophyll	0.20 (Kimpa *et al*., 2012)
Pomegranate leaf	Chlorophyll	0.72 (Chang & Lo, 2010)

Ruthenium dyes such as N3 (red dye), N719 and N749 (black dyes) have been developed by Grätzel group as sensitizer in DSSC. Ruthenium complex are good sensitizer due to the variety of photochemical properties and high stability in oxidized state (Kohle *et al*., 1997). The chemical structure of N3, N719 and N749 are shown in the Figure 2.3. Table 2.4 shows the DSSC performance using N3, N719 and N749 sensitizers.

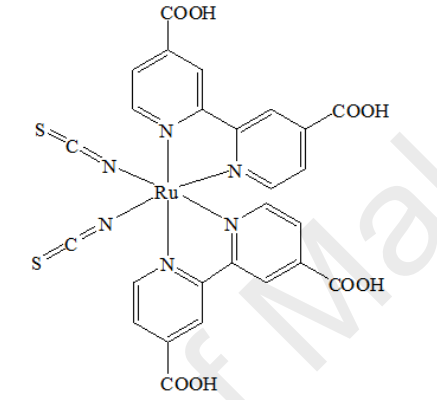

N3

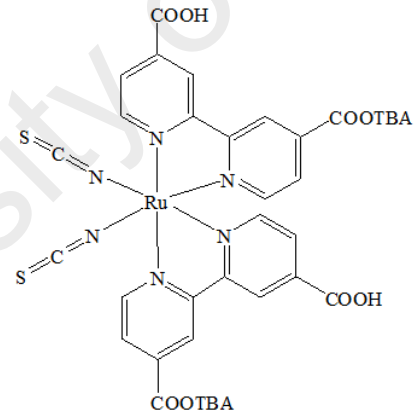

N719

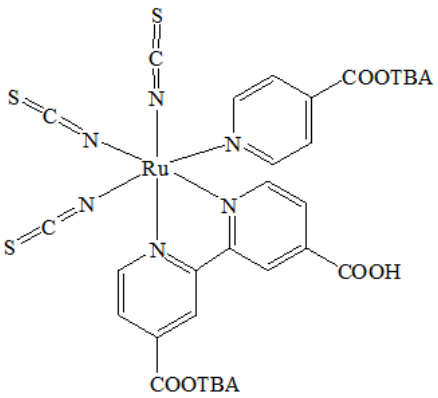

N749

Figure 2.3: Schematic diagrams for N3, N719, and N749 (Highlights, 2009)

Table 2.4: DSSCs performance using Ruthenium based sensitizer

Dye-sensitizer	Electrolyte	DSSC parameter	References
cis-Ru(II) bis (2,2'-bipyridyl-4,4'-dicarboxylate)-$(NCS)_2$ (known as N3 dye)	Lithium iodide in acetonitrile	J_{sc} : 18.20 mA cm^{-2} V_{oc} : 0.72 V *ff* :0.73 η: 10 %	(Nazeeruddin *et al*., 1993)
cis-diisothiocyanato-bis (2,2'-bipyridyl-4,4'-dicaboxylato) Ru(II) bis(tetrabutylammonium) (known as N719 dye)	Electrolyte solution	J_{sc} : 17.73 mA cm^{-2} V_{oc} : 0.85 V *ff* :0.75 η: 11.18 %	(Nazeeruddin *et al*., 2005)
cis-diisothiocyanato-bis (2,2'-bipyridyl-4,4'-dicaboxylato) Ru(II) bis(tetrabutylammonium) (known as N719 dye)	Electrolyte solution (DHS-Et23)	J_{sc} : 14.98 mA cm^{-2} V_{oc} : 0.70 V *ff* : 0.67 η: 6.97 %	(Luo *et al*., 2016)
cis-diisothiocyanato-bis (2,2'-bipyridyl-4,4'-dicaboxylato) Ru(II) bis(tetrabutylammonium) (known as N719 dye)	Fumed silica as the gelling agent, γ-butyrolactone (γ-BL) and tetrapropylammonium iodide ($Pr_4N^+I^-$)	J_{sc} : 15.70 mA cm^{-2} V_{oc} : 0.64 V *ff* : 0.63 η: 6.33 %	(Senevirathne *et al*., 2016)
Ru (II) tri(cyanato)-2,2',2"-terpyridyl-4,4',4"-tricarboxylate (known as N749)	0.6 M 1-methyl-3-propyl-imidazoliun iodide, 0.1 M LiI, 0.05 M I_2, and 0.5 M tert-butylypyridine (TBP) in acetonitrile	J_{sc} : 16.50 mA cm^{-2} V_{oc} : 0.73 V *ff* : 0.71 η: 8.40 %	(Bang *et al*., 2012)

2.4. Electrolyte

Electrolyte in DSSC plays the role as medium for charge transportation through a redox mediator in the photon-to-electricity conversion process. The electrolyte can be in liquid, solid or gel form.

There are some critical aspects that should be considered for any electrolytes used in the DSSC (Nogueira *et al*., 2004; Li *et al*., 2006) which are:

(a) Good interfacial contact between the electrolyte with the nano-porous crystalline TiO_2 layer electrode and counter electrode.

(b) Good identical properties such as thermal, chemical, optical, electrochemical and long-term stability.

(c) High ionic conductivity.

2.4.1. Liquid electrolyte

Liquid electrolyte contains solvent as a medium and iodide salt. Liquid electrolyte has the best ionic conductivity compared to the solid and gel electrolyte. High ionic conductivity is important in which it will affect the DSSC performance. Basically, liquid electrolyte in the DSSC fabrication should consist of three main components such as organic solvent, redox pair and additive. Liquid electrolyte should have some good properties such as less viscous, high temperature volatilities and precipitate of salts at low temperature (Jayaweera *et al*., 2015). Traditional organic liquid electrolytes pose problems such as:

- Low long-term stability
- Problem in sealing process to overcome leakage of electrolyte
- Easy evaporation of solvent.

There are some solvents that have been used such as acetonitrile, ethylene carbonate, propylene carbonate, γ-butyrolactone, ethylene glycol, tetrahydrofuran, dimethoxyethane, dimethylsulfoxide and water (O'Regan & Grätzel, 1991; Hara *et al*., 2001; Kato *et al*., 2009; Law *et al*., 2010) in the liquid electrolyte preparation for the DSSC application.

2.4.1.1. Dimethyl sulfoxide (DMSO)

Generally, DMSO with chemical formula $(CH_3)_2SO$ is an effective solvent for a wide selection of organic materials including many types of polymers. DMSO is a polar aprotic solvent (lack of acidic hydrogen) which can dissolve many kinds of inorganic salts. DMSO is also miscible with water and most organic type liquids. DMSO acts as a good solvent for PVA (Watase & Nishinari, 1989).

2.4.1.2. Ethylene carbonate (EC) and Propylene carbonate (PC)

EC is an organic compound with the specific chemical formula $(CH_2O)_2CO$. EC is colorless in solid form and practically odorless at room temperature. EC has low molecular weight and high dielectric constant (ε_r = 89). EC is widely used in research work as solvent in the electrolyte preparation (Ding *et al*., 2001; Sloop *et al*., 2001). PC has low molecular weight and high dielectric constant (ε_r = 65). There are some works that have been done using the PC as attractive solvent in the electrolyte for devices (Jasinski & Burrows, 1969; Yao *et al*., 2009).

Since both EC and PC have good properties, EC-PC combination has been used as solvents in the electrolyte preparation (Tobishima & Yamaji, 1984; Katayama *et al*., 2002).

2.4.1.3. Diethyl carbonates (DEC)

Diethyl carbonate (DEC) is colorless in liquid form with molecular weight of 118.13 and density of 0.97 g cm^{-3}. DEC has high boiling point of 126.8 ^{o}C and a melting point of -43 ^{o}C. DEC is a high quality solvent which can be used as plasticizer and in electrolyte preparation for capacitor, battery and lithium battery application. The chemical structure of DEC is shown in Figure 2.4.

Ionic conductivity of the electrolyte can be improved by the addition of plasticizer. The addition of low molecular weight and high dielectric constant plasticizers in the gel polymer electrolyte has significantly increase the amorphous phase of the polymer. This would affect the flexibility of polymer backbone and mobility of charge carriers (Pitawala *et al*., 2008). The addition of plasticizer also increases the volume of electrolyte system and decreases the viscosity of the electrolyte for the ion movement (Rahman *et al*., 2011).

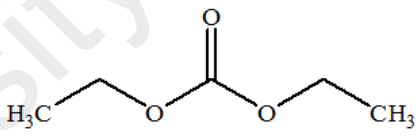

Figure 2.4: Diethyl carbonate chemical structure

2.4.2. Gel polymer electrolyte

Although solid form electrolytes may be the ideal state for DSSCs since they give high stability, easily in assembly and no-leakage problem but due to them having low ionic conductivity and poor contact with the TiO_2 nanoparticles layer electrode, the efficiency of DSSC is low. Thus, the best method to avoid this problem is using quasi-solid state polymer electrolytes or gel polymer electrolytes since they have better contact and high filling property between electrolyte and electrode. Gel polymer electrolyte is a circumventing approach for the solid and liquid electrolytes problem. In

addition, gel-form electrolyte can attain high conductivities since this kind of electrolyte has properties of holding liquid electrolyte by trapping in cages with the polymer host matrices (Wu *et al*., 2006).

2.4.2.1. Polymer

There are some research work that used various polymers or co-polymers as host matrices for the gel-form electrolyte in DSSCs, such as poly(methyl methacrylate) (PMMA) (Yang *et al*., 2008; Dissanayake *et al*., 2014), poly(acrylonitrile) (PAN) (Ileperuma *et al*., 2002; Dissanayake *et al*., 2012), poly(acrylonitrile-co-styrene) (SAN) (Lan *et al*., 2006; Wu *et al*., 2006), poly(ethylene oxide) (PEO) (Agarwala *et al*., 2011), poly(vinylidenefluoride-co-hexafluoropropylene) (PVDF-HFP) (Tsai *et al*., 2013), and polyvinyl pyrrolidone (PVP) / polyethylene glycol (PEG) (Wu *et al*., 2007). Some efficiency results using the abovementioned polymer have been shown in Table 2.5.

Table 2.5: Various researches on the GPE for the DSSC fabrication

Gel polymer electrolyte	Dye	Efficiency (%)	References
PMMA-KI-TPAI	N719	3.99	(Dissanayake *et al*., 2014)
PMMA-NaI	N719	4.78	(Yang *et al*., 2008)
PAN-TMAI	N719	2.99	(Ileperuma *et al*., 2002)
PAN-KI-TPAI	N719	~ 5.00	(Dissanayake *et al*., 2012)
SAN -NaI	N719	3.10	(Lan *et al*., 2006)
PEO– KI-LiI	N719	5.80	(Agarwala *et al*., 2011)
PVDF-HFP-KI-LiI	N3	5.52	(Tsai *et al*., 2013)
(PVP) / (PEG)-KI	N719	4.01	(Wu *et al*., 2007)

2.4.2.2. Poly (vinyl alcohol) (PVA)

Since there are various types of polymers that have been used as polymer host, PVA has been chosen due to the outstanding properties such as (Jia *et al*., 2007):

- Non-toxic
- Biocompatible
- Biodegradable
- Highly chemical resistance
- Show good performance in mechanical strength
- Easily preparation.

PVA is also a potential electrolyte material with high dielectric strength for charge storage capacity (Mohamed *et al*., 2014). PVA also has high capability of solvent holding and wide temperature window (Agrawal & Shukla, 2000). PVA also widely used for binder in solid pigments, ceramic products, plastic, cement, fibers, non-woven fabrics, catalyst pellets, and cork compositions (Attia & El-Kader, 2013). This kind of water-soluble polymer is used widely for the paper coating, textile sizing, and flexible water-soluble packaging films (Bassner & Klingenberg, 1998). Figure 2.5 shows PVA's chemical structure.

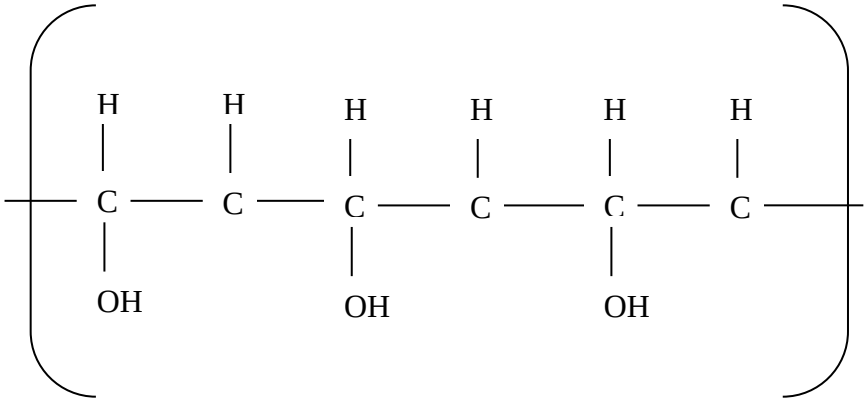

Figure 2.5: Polyvinyl alcohol (PVA) chemical structure

Polyvinyl alcohol (PVA) has also been used by researchers in severals applications such as electrical double layer capacitors (Senthilkumar *et al*., 2013), supercapacitors (Liew, *et al*., 2015), electrochromic windows (Singh *et al*., 1995), sensors (Penza & Cassano, 2000), batteries (Kadir *et al*., 2010), Li-ion batteries (Subramania *et al*., 2006) and fuel cell (Liew *et al*., 2014).

Therefore, polyvinyl alcohol (PVA) can also be used in the dye-sensitized solar cell as polymer host for the electrolyte (Aziz *et al*., 2014).

2.4.2.3. Potassium Iodide (KI)

KI is an inorganic compound containing two ions, K^+ as cation and I^- as anion as shown in Figure 2.6.

Figure 2.6: Potassium iodide chemical structure

There are some researches on the gel polymer electrolytes employing LiI, NaI and KI for DSSC applications (An *et al*., 2006; Aziz *et al*., 2014; Noor *et al*., 2014). Table 2.6 shows some researches on DSSCs that used KI as salt in electrolyte.

Table 2.6: DSSCs performance using potassium iodide based gel polymer electrolyte

Gel polymer electrolyte	Efficiency (%)	References
PEO-DMPII-KI	4.05	(Chen *et al*., 2011)
Poly(acrylamide)-PEG-EC-PC-KI	3.00	(Wu *et al*., 2006)
PEO-KI	2.04	(Kalaignan *et al*., 2006)

Table 2.6, continued.

Gel polymer electrolyte	Efficiency (%)	References
PVdF-HFP-EC-PC-KI	2.20	(Noor *et al*., 2011)
PEG-KI	2.67	(Park *et al*., 2008)
PEO-KI	4.50	(Agarwala *et al*., 2011)

2.4.2.4. Quaternary ammonium iodide

Quaternary ammonium iodide (QAI) is generally known as quaternary ammonium salts or compounds. This kind of salt contains quaternary ammonium cation and an iodide ion. The quaternary ammonium cation is a positive charge and has four branches as shown in Figure 2.7.

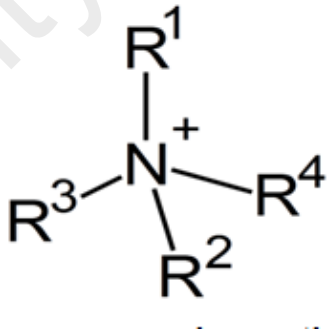

Figure 2.7: Quaternary ammonium cation chemical structure

Quaternary ammonium iodide salts are widely used in gel electrolyte for DSSC. These quaternary ammonium iodide salts includes tetraethyl ammonium iodide (TEAI), tetrapropyl ammonium iodide (TPAI), tetrametyhl ammonium iodide (TMAI), and tetrabutyl ammonium iodide (TBAI) (Bandara *et al*., 2013). The chemical structure of these salts are shown in Figure 2.8.

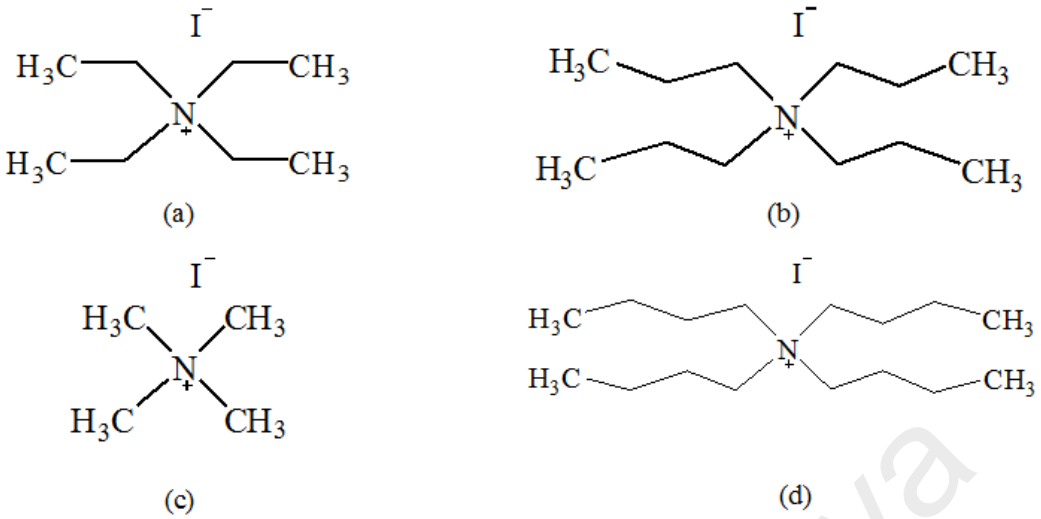

Figure 2.8: Example of quaternary ammonium iodide (a) Tetraetyhl ammonium iodide (TEAI) (b) Tetrapropyl ammonium iodide (TPAI) (c) Tetramethyl ammonium iodide (TMAI) (d) Tetrabutyhl ammonium iodide (TBAI)

The presence of quaternary ammonium iodide in the gel electrolyte system gives an advantage for dye-sensitized solar cell. This is because the quaternary ammonium iodide has large cation. Hence, this salt is expected to provide more number of iodide ions. The large number of iodide ions contributes to the short circuit current density and also the efficiency of DSSC (Arof *et al*., 2014).

2.4.2.5. Redox couple

In the DSSC, the redox couple should be playing the main role in the electrolyte. There are some properties for an ideal redox shuttles in DSSC to attain good efficiency as shown in Table 2.7 and Figure 2.9.

From the Figure 2.9, the redox shuttle system (R/R^-) is the main component for the open-circuit voltage of the dye-sensitized solar cell. The gap between the redox shuttle (R/R^-) potential in electrolyte and Fermi level of TiO_2 is a measure of the open circuit voltage (V_{oc}).

Table 2.7: Properties of ideal redox couple

Ideal redox shuttles
Reasonable value of redox potential
Rational solubility
Able to prevent the insignificant spectral characteristics in the visible light
Redox couple should in the stable mode
Highly reversible process
No chemical reactivity and surface activity

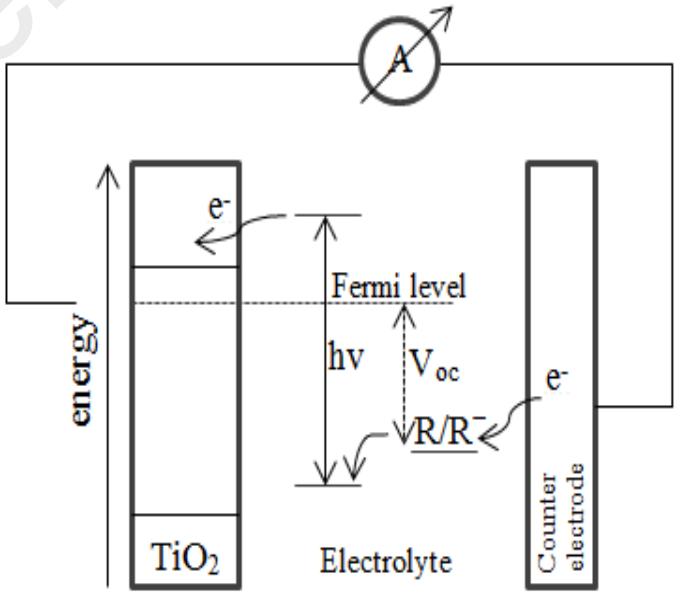

Figure 2.9: Properties of ideal redox couple (Wolfbauer *et al*., 2001)

There are some examples of redox couple that has been used in the dye-sensitized solar cell such as I^- / I_3^- (Boschloo & Hagfeldt, 2009), Br^- / Br_2 (Hara et al., 2001), SCN^- / $(SCN)_2$ with $SeCN^-$ / $(SeCN)_2$ (Oskam *et al*., 2001), Fe^{2+} / Fe^{3+} (Sönmezoğlu, *et al*., 2012), Co(II/III) (Yella *et al*., 2011) and $Co(phen)_3^{2+}$/ $Co(phen)_3^{3+}$ (Wen *et al*., 2000).

2.5. Counter electrode

The last component of dye-sensitized solar cell is counter electrode. Counter electrode should play well for the electrons transfers from the external circuit to the redox couple in electrolyte. A good counter electrode should have these properties such as (Koo *et al*., 2006):

- Good catalytic effect on the reduction of redox couple
- Large surface area.

Platinum has been used widely for dye-sensitized solar cell as counter electrode (Özkan, *et al.*, 2017). Other counter electrodes that have been used in DSSC fabrication include graphite-based (Wei *et al*., 2011) and carbon-nanotube (Yang *et al*., 2013).

2.6. Summary

In this chapter, the properties and background of dye-sensitized solar cell have been discussed properly with some important details. The next chapter presents the materials used, electrolyte preparation and some various experimental characteristics.

CHAPTER 3: METHODOLOGY

3.1. Introduction

In present work, the polymer host which is poly vinyl alcohol (PVA) was used for electrolyte preparation. Three systems were done in this work i.e single salt system, double salt system and double salt with plasticizer system.

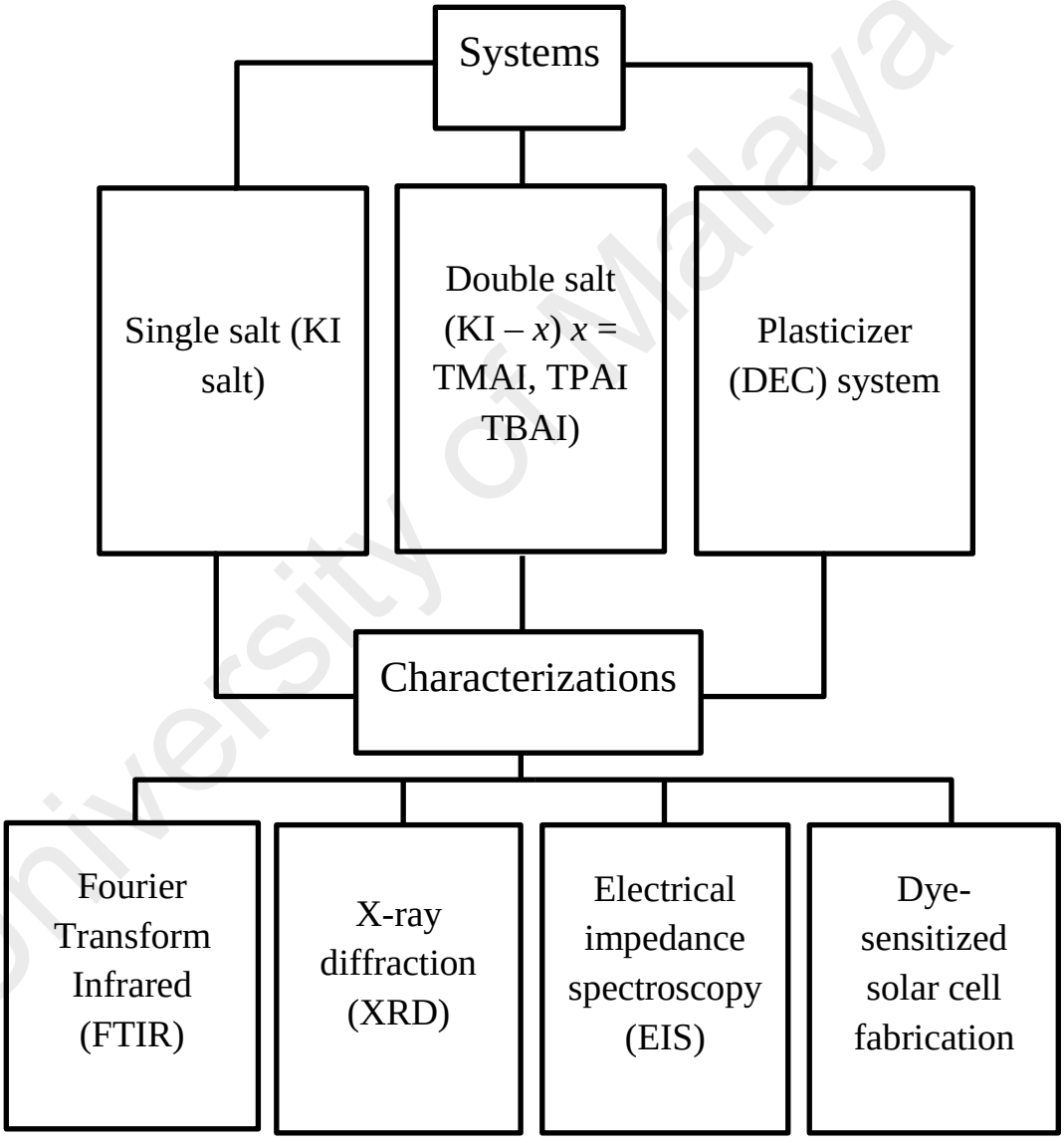

Figure 3.1: Flow chart of work systems

3.2. Chemicals

Ethylene carbonate (EC) and propylene carbonate (PC) were purchased from Sigma Aldrich. Dimethyl sulfoxide (DMSO) solvent was purchased from Friendmann Schmidt Chemicals. The salts such as potassium iodide (KI), tetrapropyl ammonium iodide (TPAI), tetrametyhl ammonium iodide (TMAI) and tetrabutyl ammonium iodide (TBAI) were purchased from Sigma Aldrich. Titanium dioxide powder (P90 and P25) were purchased from Aeroxide. Ruthenium N3 dye and Platinum (Pt) solution were purchased from Solaronix.

3.3. Gel polymer electrolyte preparation

3.3.1. PVA-EC-PC-DMSO-KI-I_2 system

The gel polymer electrolytes were prepared by keeping the amounts of PVA (0.2 g), EC (0.3 g), PC (0.4 g) and DMSO (2.2 g) fixed and varying the amounts of KI and I_2. The composition of the gel polymer electrolytes have been shown in Table 3.1.

Table 3.1(a): Amount of KI salt and I_2

Label	KI (g)	I_2 (g)
A1	0.0412	0.0060
A2	0.0868	0.0132
A3	0.1380	0.0212
A4	0.1952	0.0298
A5	0.2600	0.0400
A6	0.3346	0.0512
A7	0.4200	0.0646
A8	0.5202	0.0798
A9	0.6384	0.0980

Table 3.1(b): Composition for gel polymer electrolytes with KI salt

Label	PVA (wt. %)	EC (wt. %)	PC (wt. %)	DMSO (wt. %)	KI (wt. %)	I_2 (wt. %)
A1	6.36	9.53	12.71	69.90	1.31	0.19
A2	6.25	9.38	12.50	68.75	2.71	0.41
A3	6.14	9.20	12.27	67.50	4.23	0.66

Table 3.1(b), continued.

Label	PVA (wt. %)	EC (wt. %)	PC (wt. %)	DMSO (wt. %)	KI (wt. %)	I_2 (wt. %)
A4	6.02	9.02	12.03	66.17	5.87	0.89
A5	5.88	8.82	11.76	64.71	7.65	1.18
A6	5.74	8.61	11.48	63.11	9.59	1.47
A7	5.58	8.37	11.16	61.37	11.72	1.80
A8	5.41	8.11	10.81	59.46	14.06	2.15
A9	5.21	7.82	10.43	57.35	16.64	2.55

For the preparation of GPEs, precise amounts of KI were first dissolved in right amounts of EC, PC and DMSO contained in a glass container. Then, required amount of PVA was added to the salt solution and stirred at 383 K until a homogeneous mixture is obtained. The mixture has been cooled down until temperature reached 323 K before adding iodine (I_2) crystals and continuously stirred for few more minutes. The amount of I_2 added was 10 % molar ratio of total iodide ions available from salts. The final product is in gel form where the I_2 is dissolved well in the mixture.

3.3.2. PVA-EC-PC-DMSO-KI-*x*-I_2 (*x* = TMAI, TPAI, TBAI) system

From the first system, some parts of KI salt in A7 gel polymer electrolyte composition was replaced with tetramethyl ammonium iodide (TMAI), tetrapropyl ammonium iodide (TPAI) and tetrabutyl ammonium iodide (TBAI). Table 3.2 (a), (b), 3.3 (a), (b) and 3.4 (a), (b) list the composition details of gel polymer electrolyte composition containing TMAI, TPAI and TBAI, respectively.

Table 3.2(a): Amount of KI-TMAI salt and I_2

Label	KI (g)	TMAI (g)	I_2 (g)
B1	0.294	0.126	0.061
B2	0.210	0.210	0.058
B3	0.126	0.294	0.056
B4	0.000	0.420	0.053

Table 3.2(b): Composition for gel polymer electrolytes with KI-TMAI salt

Label	PVA (wt. %)	EC (wt. %)	PC (wt. %)	DMSO (wt. %)	KI (wt. %)	TMAI (wt. %)	I_2 (wt. %)
B1	5.59	8.38	11.17	61.43	8.21	3.52	1.70
B2	5.59	8.38	11.18	61.49	5.87	5.87	1.62
B3	5.59	8.39	11.19	61.52	3.52	8.22	1.57
B4	5.60	8.40	11.20	61.57	0.00	11.75	1.48

Table 3.3(a): Amount of KI-TPAI salt and I_2

Label	KI (g)	TPAI (g)	I_2 (g)
C1	0.294	0.126	0.055
C2	0.210	0.210	0.049
C3	0.126	0.294	0.043
C4	0.000	0.420	0.034

Table 3.3(b): Composition for gel polymer electrolytes with KI-TPAI salt

Label	PVA (wt. %)	EC (wt. %)	PC (wt. %)	DMSO (wt. %)	KI (wt. %)	TPAI (wt. %)	I_2 (wt. %)
C1	5.60	8.39	11.19	61.54	8.22	3.52	1.54
C2	5.61	8.41	11.21	61.64	5.88	5.88	1.37
C3	5.61	8.42	11.23	61.74	3.54	8.25	1.21
C4	5.63	8.44	11.25	61.90	0.00	11.82	0.96

Table 3.4(a): Amount of KI-TBAI salt and I_2

Label	KI (g)	TBAI (g)	I_2 (g)
D1	0.294	0.126	0.0497
D2	0.210	0.210	0.0464
D3	0.126	0.294	0.0394
D4	0.000	0.420	0.0288

Table 3.4(b): Composition for gel polymer electrolytes with KI-TBAI salt

Label	PVA (wt. %)	EC (wt. %)	PC (wt. %)	DMSO (wt. %)	KI (wt. %)	TBAI (wt. %)	I_2 (wt. %)
D1	5.60	8.40	11.21	61.63	8.24	3.53	1.39
D2	5.61	8.41	11.22	61.68	5.89	5.89	1.30
D3	5.62	8.43	11.24	61.80	3.54	8.26	1.11
D4	5.64	8.45	11.27	61.99	0.00	11.84	0.81

3.3.3. Plasticizer system

In this part, the diethyl carbonate was used in the gel polymer electrolyte as plasticizer. Two kinds of samples have been chosen from the previous double iodide system (KI-TPAI and KI-TBAI) for plasticizer system. Table 3.5 and Table 3.6 shows the composition of PVA-EC-PC-DMSO-KI-TPAI-I_2-DEC and PVA-EC-PC-DMSO-KI-TBAI-I_2-DEC gel polymer electrolyte system respectively.

Table 3.5: Composition for gel polymer electrolytes (KI-TPAI-I_2-DEC)

Label	PVA (wt. %)	EC (wt. %)	PC (wt. %)	DMSO (wt. %)	KI (wt. %)	TPAI (wt. %)	I_2 (wt. %)	DEC (wt. %)
E1	5.52	8.28	11.04	60.70	5.79	5.79	1.35	1.53
E2	5.46	8.19	10.92	60.06	5.73	5.73	1.34	2.57
E3	5.40	8.10	10.80	59.40	5.67	5.67	1.32	3.64
E4	5.31	7.96	10.62	58.39	5.57	5.57	1.30	5.28

Table 3.6: Composition for gel polymer electrolytes (KI-TBAI-I_2-DEC)

Label	PVA (wt. %)	EC (wt. %)	PC (wt. %)	DMSO (wt. %)	KI (wt. %)	TBAI (wt. %)	I_2 (wt. %)	DEC (wt. %)
F1	5.56	8.33	11.11	61.12	3.50	8.17	1.10	1.11
F2	5.47	8.21	10.95	60.22	3.45	8.05	1.08	2.57
F3	5.40	8.10	10.80	59.40	5.67	5.67	1.32	3.64
F4	5.30	7.95	10.61	58.33	3.34	7.80	1.04	5.63

3.4. Electrical Impedance Spectroscopy (EIS)

The HIOKI LCR Hi-Tester *ac* impedance bridge was used for impedance measurements in the frequency range between 1 Hz to 100 kHz. The gel polymer electrolyte was sandwiched between two clean stainless steel electrodes. The measurement was performed at various temperatures (298 K to 373 K).

Figure 3.2: Electrochemical impedance spectroscopy (EIS) instrument

Conductivity was calculated using the following equation:

$$\sigma = \frac{t}{R_b A} \tag{3.1}$$

where, t is gel polymer electrolyte thickness, R_b is the bulk resistance which can be obtained from the intersection of Cole-Cole plot with the real impedance axis and A is the electrolyte surface area.

In impedance spectroscopy, the applied voltage (V) is defined as

$$V(t) = V_o \sin(\omega t) \tag{3.2}$$

where V_o is the voltage amplitude and $\omega = 2\pi f$, where f is frequency.

The resulting electric current (I) through the sample is given by,

$$I(t) = I_o \sin(\omega t + \varphi) \tag{3.3}$$

where I_o is the current amplitude and φ is the phase angle between the applied voltage and the resultant current. The electrical impedance, $Z(\omega)$ is defined as

$$Z(\omega) = \frac{V(t)}{I(t)} \tag{3.4}$$

and also can be expressed as

$$Z(\omega) = Z_r + jZ_i \tag{3.5}$$

where Z_r is real impedance and Z_i is imaginary impedance.

The real and imaginary parts of the complex impedance can be defined as

$$Z_r = Z\cos\theta \tag{3.6}$$

$$Z_i = Z\sin\theta \tag{3.7}$$

Nyquist plot is the plot of the negative imaginary part ($-Z_i$) against the real part (Z_r) of impedance.

Another related function such as complex permittivity $\varepsilon(\omega)$ can be expressed by

$$\varepsilon(\omega) = \varepsilon_r + j\varepsilon_i \tag{3.8}$$

where ε_r is the real part of complex permittivity and ε_i is the imaginary part.

The real and imaginary parts of the complex permittivity is given by

$$\varepsilon_r = \frac{Z_i}{\omega C_o (Z_r^{\,2} + Z_i^{\,2})} \tag{3.9}$$

$$\varepsilon_i = \frac{Z'}{\omega C_o (Z_r^{\,2} + Z_i^{\,2})} \tag{3.10}$$

Here, $C_o = \varepsilon_o A/t$ where ε_o, A and t is permittivity of space, area and thickness of the electrolyte, respectively.

In this study, the Nyquist plot or Cole-Cole plot has been used to extract the bulk resistance of gel polymer electrolyte where the conductivity value can be obtained from Equation (3.1). In order to understand ionic transportation, the diffusion coefficient (D), the ionic mobility (μ) and number density of charge carrier (n) for all gel polymer electrolytes have been calculated using the following equations (Bandara *et al*., 2011):

$$D = \frac{(\varepsilon_r \varepsilon_o A)^2}{\tau (k^{-1})^2} \tag{3.11}$$

$$\mu = \frac{eD}{k_B T} \tag{3.12}$$

$$n = \frac{\sigma}{e\mu} \tag{3.13}$$

where $\tau = 1/\omega$, ω is the angular frequency at the intercept of spike plot with the x-axis in the Cole-Cole plot, A is the area of the sample, k^{-1} is obtained from the fitting of the experimental data, ε_o is the vacuum permittivity, ε_r is the dielectric constant of gel polymer electrolyte which can be obtained from equation (3.9), k_b is Boltzmann's constant and e is electron charge.

3.5. X-ray diffraction (XRD)

X-ray diffraction is an important technique to identify the crystalline or amorphous state of the polymer electrolytes. The XRD was carried out by applying an X-ray beam with a certain wavelength λ at different angles on the sample. Figure 3.3 shows an example of x-ray diffractrograms for polyvinyl alcohol (PVA)-poly vinylidene fluorine (PVdF) blend polymer electrolyte. From Figure 3.3, the PVA peaks shown at 2θ=19.5^o and 22.3^o and the PVdF peaks shown at 2θ =20^o and 23^o. These peaks indicate that the PVA and PVdF are semicrystalline. The peaks corresponding $LiClO_4$ do not appear in the PVA-PVdF. $LiClO_4$ spectra indicates that the salt is completely dissolved in the

polymer matrices. In this work, the XRD of the gel electrolytes was performed using an X-ray diffractometer (BTX-II Olympus Benchtop). The source of X-ray is Cu-kα radiation with wavelength λ=1.540598 Å. The percentage of the gel polymer electrolyte that is crystalline can be determined from equation:

$$\%Crystallinity = \frac{Area\ under\ crystalline\ peaks}{Total\ Area\ under\ all\ peaks} \times 100\% \qquad (3.14)$$

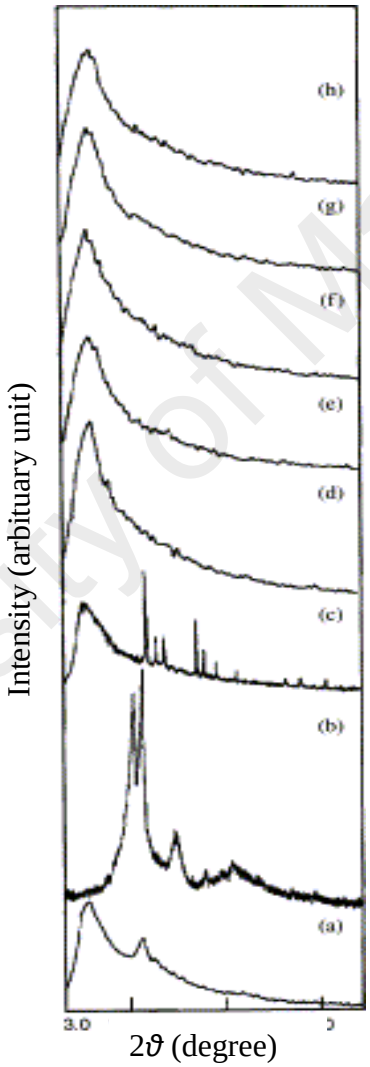

Figure 3.3: X-ray diffraction patterns of (a) PVA, (b) PVdF, (c) $LiClO_4$, (d) PVA–PVdF (0:90)–$LiClO_4$ (10 wt.%), (e) PVA–PVdF (22.5:67.5)–$LiClO_4$(10 wt.%), (f) PVA–PVdF (45:45)–Li-ClO_4 (10 wt.%), (g) PVA–PVdF (67.5:22.5)–$LiClO_4$(10 wt.%), (h)PVA–PVdF(90:0)–$LiClO_4$ (10 wt.%) (Rajendran *et al*., 2004)

3.6. Fourier transform infrared (FTIR) spectroscopy

The functional group of gel polymer electrolytes such as alkyl, hydroxyl, amino group can be determined using FTIR spectroscopy. In this work, FTIR spectrophotometer (Nicolet iS10 Thermo Scientific) has been used. The measurement was carried out in the range between 4000 and 650 cm^{-1} with 2 cm^{-1} resolution.

3.7. Fabrication of Dye-sensitized solar cell (DSSC)

3.7.1. Photo-anode preparation

The photoanode was prepared by coating two layer of TiO_2 on top of conducting side of FTO glass. The first layer is compact layer and the second is porous layer. The compact TiO_2 layer was prepared using the following procedure. 0.5 g of TiO_2 (P90) powder was grounded for about 30 minutes with 2 ml of HNO_3 (pH=1) in an agate mortar. Then a drop of resulted slurry was spin coated on the well cleaned FTO glass in two steps. Spin coating was done first at 1000 rpm for 5 seconds and followed by another spin coating at 2300 rpm for 60 seconds. The spin coated glass plates were sintered at 450 $^{\circ}C$ for about 30 minutes in a furnace.

The porous TiO_2 layer was prepared using the following procedure. 0.5 g of TiO_2 powder (Degussa P25) and 0.1 g of carbowax was grounded with 2 ml HNO_3 (pH=1) for 30 minutes in an agate mortar. Two drops of Triton X-100 were added as the surfactant during the last stage of grinding. Resulted TiO_2 slurry was spread on top compact layer using the 'Doctor Blade' method. It was the sintered at 450 $^{\circ}C$ for 30 minutes in a furnace.

In order to adsorb dye molecules, the TiO_2 coated electrodes were immersed in 0.3 mM of N3 dye solution held for 24 hours. The N3 dye solution was prepared by dissolved 1 mg of N3 powder in 5 mL of ethanol.

3.7.2. Platinum (Pt) electrode preparation

The platinum (Pt) solution was spread onto the clean conducting surface of FTO glass. The counter electrode was then heated at 450 ^{o}C in the furnace for 30 minutes.

3.7.3. Dye-sensitized solar cells (DSSCs) assembly

DSSCs were prepared by sandwiching the gel electrolyte between the dye-sensitized TiO_2 working electrode and the counter electrode and thus with the configuration of glass/FTO/TiO_2/Dye/Gel polymer electrolyte/Pt/FTO/glass. A platinum coated glass electrode was used as the counter electrode.

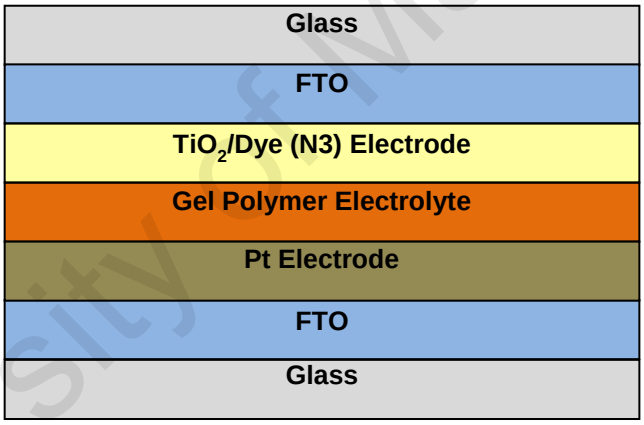

Figure 3.4: Configuration of Dye-sensitized solar cell (DSSC)

3.8. *J-V* measurement of DSSC

DSSC were tested under white light intensity of 100 mW cm^{-2}. The *J-V* characteristics were obtained using a Keithley 2400 source meter. The fill factor (*ff*) was calculated using the following equation:

$$ff = \frac{V_{max} \; x \; J_{max}}{V_{oc} \; x \; J_{sc}} \qquad (3.15)$$

where J_{sc} is the short-circuit current density (mA cm^{-2}) and V_{oc} is the open-circuit voltage (V). J_{max} (mA cm^{-2}) and V_{max} (V) are the current density and voltage at the maximum point of power output as shown in Figure 3.5

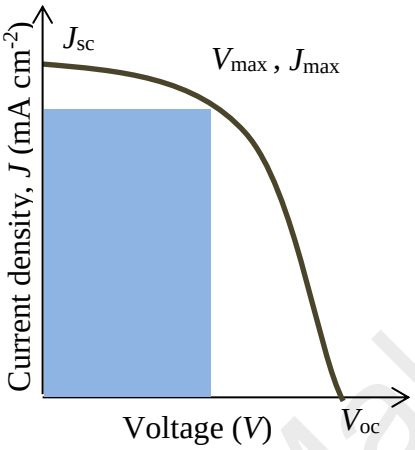

Figure 3.5: *J-V* curve for dye-sensitized solar cell (DSSC)

The conversion efficiency from the external light into electricity can be calculated by following relationship:

$$\eta\,(\%) = \frac{V_{oc}\ J_{sc}\ ff}{P_{in}}\ X\ 100\% \qquad (3.16)$$

where P_{in} is the incident light power (100 mW cm^{-2}).

Figure 3.6 shows a complete fabricated dye-sensitized solar cell.

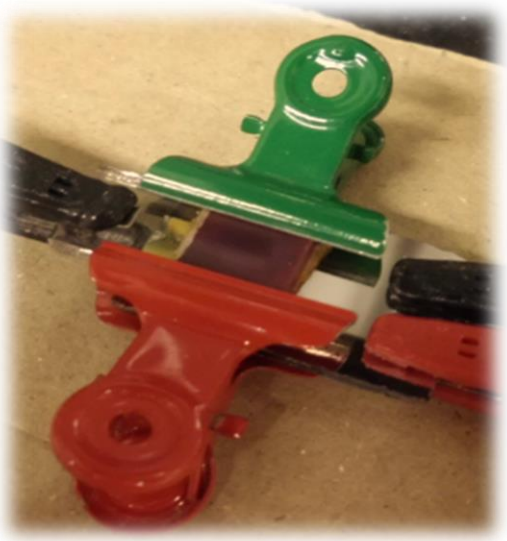

Figure 3.6: Completely fabricated Dye-sensitized solar cell

3.9. Summary

The preparation of gel polymer electrolytes which are PVA-EC-PC-DMSO-KI system, PVA-EC-PC-DMSO-KI-*x*-I_2 (*x* = TMAI, TPAI, TBAI) system and PVA-EC-PC-DMSO-KI-*x*-I_2-DEC (*x*=TPAI, TBAI) system have been shown in details. The gel polymers electrolytes have been characterized using x-ray diffraction (XRD), fourier transform infrared (FTIR) and electrical impedance spectroscopy (EIS). All gel polymer electrolytes have been used in the DSSC fabrication.

CHAPTER 4: FOURIER TRANSFORM INFRARED (FTIR) SPECTROSCOPY

4.1. Introduction

The interaction among the materials in the gel polymer electrolyte systems have been investigated using fourier transform infrared (FTIR) spectroscopy. The interactions can be determined by observing the shifting of peaks or wavenumbers of the functional groups in the spectrum. For example, PVA structure contains the alcohol functional group (hydroxyl). This hydroxyl band is expected to shift when O-H bond interacts with the cation of salt used.

4.2. Interaction between PVA-DMSO

Figure 4.1 shows the infrared spectra for PVA, DMSO and PVA-DMSO in the region between (a) 1060 to 1000 cm^{-1} and (b) 3600 to 3000 cm^{-1}. The functional group of S=O for DMSO was observed at 1026 cm^{-1} (Nakamoto, 1986). The peak has been shifted to a lower wavenumber at 1017 cm^{-1} for the PVA-DMSO sample. Since PVA does not have S=O group, there is no peak can be observed in this region. The band at 3316 cm^{-1} attributed to the hydroxyl band of PVA has been shifted to 3405 cm^{-1} as shown in Figure 4.1 (b). This shows that there is an interaction between PVA and DMSO. All the shifted wavenumber for PVA-DMSO have been listed in Table 4.1.

(a)

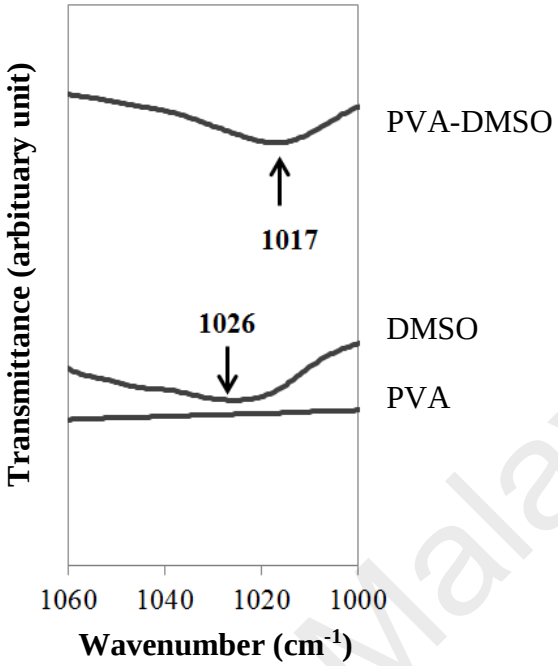

(b)

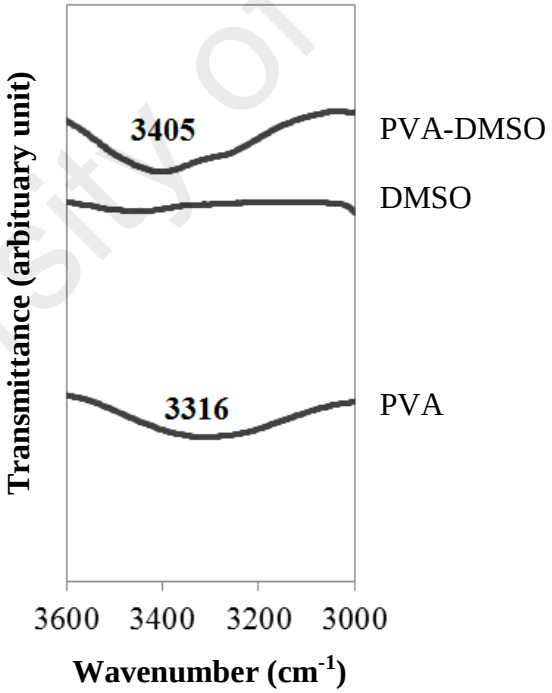

Figure 4.1: FTIR spectra for PVA, DMSO and PVA-DMSO (a) (1060-1000 cm^{-1}) and (b) (3600-3000 cm^{-1})

Table 4.1: Bands for PVA, DMSO and PVA-DMSO with their wavenumber

Wavenumber (cm^{-1})			
Assignments	PVA	DMSO	PVA-DMSO
Symmetry C-S Stretch	-	662	657
Asymmetry C-S Stretch	-	694	700
Skeletal; C-O stretch	840	887	892
S=O stretch	-	1026	1017
C-O stretch	1090	-	1081
CH-OH bending and CH_3	1322	1304	1312
CH_2 bending	-	1435	1434
C=O stretch, combination of υ(CH) and υ(CS) and C=C stretch	1648	1649	1655
Symmetry C-H stretch	2925	2983	2988
OH	3316	-	3405

4.3. Interaction between DMSO with EC-PC

Figure 4.2 shows the FTIR spectra for DMSO, EC, PC, DMSO-PC, DMSO-EC and DMSO-EC-PC in the region of 1040 to 1000 cm^{-1}. It can be seen that the DMSO peak at 1026 cm^{-1} was shifted to 1019 cm^{-1} for DMSO-PC, 1018 cm^{-1} for DMSO-EC and 1017 cm^{-1} for DMSO-EC-PC. The shifting of the band shows that there is an interaction between DMSO, EC and PC at the S=O band.

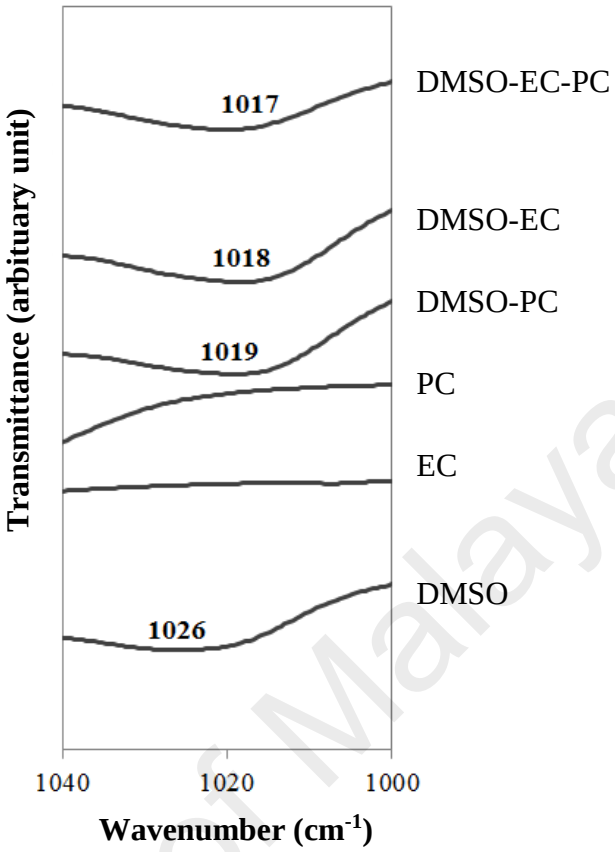

Figure 4.2: FTIR spectra for DMSO, EC, PC, DMSO-PC, DMSO-EC and DMSO-EC-PC (1040-1000 cm^{-1})

Figure 4.3 shows the FTIR spectra for the DMSO, EC, PC, DMSO-PC, DMSO-EC and DMSO-EC-PC in the range of 1200 to 1150 cm^{-1}. This region is contributing to the band of C-O-C stretching (Zhang *et al.*, 2013). There is no peak observed for the spectrum of DMSO. The C-O-C peak was observed for EC and PC at 1156 cm^{-1} and 1180 cm^{-1} respectively. This peak was shifted to 1184 cm^{-1} for DMSO-PC and 1163 cm^{-1} for DMSO-EC. Since the resolution used in this work was 2 cm^{-1}, this shifting indicates that there is an interaction occurs at the C-O-C band of EC and PC with the DMSO. The DMSO-EC-PC spectrum shows two peaks at 1180 cm^{-1} attributed to the interaction between DMSO and PC at 1169 cm^{-1} attributed to the interaction between DMSO and EC.

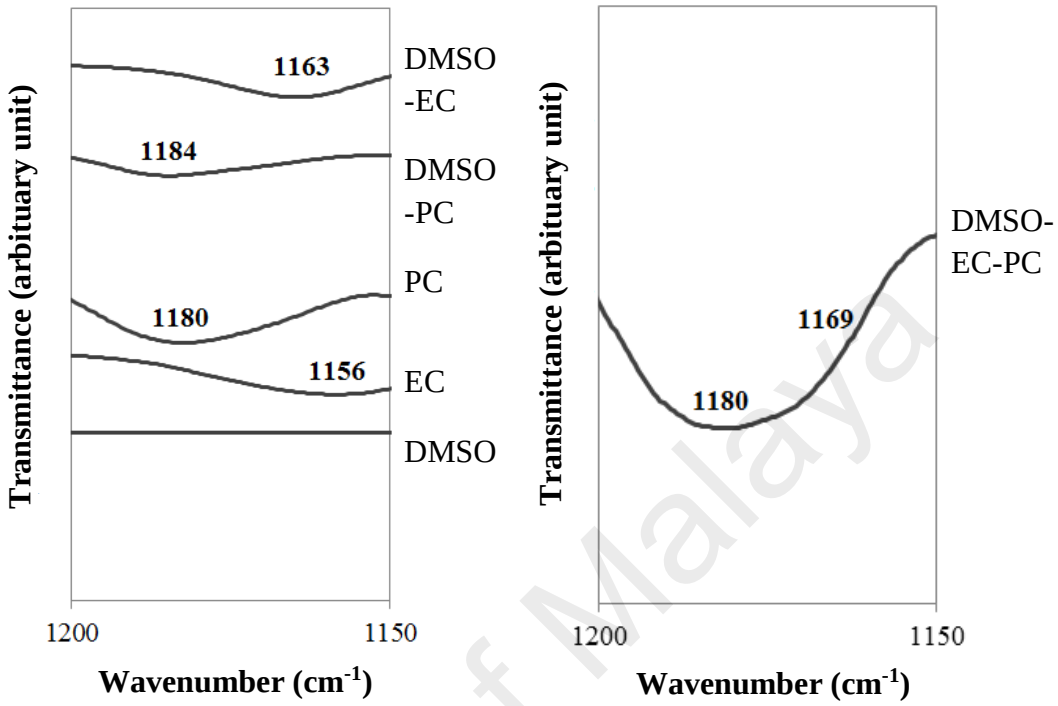

Figure 4.3: FTIR spectra for DMSO, EC, PC, DMSO-PC, DMSO-EC and DMSO-EC-PC (1200-1150 cm^{-1})

Figure 4.4 shows the FTIR spectra for DMSO, EC, PC, DMSO-PC, DMSO-EC and DMSO-EC-PC in the range of 1850 to 1750 cm^{-1} which is contributing to the C=O stretch band (Osman & Arof, 2003). There is no peak observed for the spectrum of DMSO. There are two peaks attributed to the C=O band was observed in the spectrum of EC which is at 1767 cm^{-1} and 1794 cm^{-1}. In the spectrum of PC, the C=O band was observed at 1782 cm^{-1}. This band was shifted to 1786 cm^{-1} for DMSO-PC where 1771 cm^{-1} and 1798 cm^{-1} for DMSO-EC. The DMSO-EC-PC spectrum shows the new shifted peak at 1775 cm^{-1} and 1800 cm^{-1} for DMSO-EC-PC. This indicates that the DMSO has been interacted with EC-PC solvent. The S=O, C-O-C and C=O bands of DMSO-EC-PC have been listed in Table 4.2.

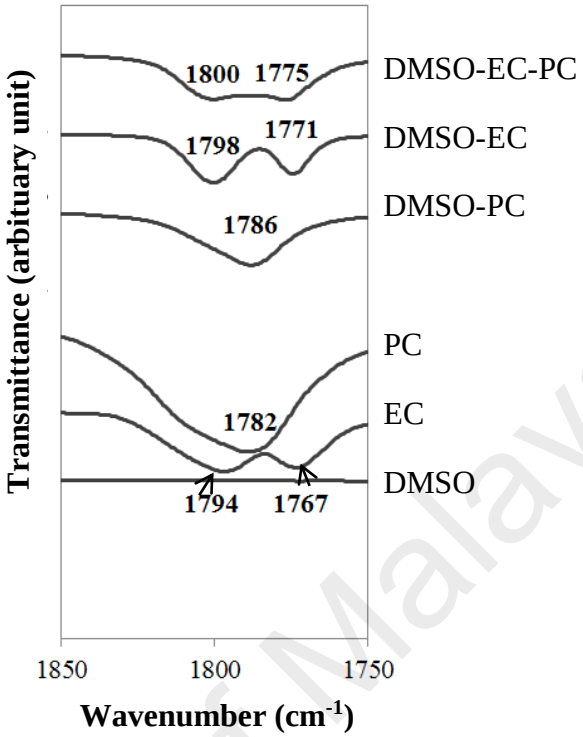

Figure 4.4: FTIR spectra for DMSO, EC, PC, DMSO-PC, DMSO-EC and DMSO-EC-PC (1850-1750 cm^{-1})

Table 4.2: Bands for DMSO, EC, PC, DMSO-EC, DMSO-PC and DMSO-EC-PC with their wavenumber

Wavenumber (cm^{-1})						
Assignment of bands	DMSO	EC	PC	DMSO-EC	DMSO-PC	DMSO-EC-PC
S=O	1026	-	-	1018	1019	1017
C-O-C stretch	-	1156	1180	1163	1184	1180, 1169
C=O stretch	-	1767, 1794	1782	1771,1798	1786	1775,1800

4.4. Interaction between PVA-DMSO-EC-PC with KI salt

Figure 4.5 shows the FTIR spectra for PVA-DMSO-EC-PC and PVA-DMSO-EC-PC-KI gel polymer electrolytes in the region of 3700 to 3100 cm^{-1}. The hydroxyl band for PVA-DMSO-EC-PC was observed at 3417 cm^{-1}. The band was shifted when the potassium iodide salt was added into the PVA-DMSO-EC-PC. The shifted bands appear at 3410, 3410, 3410, 3410, 3410, 3407, 3400, 3403 and 3406 cm^{-1} for samples A1, A2, A3, A4, A5, A6, A7, A8 and A9, respectively. This indicates that the cation of potassium iodide do interact with the hydroxyl band of PVA.

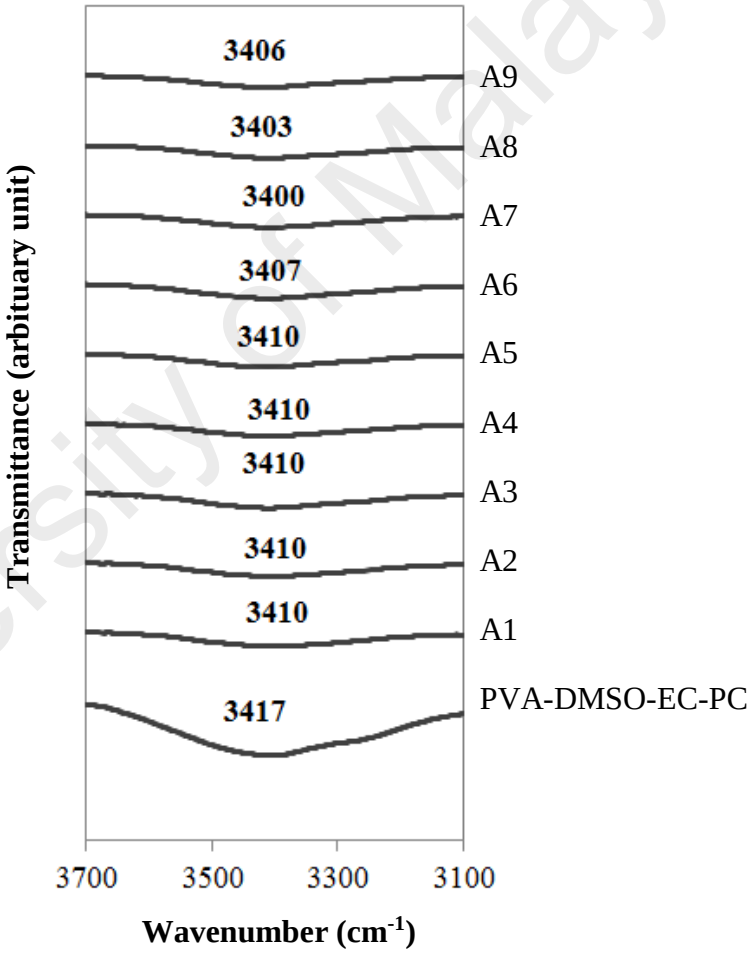

Figure 4.5: FTIR spectra for PVA-DMSO-EC-PC and PVA-DMSO-EC-PC-KI (3700 – 3100 cm^{-1})

Figure 4.6 shows the FTIR spectra for PVA-DMSO-EC-PC gel and PVA-DMSO-EC-PC-KI gel polymer electrolytes in the region of (a) 1250 to 1150 cm^{-1} and (b) 1850 to 1750 cm^{-1}.

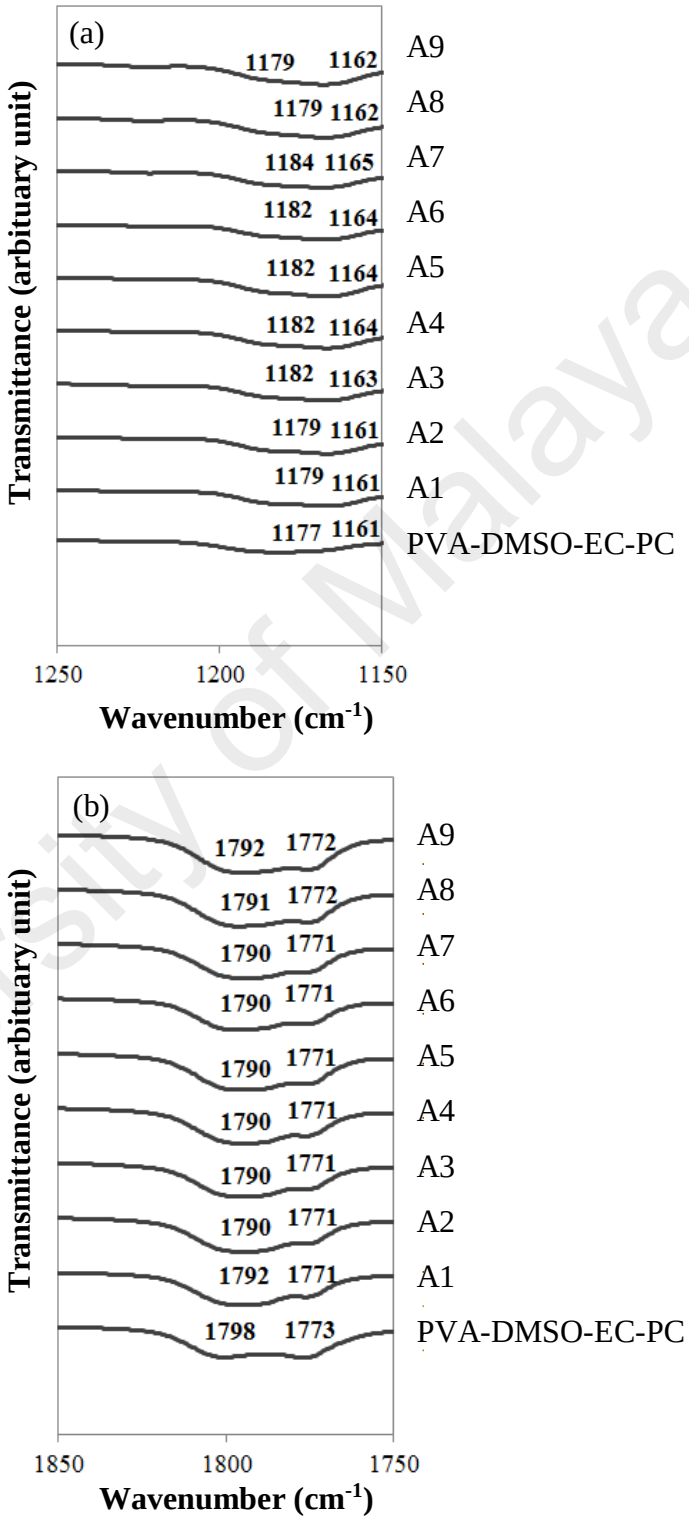

Figure 4.6: FTIR spectra for PVA-DMSO-EC-PC and PVA-DMSO-EC-PC-KI (a) 1250 –1150 cm^{-1} and (b) 1850 – 1750 cm^{-1}

The peaks observed for PVA-DMSO-EC-PC and samples A1, A2, A3, A4, A5, A6, A7, A8 and A9 have been listed in Table 4.3. It can be seen that C-O-C band is slightly shifted with the addition of KI. The C=O band of PVA-DMSO-EC-PC at 1773 cm^{-1} seems unchanged when KI is added. But, the band at 1798 cm^{-1} was shifted to lower wavenumber for sample A1 to A9. This indicates that there is an interaction between PVA-DMSO-EC-PC and KI at C-O-C and C=O bands.

Table 4.3: Bands for PVA-DMSO-EC-PC, A1, A2, A3, A4, A5, A6, A7, A8 and A9 with their wavenumber

Wavenumber (cm^{-1})			
Assignment of bands	O-H	C=O	C-O-C
PVA-DMSO-EC-PC	3417	1773, 1798	1161, 1177
A1	3410	1771, 1792	1161, 1179
A2	3410	1771, 1790	1163, 1182
A3	3410	1771, 1790	1164, 1182
A4	3410	1771, 1790	1164, 1182
A5	3410	1771, 1790	1164, 1182
A6	3407	1771, 1790	1164, 1182
A7	3400	1771, 1790	1165, 1184
A8	3403	1772, 1791	1162, 1179
A9	3406	1772, 1792	1162, 1179

4.5. Interaction between PVA-DMSO-EC-PC with KI-TMAI salt

Figure 4.7 shows the FTIR spectra for PVA-DMSO-EC-PC-KI-TMAI gel polymer electrolytes in the region of 3700 to 3100 cm^{-1}. The band observed at this region was hydroxyl band. The hydroxyl band of PVA-DMSO-EC-PC-KI-TMAI gel polymer electrolytes has been listed in Table 4.4. Without KI-TMAI salts, the band was observed at 3417 cm^{-1} (Figure 4.5 and Table 4.3). This band shifted to lower wavenumber when KI-TMAI salts were added to PVA-DMSO-EC-PC.

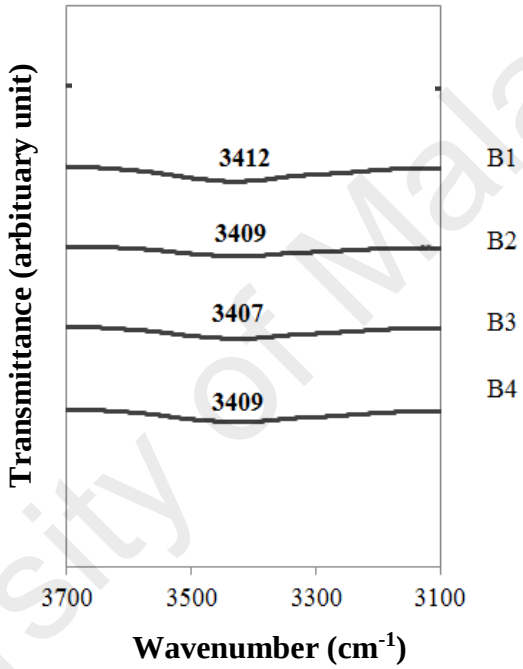

Figure 4.7: FTIR spectra for PVA-DMSO-EC-PC-KI-TMAI (3700 – 3100 cm^{-1})

Figure 4.8 shows the FTIR spectra for PVA-DMSO-EC-PC-KI-TMAI gel polymer electrolytes in the region of 1250 to 1150 cm^{-1} and 1850 to 1750 cm^{-1}. The band observed at this region was C-O-C and C=O respectively. The peaks observed for PVA-DMSO-EC-PC-KI-TMAI have been listed in Table 4.4. It can be seen that C-O-C band of PVA-DMSO-EC-PC at 1161 cm^{-1} and 1177 cm^{-1} have been shifted to higher wavenumber with the addition of KI-TMAI. The C=O band of PVA-DMSO-EC-PC at 1773 cm^{-1} seems unchanged when KI-TMAI is added and the band at 1798 cm^{-1} slightly

shifted to lower wavenumber. This indicates that there is an interaction between PVA-DMSO-EC-PC and KI-TMAI at O-H, C-O-C and C=O bands.

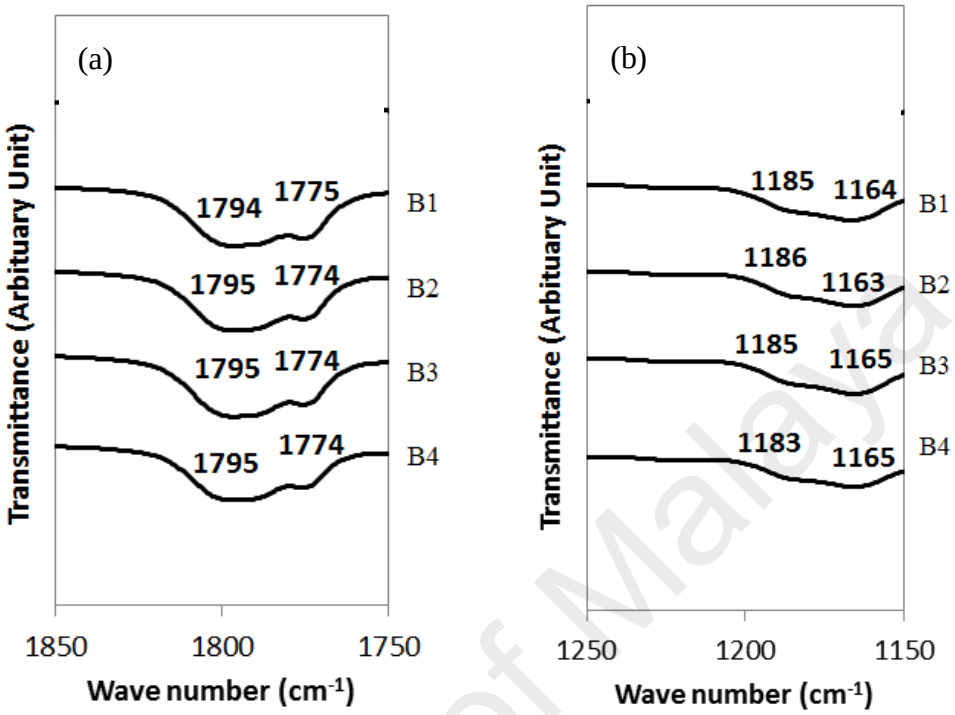

Figure 4.8: FTIR spectra for PVA-DMSO-EC-PC-KI-TMAI (a) (1850 – 1750 cm^{-1}) and (b) (1250 – 1150 cm^{-1})

Table 4.4: Band for B1, B2, B3, B4 with their wavenumber

Wavenumber (cm^{-1})				
Assignment of bands	B1	B2	B3	B4
O-H	3412	3409	3407	3409
C=O	1775,1794	1774,1795	1774,1795	1774,1795
C-O-C	1164,1185	1163,1186	1165,1185	1165,1183

4.6. Interaction between PVA-DMSO-EC-PC with KI-TPAI salt

Figure 4.9 shows the FTIR spectra for samples PVA-DMSO-EC-PC-KI-TPAI gel polymer electrolytes in the region of 3700 to 3100 cm^{-1}. The hydroxyl band was observed at 3411, 3415, 3417 and 3419 cm^{-1} for sample C1, C2, C3 and C4 respectively. Without KI-TPAI, the band was observed at 3417 cm^{-1} (Figure 4.5 and Table 4.3). Therefore, the hydroxyl band of C2 and C4 gel polymer electrolytes is considered unchanged. The shifted peak only observed for C1 sample.

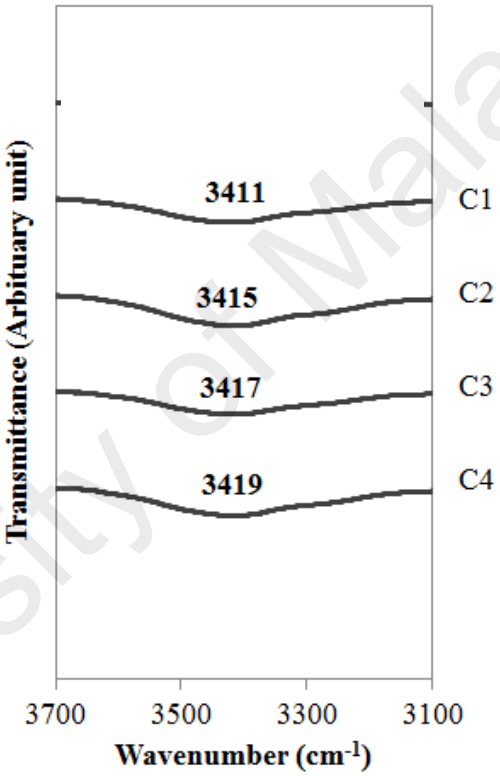

Figure 4.9: FTIR spectra for PVA-DMSO-EC-PC-KI-TPAI (3700 – 3100 cm^{-1})

Figure 4.10 shows the FTIR spectra for PVA-DMSO-EC-PC-KI-TPAI gel polymer electrolytes in the region of 1250 to 1150 cm^{-1} and 1850 to 1750 cm^{-1}. The band observed at this region was C-O-C and C=O respectively.

The peaks observed for PVA-DMSO-EC-PC-KI-TPAI have been listed in Table 4.5. It can be seen that C-O-C band of PVA-DMSO-EC-PC at 1161 cm^{-1} and 1177 cm^{-1} is shifted with the addition of KI-TPAI.

The C=O band of PVA-DMSO-EC-PC at 1773 cm^{-1} and 1798 cm^{-1} seems on changed when KI-TPAI is added. This indicates that the interaction between PVA-DMSO-EC-PC and KI-TPAI has been occurred at C-O-C bands.

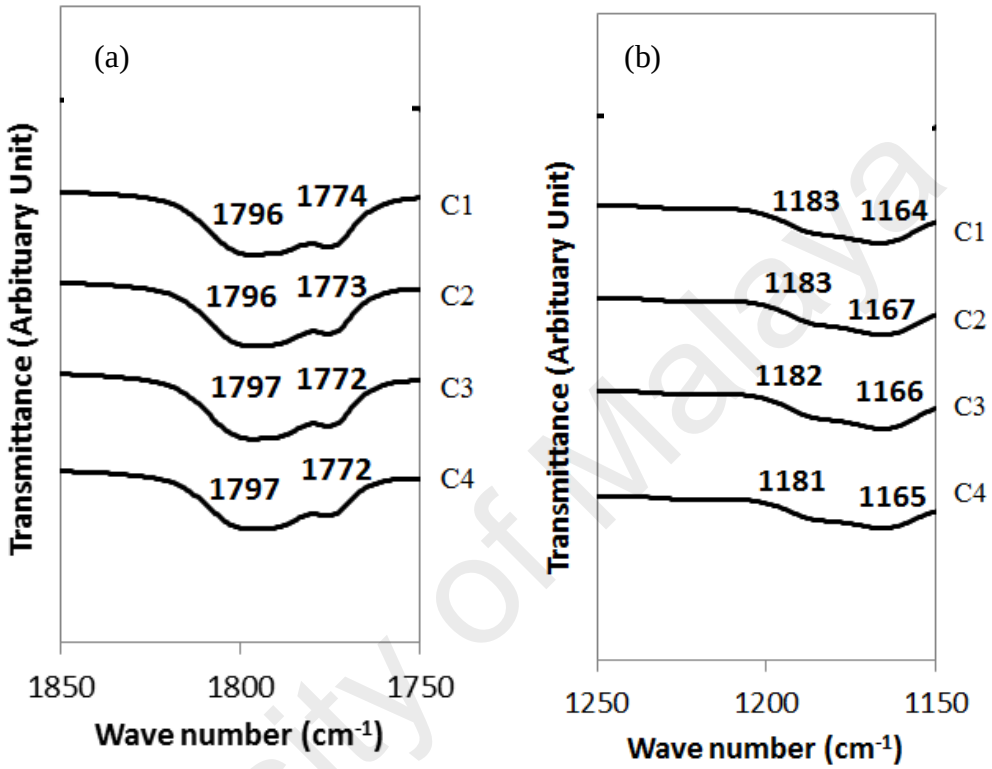

Figure 4.10: FTIR spectra for PVA-DMSO-EC-PC-KI-TPAI (a) (1850 – 1750 cm^{-1}) and (b) (1250 – 1150 cm^{-1})

Table 4.5: Band for C1, C2, C3, C4 with their wavenumber

Wavenumber (cm^{-1})				
Assignment of bands	C1	C2	C3	C4
O-H	3411	3415	3417	3419
C=O	1774,1796	1773,1796	1772,1797	1772,1797
C-O-C	1164,1183	1167,1183	1166,1182	1165,1181

4.7. Interaction between PVA-DMSO-EC-PC with KI-TBAI salt

Figure 4.11 shows the spectra for sample PVA-DMSO-EC-PC-KI-TBAI gel polymer electrolytes in the region of 3700 to 3100 cm^{-1}. It can be observed that the hydroxyl band is slightly shifted to higher wavenumber for D1 gel polymer electrolyte and lower wavenumber for D2 gel polymer electrolyte. Due to the resolution used is 2 cm^{-1}, the hydroxyl band of D3 and D4 gel polymer electrolytes are not consider shifted as the O-H band without KI-TBAI salt (PVA-DMSO-EC-PC) is 3417 cm^{-1} (Figure 4.5 and Table 4.3)

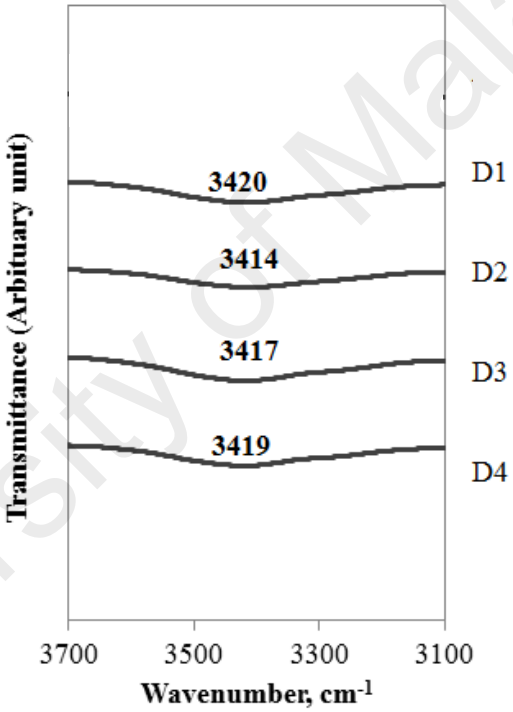

Figure 4.11: FTIR spectra for PVA-DMSO-EC-PC-KI-TBAI (3700 – 3100 cm^{-1})

Figure 4.12 shows the FTIR spectra for PVA-DMSO-EC-PC-KI-TBAI gel polymer electrolytes in the region of 1250 to 1150 cm^{-1} and 1850 to 1750 cm^{-1}. The band observed at this region was C-O-C and C=O respectively.

The peaks observed for PVA-DMSO-EC-PC-KI-TBAI have been listed in Table 4.6. It can be seen that C-O-C band of PVA-DMSO-EC-PC at 1161 cm^{-1} and 1177 cm^{-1} is shifted with the addition of KI-TBAI. The C=O band of PVA-DMSO-EC-PC at 1798

cm^{-1} was shifted to lower wavenumber when KI-TBAI is added. This indicates that there is interaction between PVA-DMSO-EC-PC and KI-TBAI at C-O-C and C=O bands.

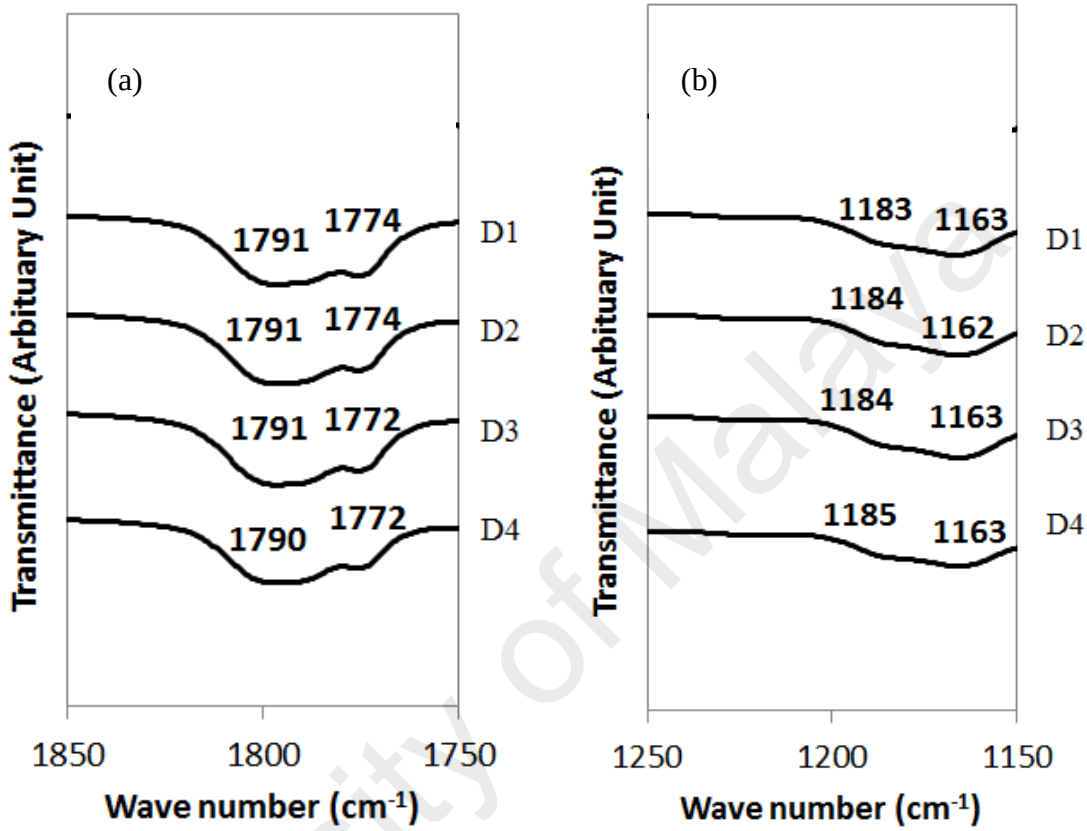

Figure 4.12: FTIR spectra for PVA-DMSO-EC-PC-KI-TBAI (a) (1850 – 1750 cm^{-1}) and (b) (1250 – 1150 cm^{-1})

Table 4.6: Bands for D1, D2, D3, D4 with their wavenumber

Wavenumber (cm^{-1})				
Assignment of bands	D1	D2	D3	D4
O-H	3420	3414	3417	3419
C=O	1773,1793	1774,1791	1772,1791	1792,1790
C-O-C	1163,1183	1162,1184	1163,1184	1163,1185

4.8. Interaction between PVA-DMSO-EC-PC-KI-TPAI with addition of DEC

Figure 4.13 shows the spectra for sample C2 gel polymer electrolyte with the addition of various amount of DEC in the region between 3700 to 3100 cm^{-1}. The peaks observed which is attributed to the hydroxyl band are listed in Table 4.7. It can be observed that the band was shifted to lower wavenumber with the addition of DEC.

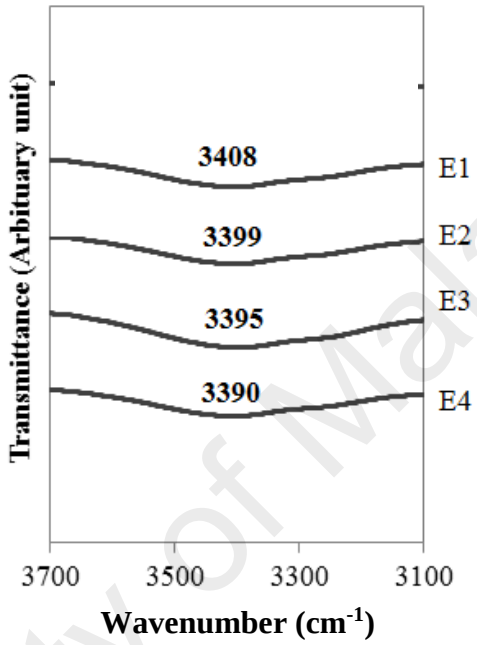

Figure 4.13: FTIR spectra for PVA-DMSO-EC-PC-KI-TPAI with variation of DEC (3700 – 3100 cm^{-1})

Figure 4.14 shows the FTIR spectra for PVA-DMSO-EC-PC-KI-TPAI-DEC gel polymer electrolytes in the region of 1250 – 1150 cm^{-1} and 1850 – 1750 cm^{-1}. The band observed at this region was C-O-C and C=O respectively.

The peaks observed for PVA-DMSO-EC-PC-KI-TPAI-DEC have been listed in Table 4.7. It can be seen that C-O-C band of PVA-DMSO-EC-PC-KI-TPAI at 1164 cm^{-1} and 1183 cm^{-1} was not changed with the addition of DEC. Similar observation can be obtained to C=O band where the band was remain unchanged when DEC is added. This indicates that there is no interaction occur between PVA-DMSO-EC-PC-KI-TPAI and DEC at C-O-C and C=O bands.

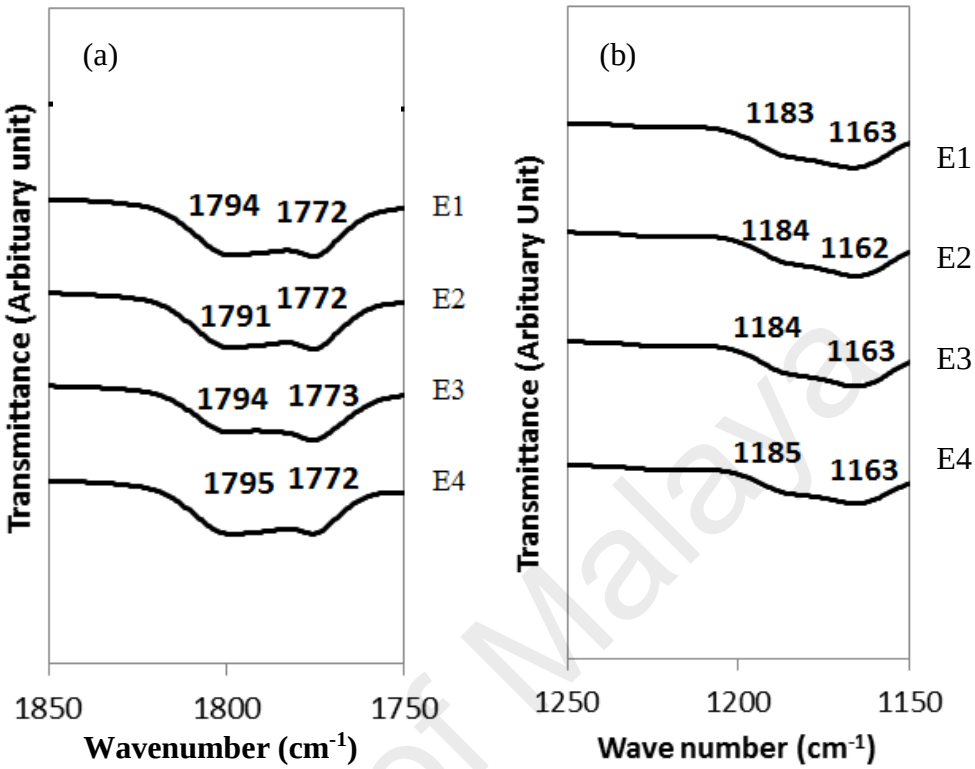

Figure 4.14: FTIR spectra for PVA-DMSO-EC-PC-KI-TPAI with variation of DEC (a) (1850 – 1750 cm^{-1}) and (b) (1250 – 1150 cm^{-1})

Table 4.7: Bands for E1, E2, E3, E4 with their wavenumber

Wavenumber (cm^{-1})				
Assignment of bands	E1	E2	E3	E4
O-H	3408	3399	3395	3390
C=O	1772,1794	1772,1791	1773,1794	1772,1795
C-O-C	1163,1183	1162,1184	1163,1184	1163,1185

4.9. Interaction between PVA-DMSO-EC-PC-KI-TBAI with addition of DEC

Figure 4.15 shows the spectra for sample D3 gel polymer electrolyte with the addition of various amount of DEC in region between 3700 to 3100 cm^{-1}. Similar to the C2 gel polymer electrolyte, the hydroxyl band of D3 gel polymer electrolyte was shifted to lower wavenumber with addition of DEC.

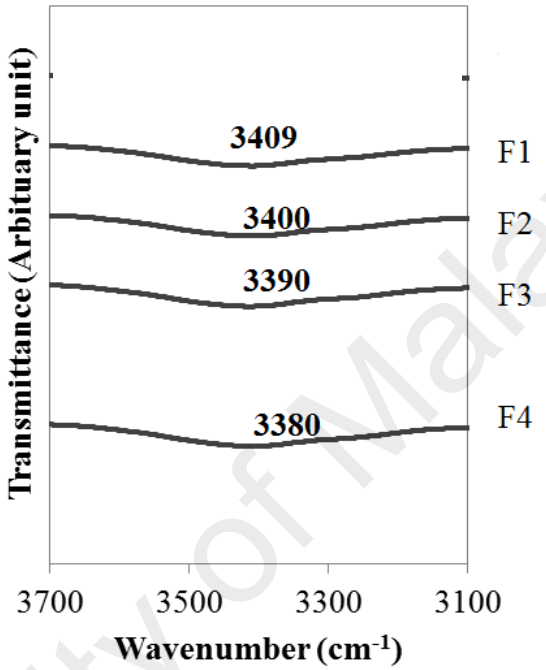

Figure 4.15: FTIR spectra for PVA-DMSO-EC-PC-KI-TBAI with variation of DEC (3700 – 3100 cm^{-1})

Figure 4.16 shows the FTIR spectra for PVA-DMSO-EC-PC-KI-TBAI-DEC gel polymer electrolytes in the region of 1250 – 1150 cm^{-1} and 1850 – 1750 cm^{-1}. The band observed at this region was C-O-C and C=O respectively.

The peaks observed for PVA-DMSO-EC-PC-KI-TBAI-DEC have been listed in Table 4.8. It can be seen that C-O-C band of PVA-DMSO-EC-PC-KI-TBAI has not shift with the additive of DEC. The C=O band of PVA-DMSO-EC-PC-KI-TBAI at 1791 cm^{-1} was shifted to higher wavenumber when DEC is added. This indicates that there is an interaction between PVA-DMSO-EC-PC-KI-TBAI and DEC at C-O-C and C=O bands.

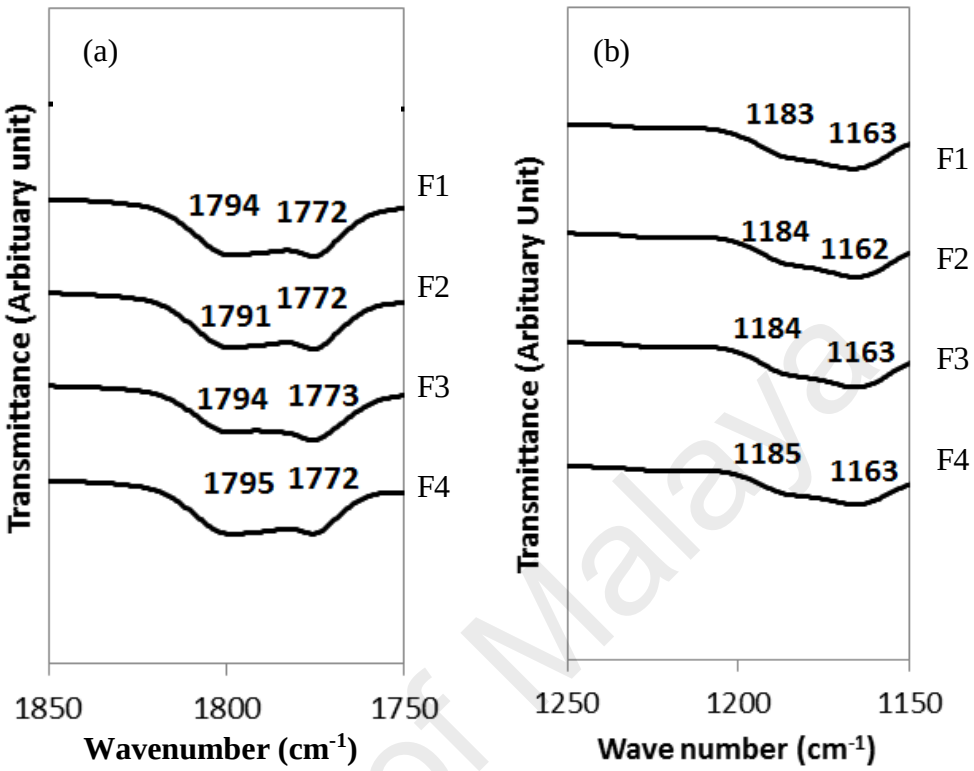

Figure 4.16: FTIR spectra for PVA-DMSO-EC-PC-KI-TBAI with variation of DEC (a) (1850 – 1750 cm^{-1}) and (b) (1250 – 1150 cm^{-1})

Table 4.8: Bands for F1, F2, F3, F4 with their wavenumber

Assignment of bands	F1	F2	F3	F4
O-H	3409	3400	3390	3380
C=O	1772,1794	1772,1791	1773,1794	1772,1795
C-O-C	1163,1183	1162,1184	1163,1184	1163,1185

4.10. Interaction between solvent (DMSO) with salts (KI, TMAI, TPAI and TBAI)

Figure 4.17 shows the FTIR spectra for the DMSO, DMSO-KI, DMSO-TMAI, DMSO-TPAI, and DMSO-TBAI in region between 1040 to 1000 cm $^{-1}$. The S=O band peak of DMSO was observed at 1026 cm^{-1}. The peak was shifted to lower wave number indicates that the interaction between salts and DMSO occurred at S=O band.

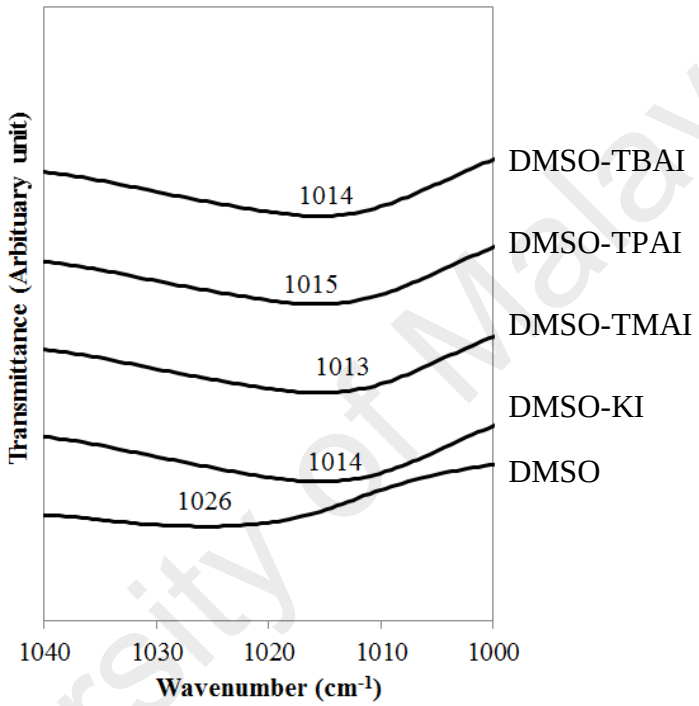

Figure 4.17: FTIR spectra for DMSO and KI, TMAI, TPAI and TBAI salts (1040 – 1000 cm^{-1})

4.11. Summary

In this chapter, the interaction between PVA-DMSO-EC-PC with the KI, TMAI, TPAI, TBAI and DEC have been analysed using FTIR spectroscopy. The shifted peaks indicates that the interaction is occurred.

CHAPTER 5: X-RAY DIFFRACTION (XRD) ANALYSIS

5.1. Introduction

X-ray diffraction is a useful tool to determine the structural phase by observing the appearance and disappearance of crystalline or amorphous region. From this study, the nature of the different gel polymer electrolytes composition can be described in more details.

In this chapter, XRD results will be presented. XRD patterns for each gel polymer electrolyte in the PVA-EC-PC-DMSO-KI, PVA-EC-PC-DMSO-KI-TMAI, PVA-EC-PC-DMSO-KI-TPAI, PVA-EC-PC-DMSO-KI-TBAI and PVA-EC-PC-DMSO-KI-TPAI-DEC and PVA-EC-PC-DMSO-KI-TBAI-DEC systems have been obtained. Each XRD pattern has been analyzed using the Origin 8 software.

5.2. PVA-EC-PC-DMSO-KI system

Figure 5.1 shows the XRD pattern for polyvinyl alcohol (PVA) powder. Obviously there are some sharp peaks located at 2θ = 5.45°, 10.90°, 19.60° and 40.25°. This indicates that the PVA powder is semicrystalline in nature.

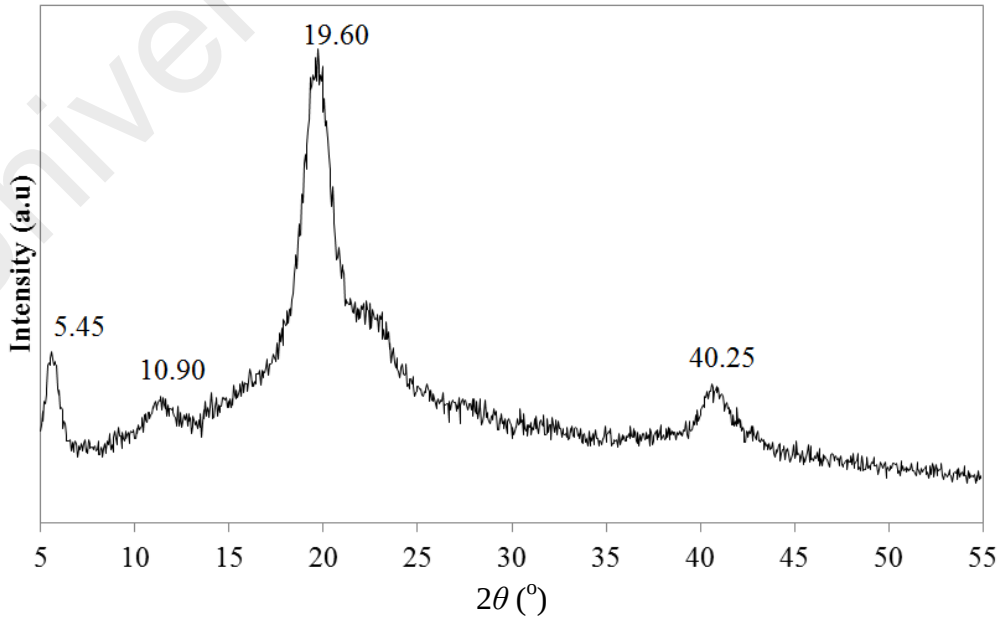

Figure 5.1: XRD pattern for polyvinyl alcohol (PVA) powder

The XRD patterns of PVA-EC-PC-DMSO-KI gel polymer electrolytes with different amounts of KI salts have been shown in Figure 5.2. All XRD patterns of the gel polymer electrolytes show a broad peak at $2\theta = 20^{o}$ which indicates that the gel polymer electrolytes are amorphous. The peak position agrees well with the peak located at $2\theta = 20^{o}$ for pure PVA which has also been reported by Krumova *et al*. (2000). The FWHM values of the XRD patterns for PVA-EC-PC-DMSO-KI gel polymer electrolytes have been obtained and shown in Figure 5.3 and Table 5.1. It can be observed that the value of FWHM increases slightly starting from 0.19 rad (A1) up to 0.22 rad (A5, A6 and A7). The increase of FWHM value indicates that the gel polymer electrolytes have become more amorphous. The value is slightly decreased to 0.21 rad for samples A8 and A9.

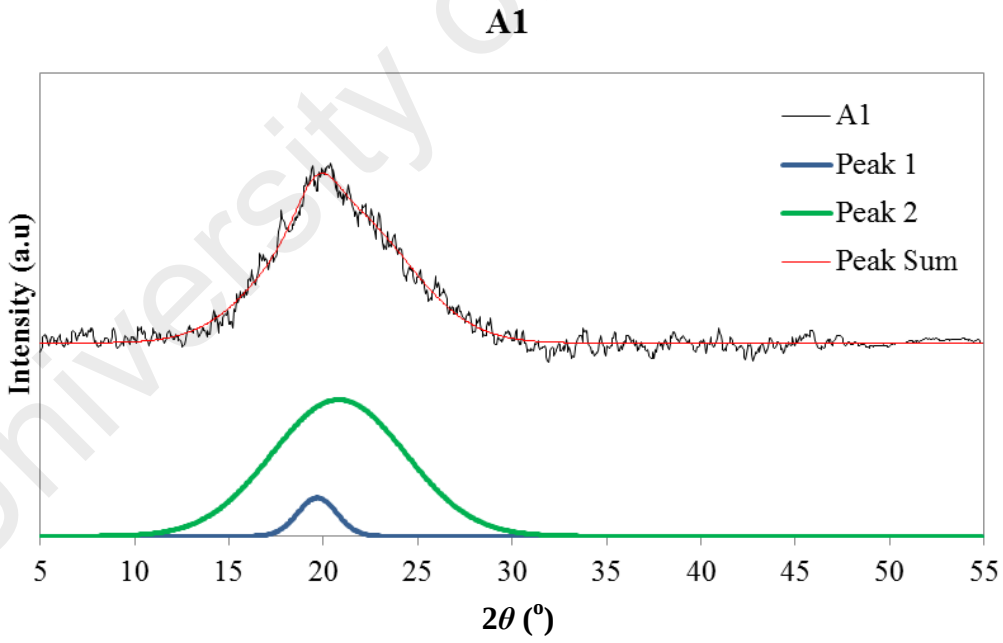

Figure 5.2: All XRD curves with fitted lines for PVA-EC-PC-DMSO-KI gel polymer electrolytes

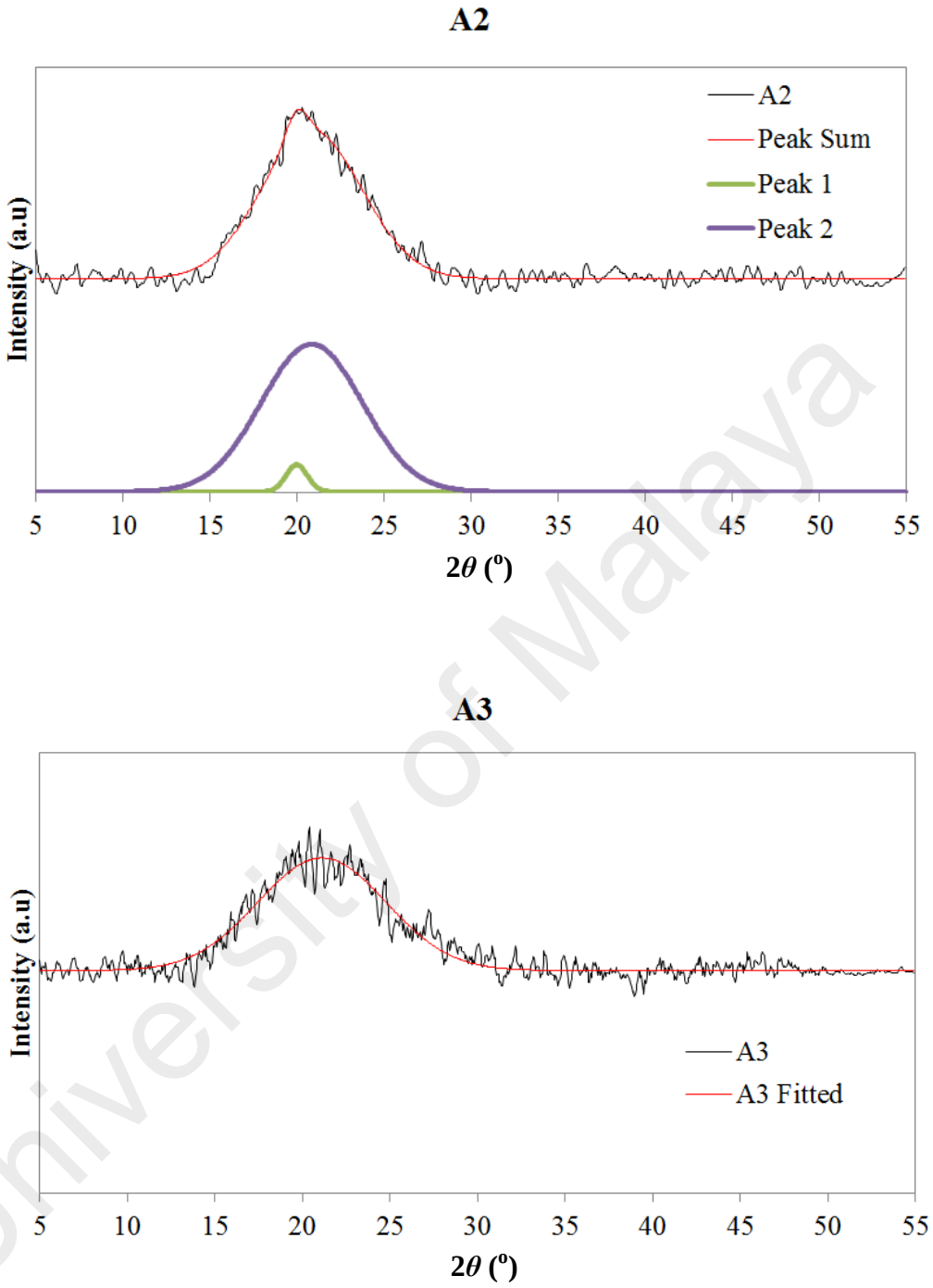

Figure 5.2, continued.

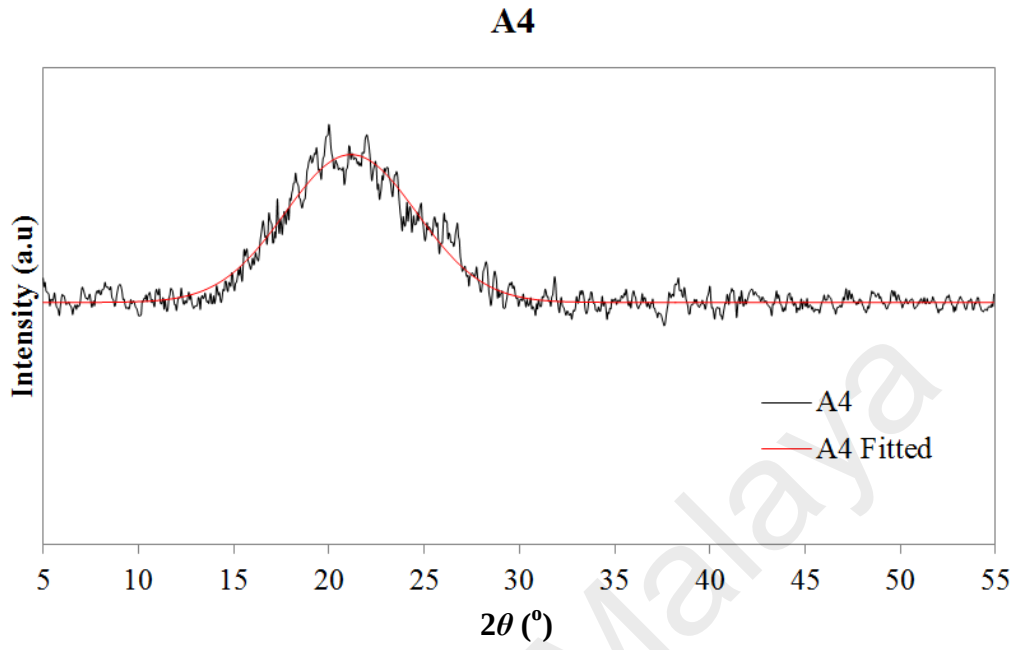

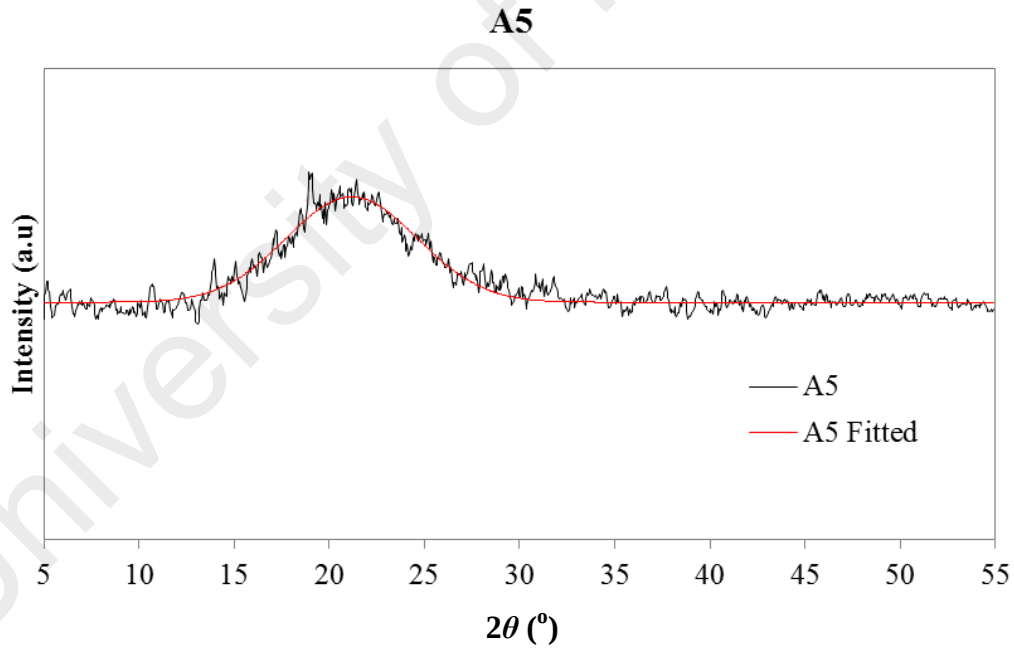

Figure 5.2, continued.

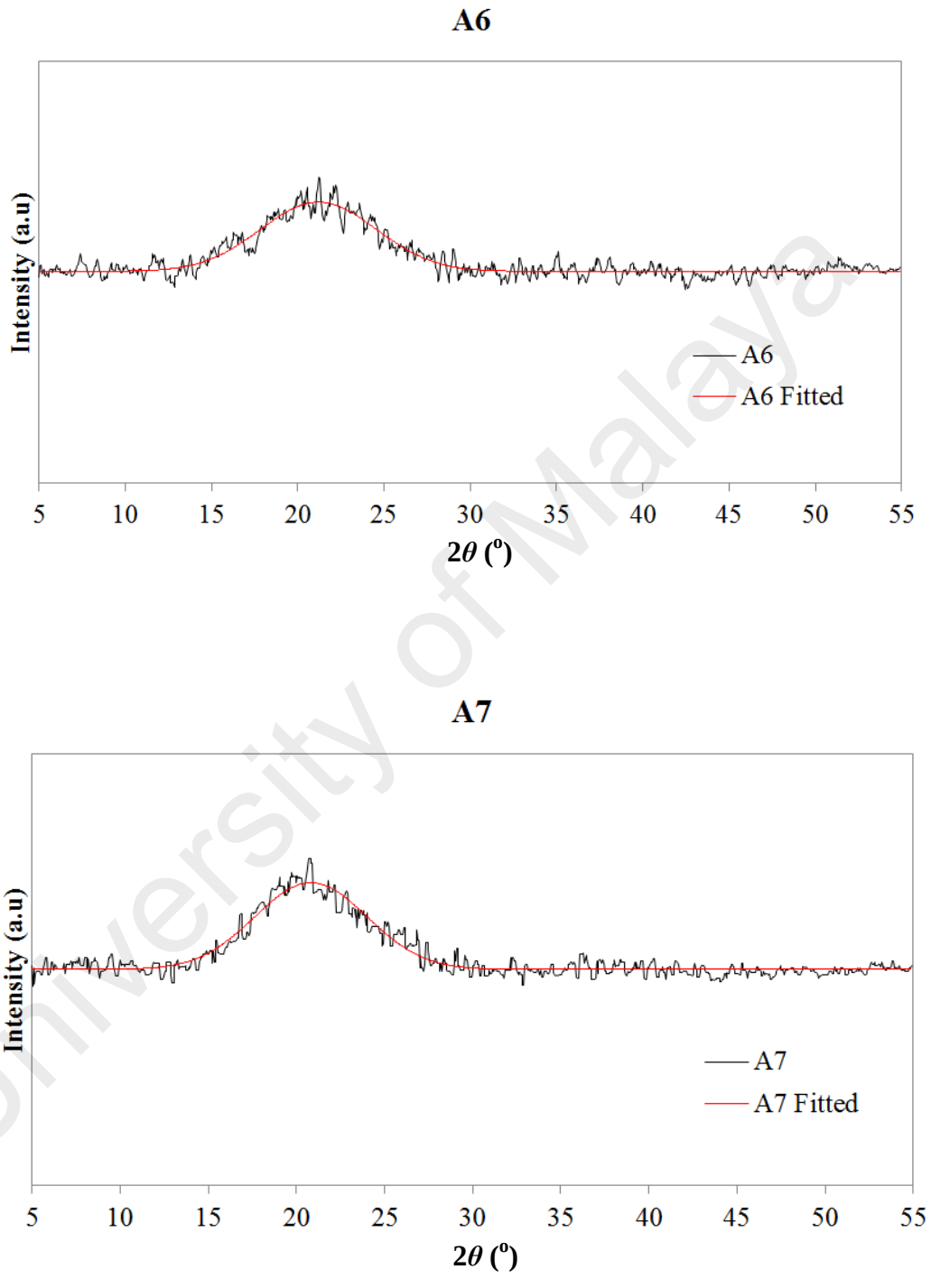

Figure 5.2, continued.

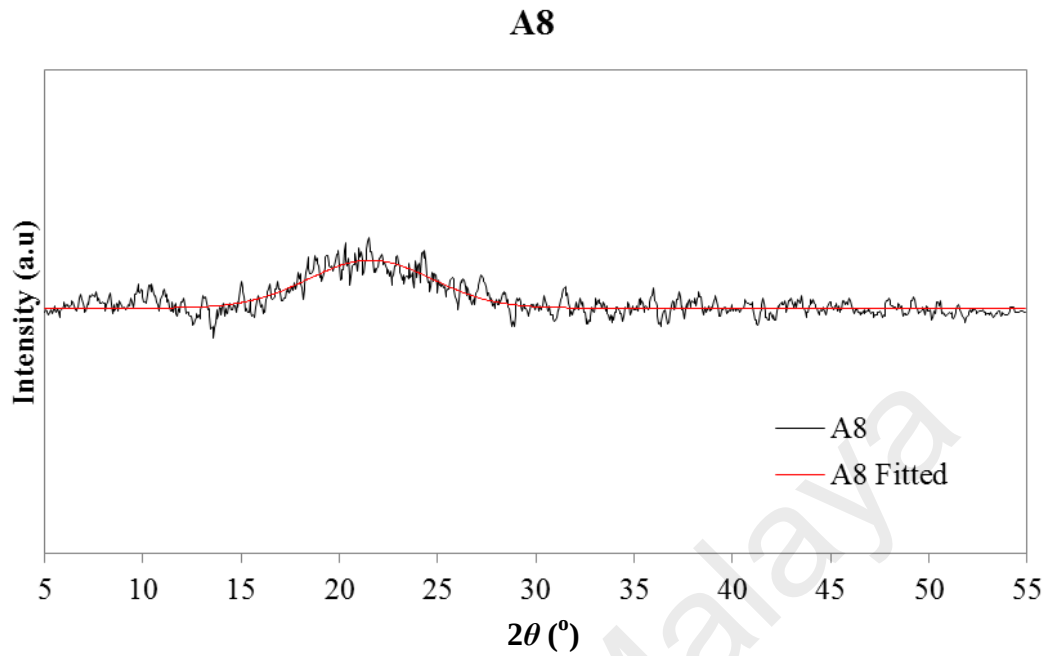

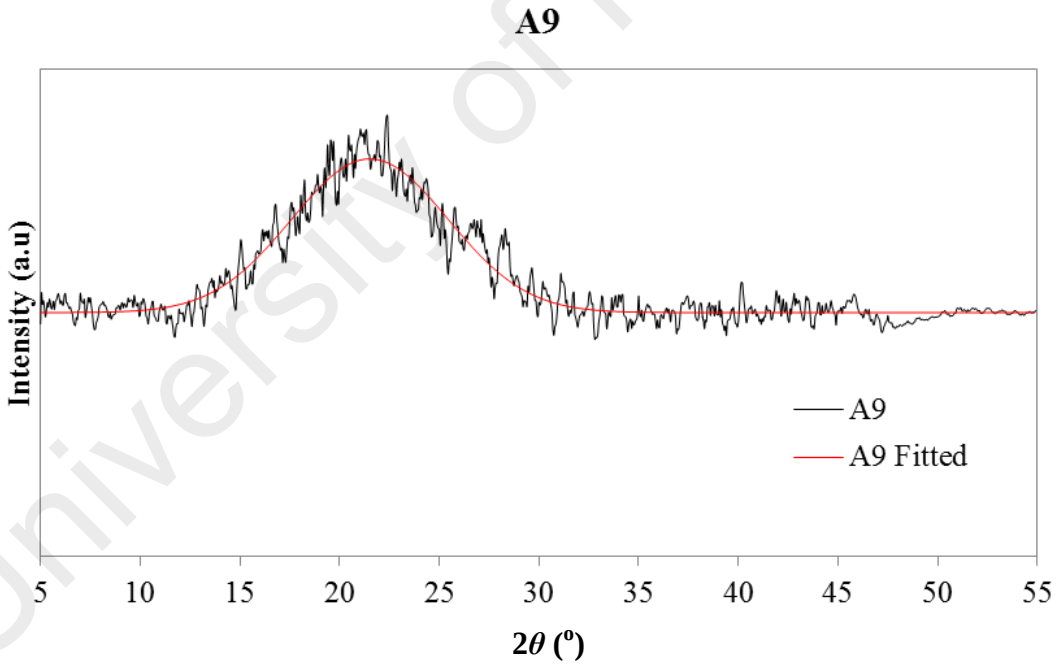

Figure 5.2, continued.

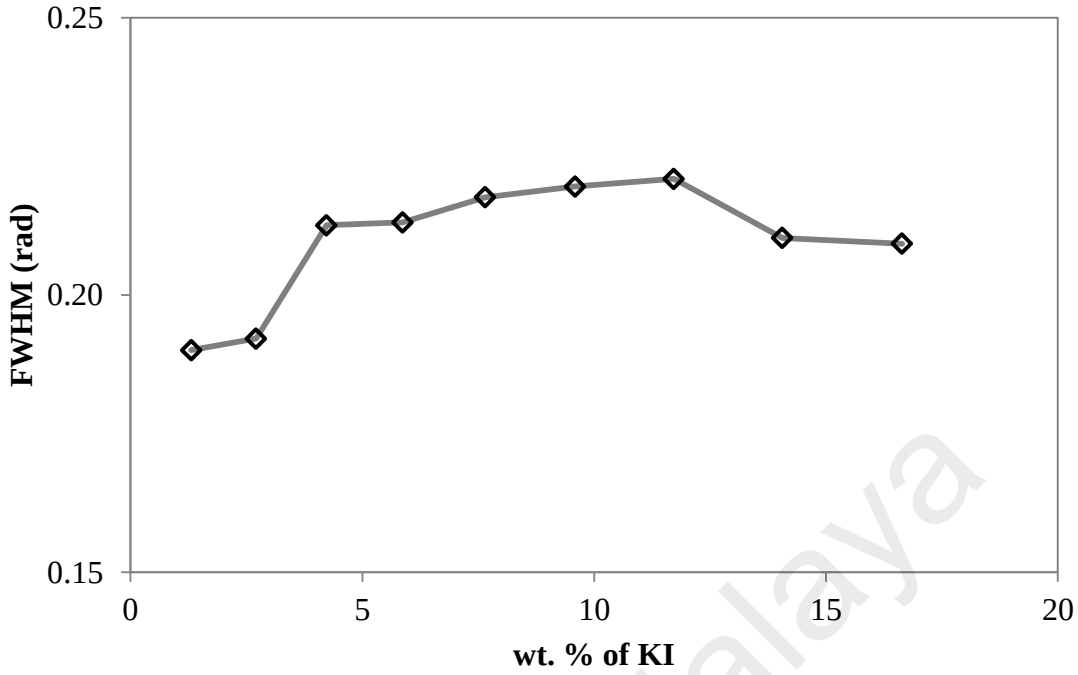

Figure 5.3: FWHM for each gel polymer electrolytes with different amount of KI salt

Table 5.1: 2θ and FWHM for gel polymer electrolytes contain different amount of KI salt

Electrolyte	2θ (^{o})	FWHM (rad)
A1	21.47	0.19
A2	21.73	0.19
A3	21.56	0.21
A4	21.61	0.21
A5	21.22	0.22
A6	21.93	0.22
A7	21.23	0.22
A8	21.67	0.21
A9	22.34	0.21

5.3. PVA-EC-PC-DMSO-KI-*x*-I_2 (*x* = TMAI, TPAI, TBAI) system

5.3.1. PVA-EC-PC-DMSO-KI-TMAI system

XRD pattern for tetramethyl ammonium iodide salt has been shown in Figure 5.4. There are some sharp peaks shown in this XRD pattern such as at 15.45°, 19.20°, 22.45°, 29.30°, 32.95°, 35.80°, 39.45°, 45.85° and 50.10°. These sharp peaks indicate that the TMAI salt is crystalline in nature.

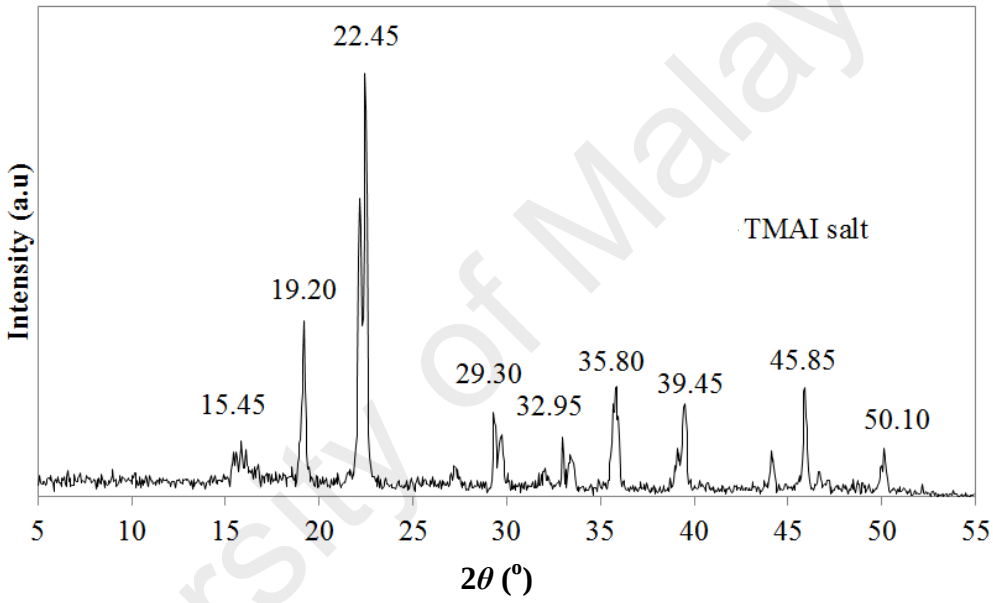

Figure 5.4: XRD pattern for tetrametyhl ammonium iodide (TMAI) salt

Figure 5.5 shows the XRD patterns of PVA-EC-PC-DMSO-KI-TMAI gel polymer electrolytes with various amounts of KI and TMAI salts. It can be observed that the B1, B2, B3 and B4 gel polymer electrolytes exhibits a sharp peak with highest intensity at $2\theta \sim 22^{o}$. This obvious sharp peak appears in the XRD pattern due to the TMAI salt which has not dissolve well in the gel polymer electrolyte. The other crystalline peaks that observed in the XRD patterns of B1, B2, B3 and B4 also belong to the TMAI salt.

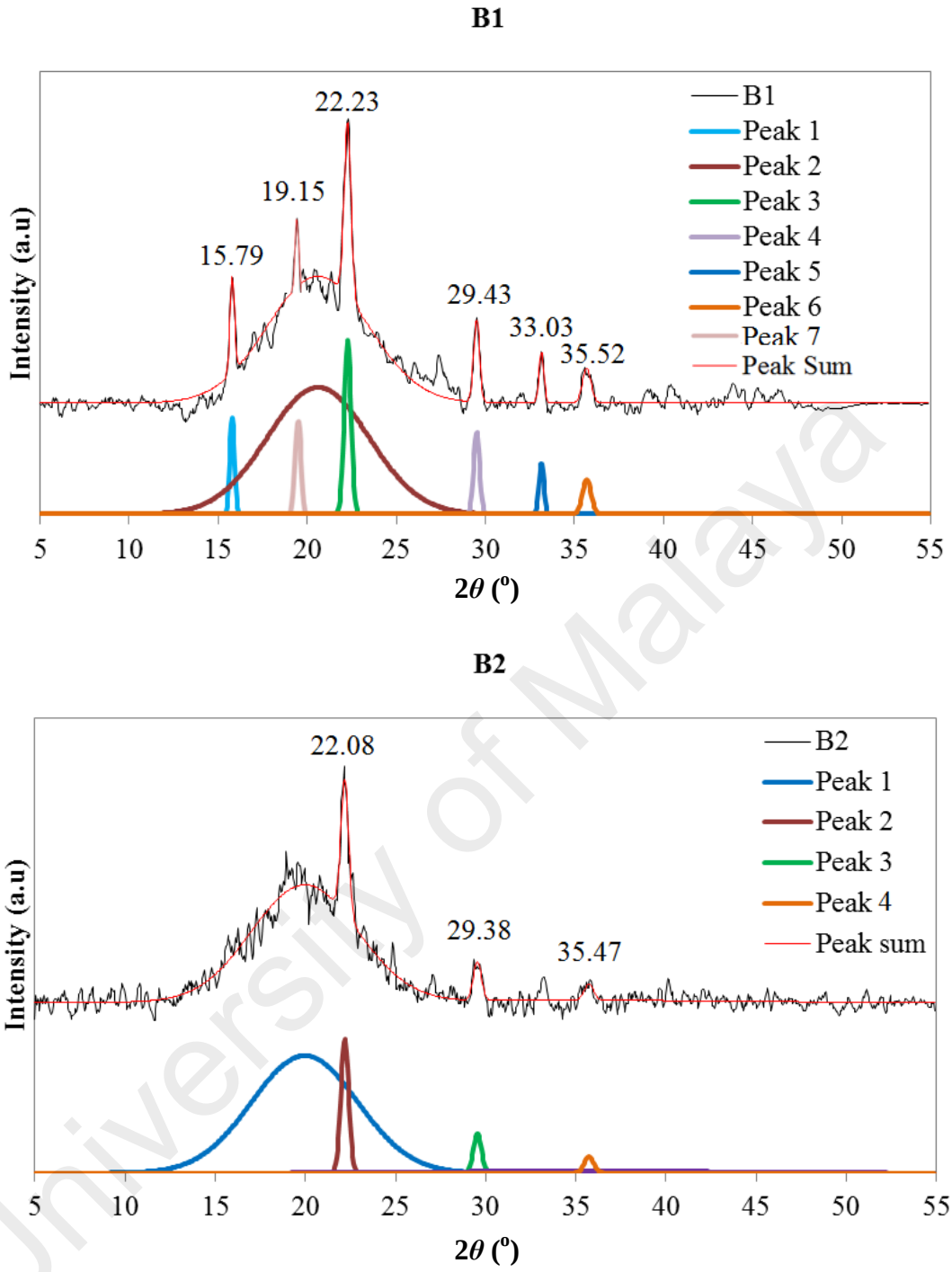

Figure 5.5: All XRD curves with fitted lines for PVA-EC-PC-DMSO-KI-TMAI gel polymer electrolytes

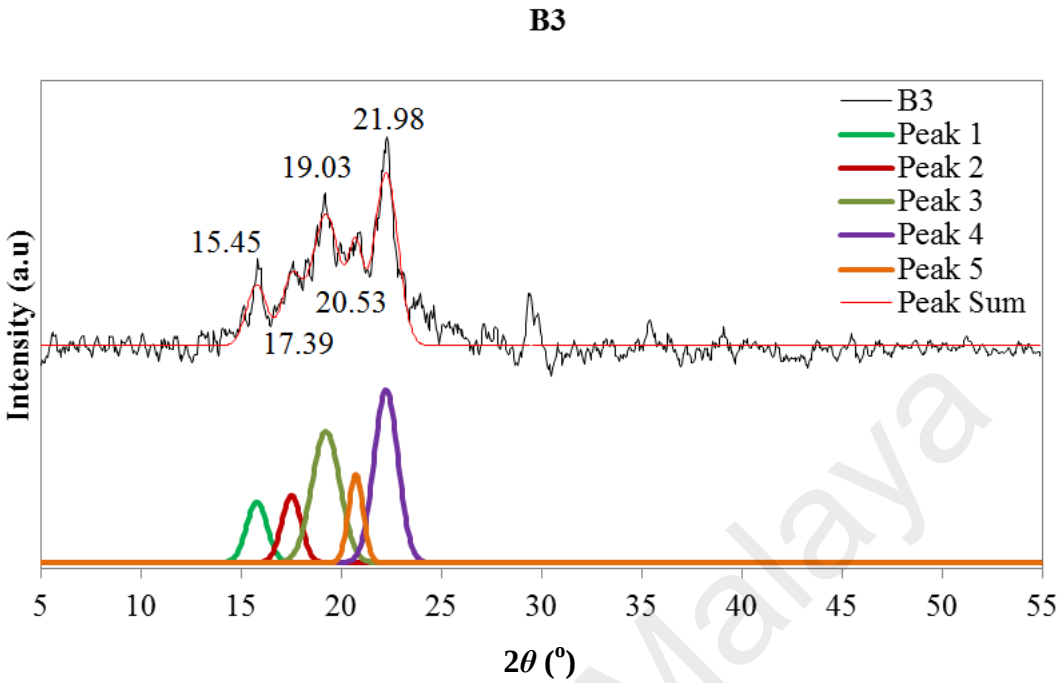

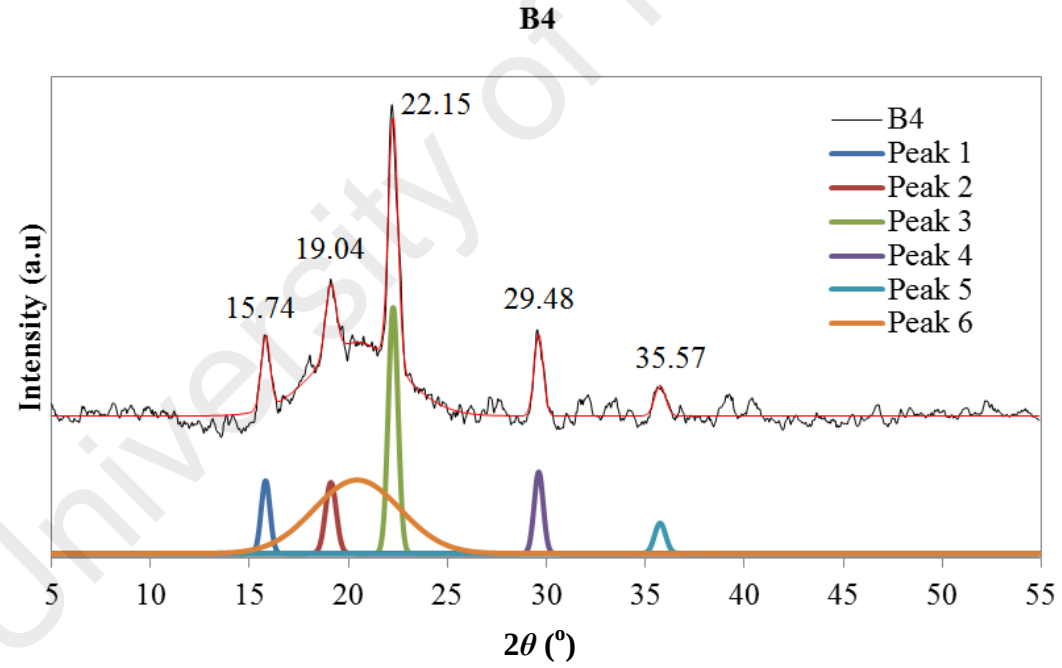

Figure 5.5, continued.

Figure 5.6 shows the degree of crystallinity χ (%) *vs* wt. % of KI-TMAI for PVA-EC-PC-DMSO-KI-TMAI gel polymer electrolytes. The degree of crystallinity χ (%) calculated using equation 3.15 show an increase trend with decreasing of KI salt and increasing of TMAI salt.

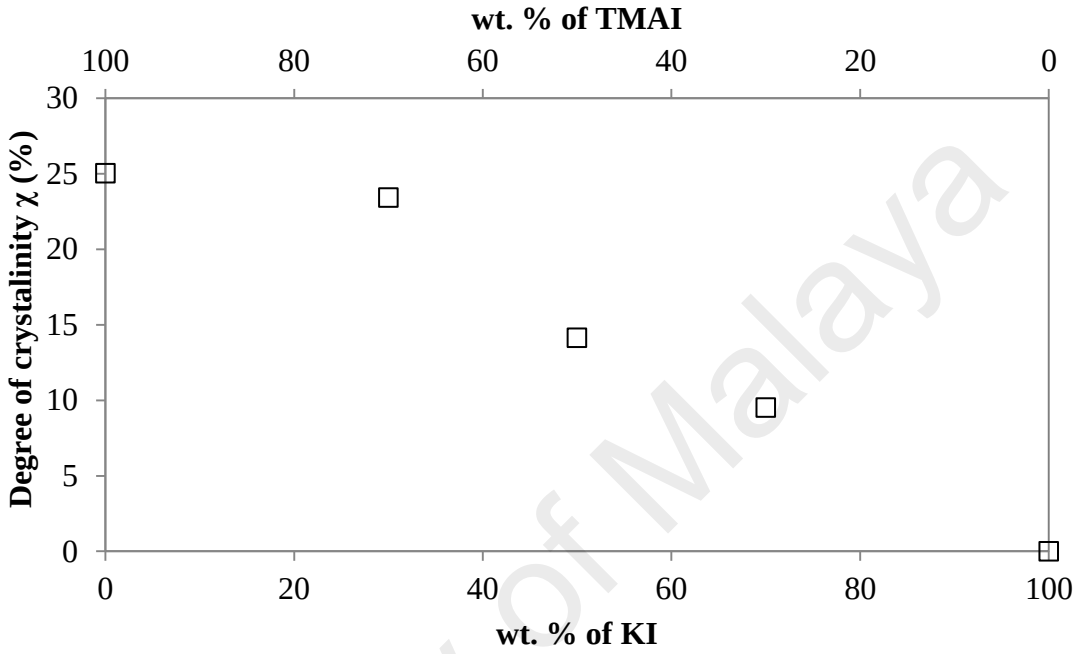

Figure 5.6: Degree of crystallinity χ (%) vs wt. % of KI-TMAI

5.3.2. PVA-EC-PC-DMSO-KI-TPAI system

Figure 5.7 shows the XRD pattern for tetrapropyl ammonium iodide salt. There are some sharp peaks are shown in this XRD pattern such as at 10.05^{o}, 12.20^{o}, 19.25^{o}, 22.75^{o}, 25.30^{o}, 27.80^{o}, 32.45^{o} and 37.65^{o}. These sharp peaks indicate that this TPAI salt is crystalline.

Figure 5.8 shows the XRD patterns of PVA-EC-PC-DMSO-KI-TPAI gel polymer electrolytes with different amounts of KI and TPAI salts. Amorphous nature has been observed in all these gel polymer electrolytes.

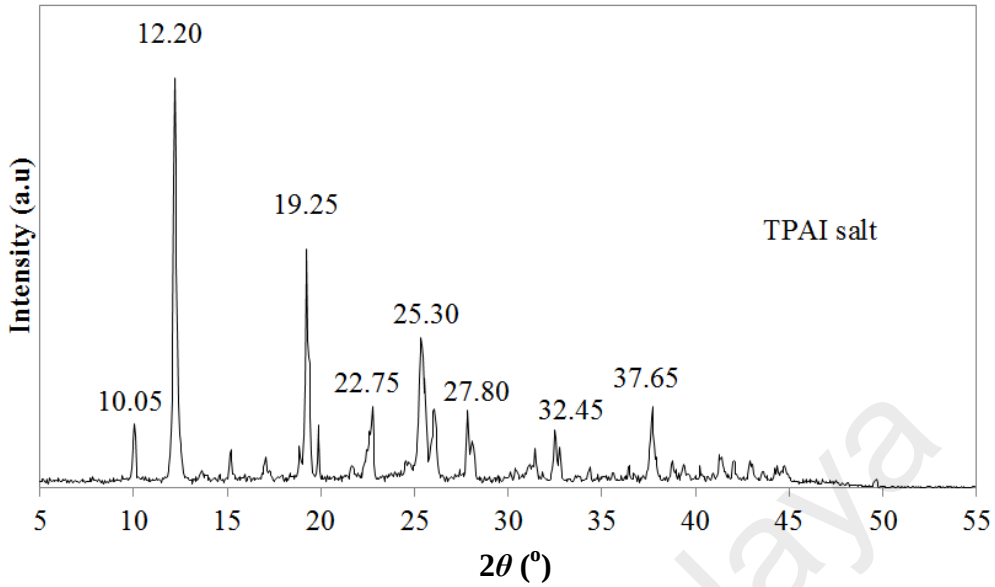

Figure 5.7: XRD pattern for tetrapropyl ammonium iodide (TPAI) salt

From Figure 5.8, it can be observed that the amorphous peak appears at $2\theta \sim 20^{o}$. The absence of TPAI crystalline peaks shows that the TPAI salt has been dissolved completely in the gel polymer electrolytes. All the XRD curves also show the fitted red line which implies close agreement to the XRD curves. The FWHM values of the PVA-EC-PC-DMSO-KI-TPAI gel polymer electrolytes have been obtained and shown in Figure 5.9 and Table 5.2. It can be observed that the FWHM value has slightly decreased with increasing TPAI concentration. This indicates that the gel polymer electrolyte becomes less amorphous in higher TPAI content.

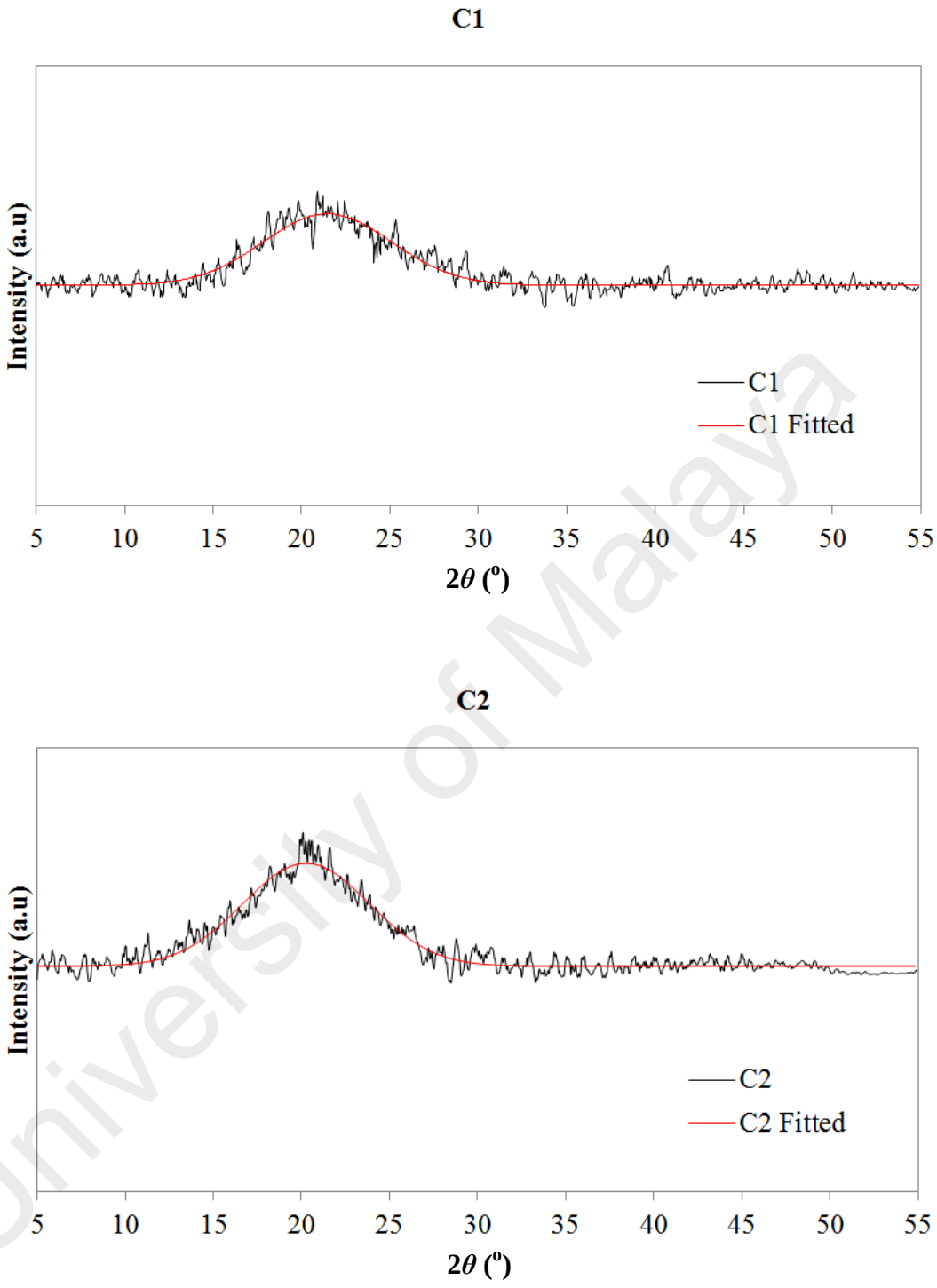

Figure 5.8: All XRD curves with fitted lines for PVA-EC-PC-DMSO-KI-TPAI gel polymer electrolytes

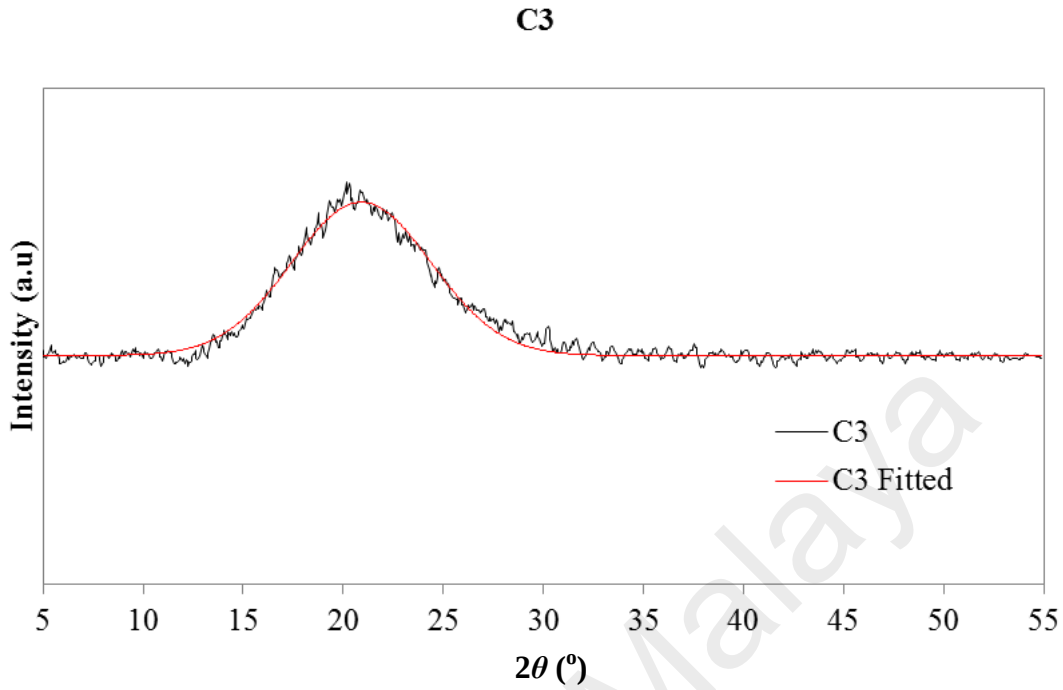

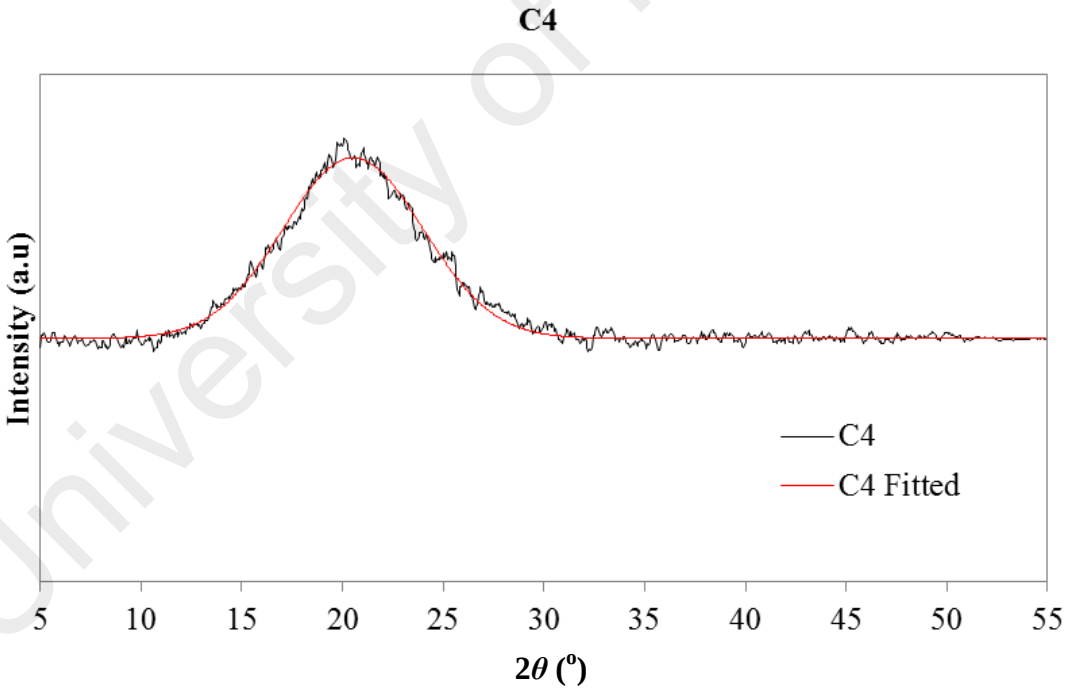

Figure 5.8, continued.

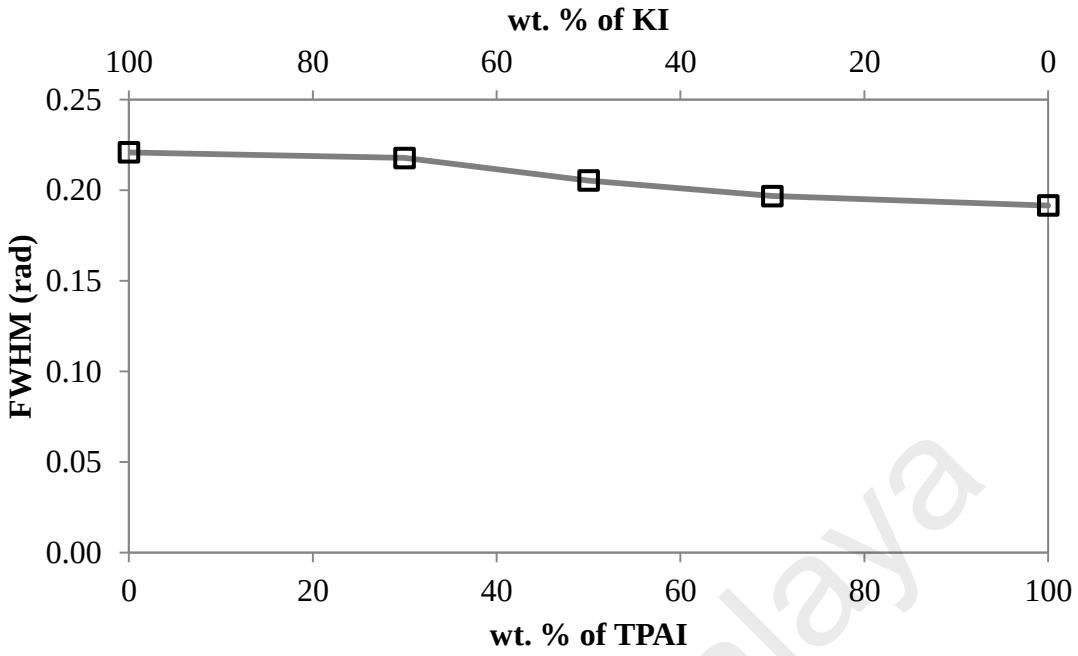

Figure 5.9: FWHM for each gel polymer electrolytes with different amount of KI-TPAI salts

Table 5.2: 2θ and FWHM for gel polymer electrolytes contain different amount of KI-TPAI salt

Electrolyte	**2θ (^{o})**	**FWHM (rad)**
A7	21.23	0.22
C1	21.42	0.22
C2	20.36	0.21
C3	21.17	0.20
C4	20.79	0.19

5.3.3. PVA-EC-PC-DMSO-KI-TBAI system

Figure 5.10 shows the XRD pattern for tetrabutyl ammonium iodide salt. There are some sharp peaks shown in this XRD pattern such as at 9.40°, 18.05°, 20.60°, 22.60°, 24.70°, 27.60°, 31.35° and 40.30°. These sharp peaks indicate that the TBAI salt is crystalline.

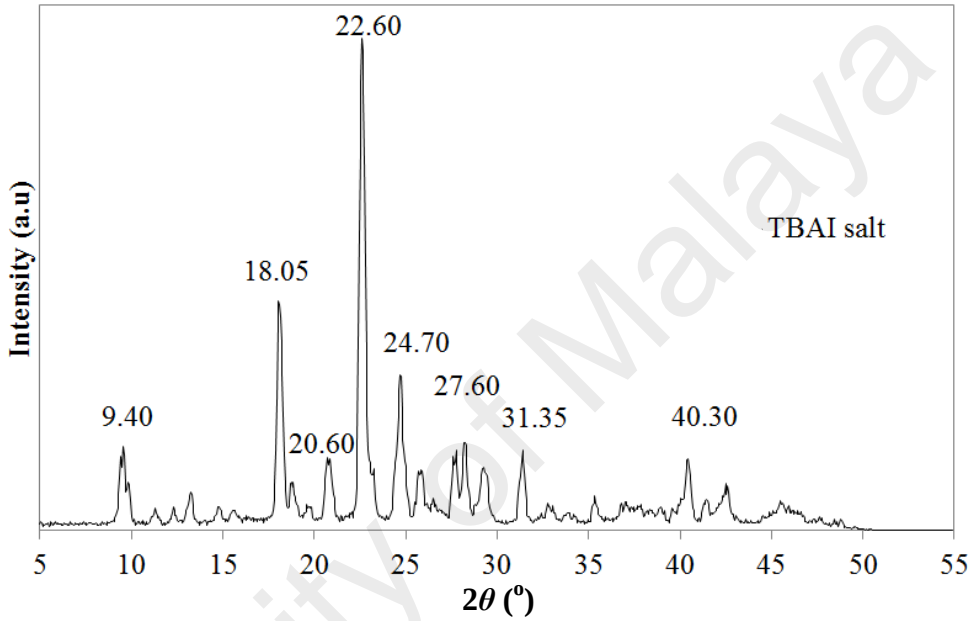

Figure 5.10: XRD pattern for tetrabutyl ammonium iodide (TBAI) salt

Figure 5.11 shows the XRD patterns of PVA-EC-PC-DMSO-KI-TBAI gel polymer electrolytes with various amounts of KI and TBAI salts. The broad peaks indicate that the amorphous nature of gel polymer electrolytes. The amorphous peak for each gel polymer electrolyte contains KI and TBAI salts observed at $2\theta \sim 20^{o}$. The FWHM value of the PVA-EC-PC-DMSO-KI-TBAI gel polymer electrolytes has been obtained and shown in Figure 5.12 and Table 5.3. It can be observed that the FWHM value is slightly decreasing with the increase of TBAI concentration which indicates that the gel polymer electrolytes becomes less amorphous.

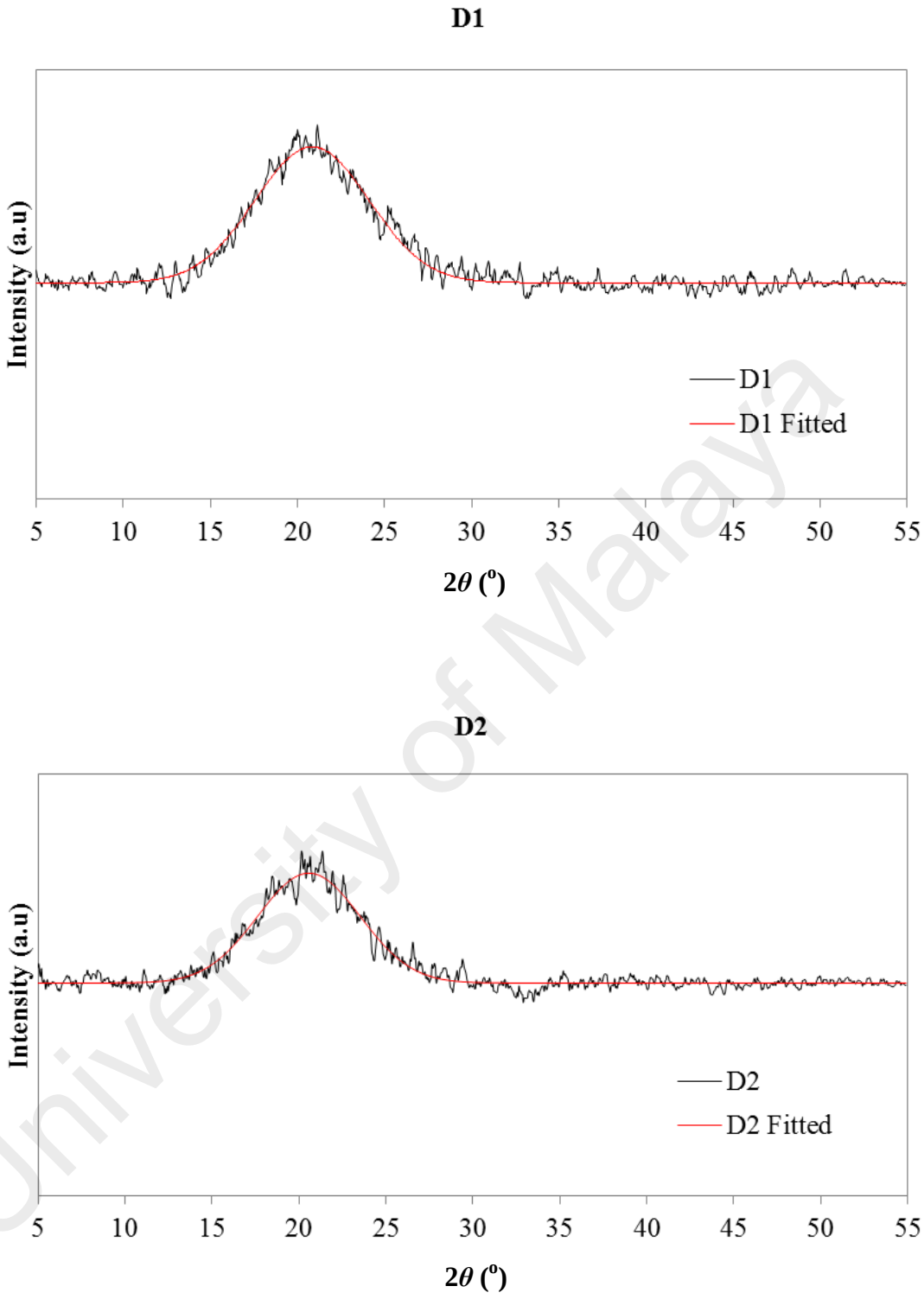

Figure 5.11: All XRD curves with fitted lines for PVA-EC-PC-DMSO-KI-TBAI gel polymer electrolytes

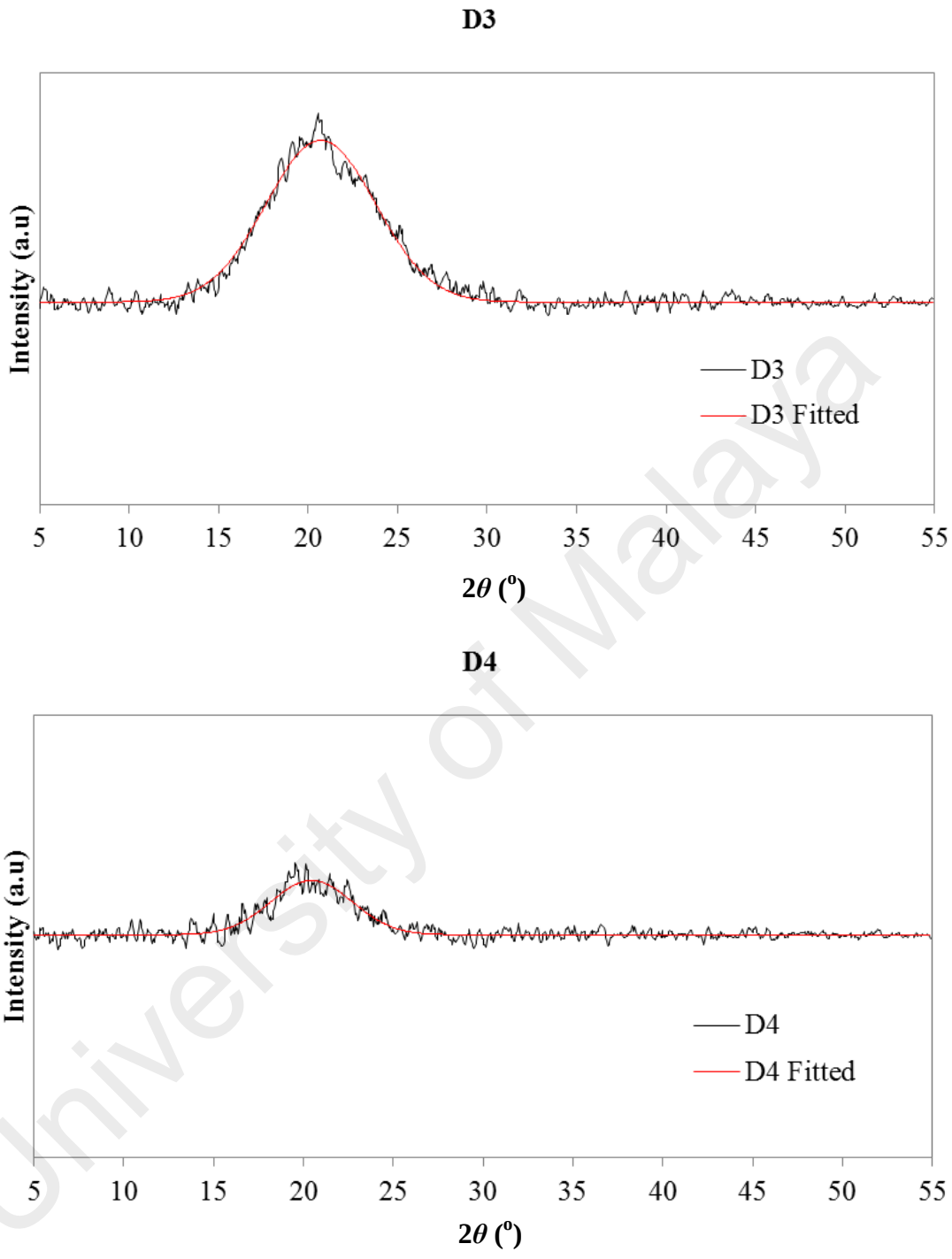

Figure 5.11, continued.

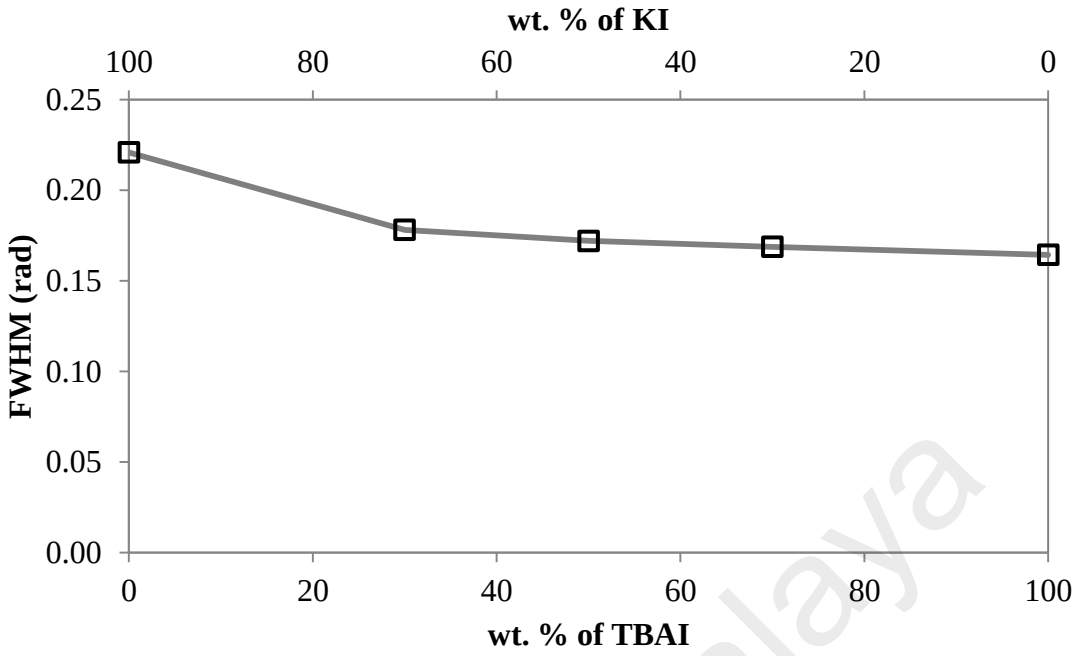

Figure 5.12: FWHM for each gel polymer electrolytes with different amount of KI-TBAI salts

Table 5.3: 2θ and FWHM for gel polymer electrolytes contain different amount of KI-TBAI salt

Electrolyte	**2θ (^{o})**	**FWHM (rad)**
A7	21.23	0.22
D1	20.94	0.18
D2	20.80	0.17
D3	20.90	0.17
D4	20.25	0.16

5.4. Plasticizer system

5.4.1. PVA-EC-PC-DMSO-KI-TPAI-DEC system

Figure 5.13 shows the XRD patterns of PVA-EC-PC-DMSO-KI-TPAI-DEC gel polymer electrolytes with various amount of DEC. All the XRD patterns exhibits a broad peak indicates that the gel polymer electrolytes are amorphous. The amorphous peak for each gel electrolytes was observed at $2\theta \sim 20^{o}$. The FWHM values of the PVA-EC-PC-DMSO-KI-TPAI-DEC gel polymer electrolytes have been obtained and shown in Figure 5.14 and Table 5.4. It can be observed the FWHM value increases with the DEC content which indicates that the gel polymer electrolytes becoming more amorphous.

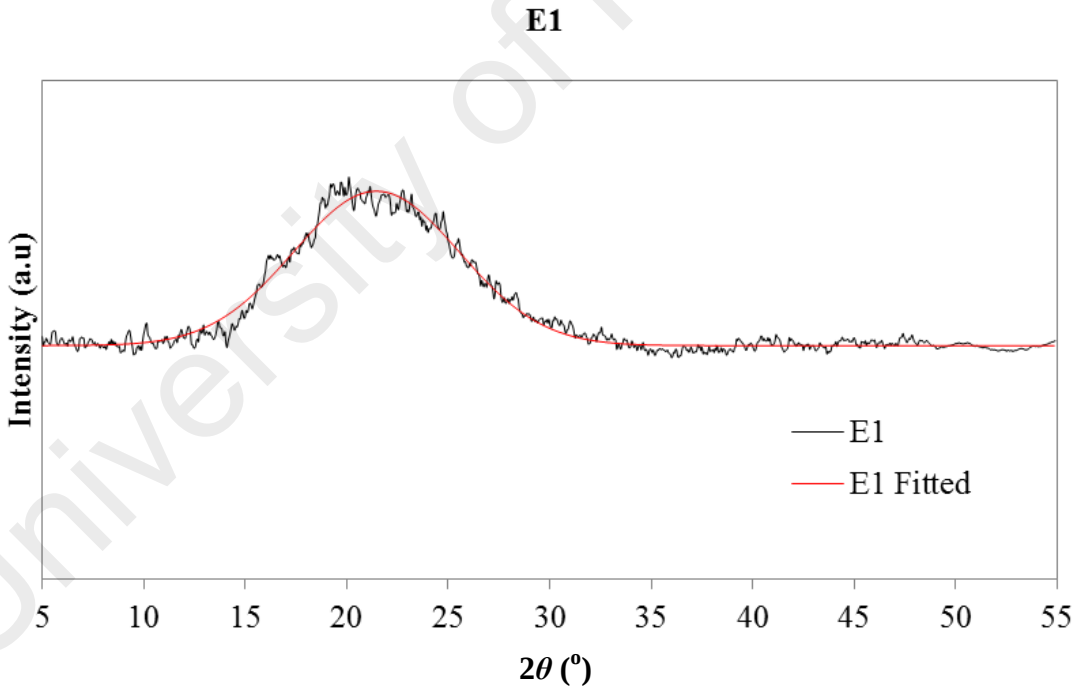

Figure 5.13: All XRD curves with fitted lines for PVA-EC-PC-DMSO-KI-TPAI-DEC gel polymer electrolytes

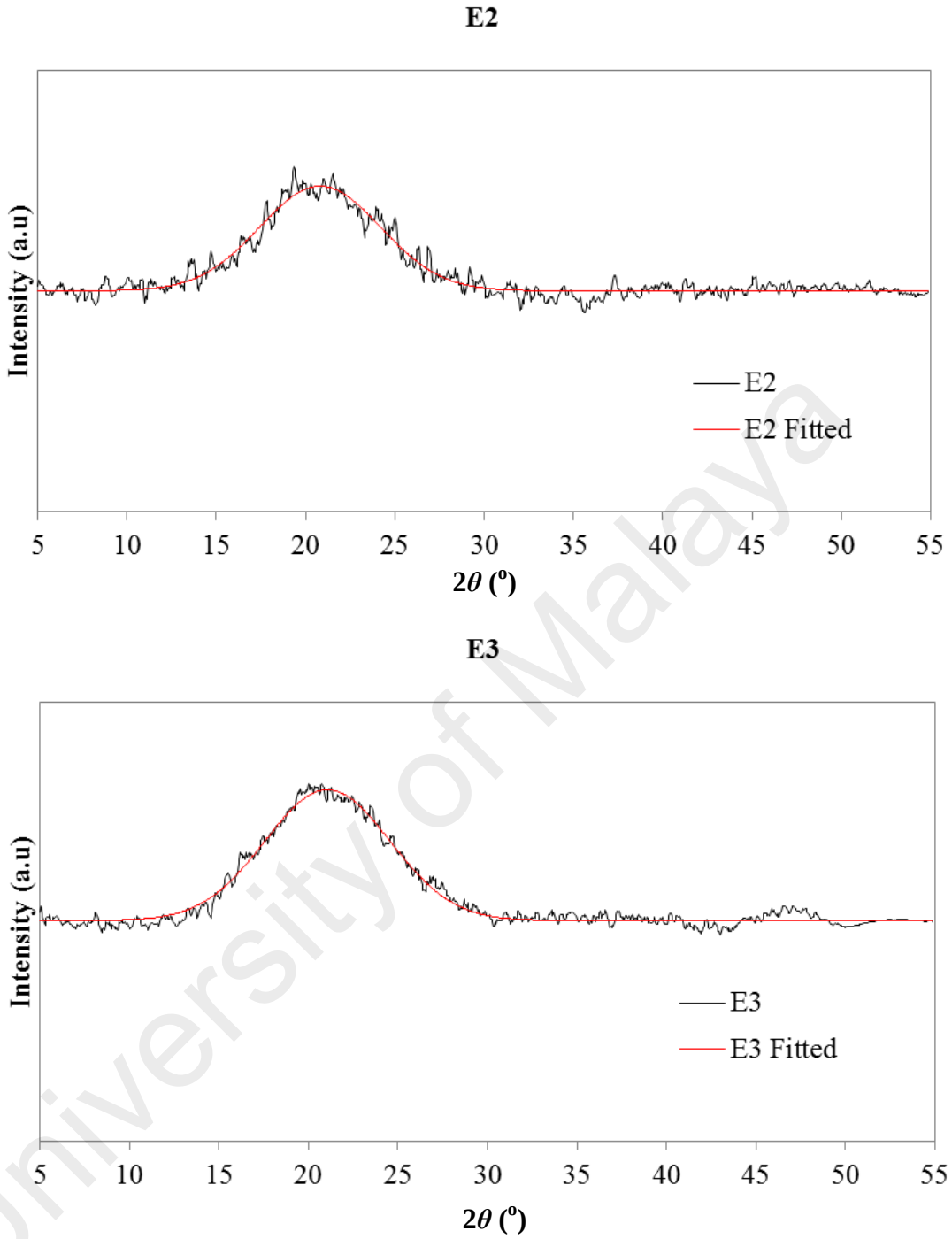

Figure 5.13, continued.

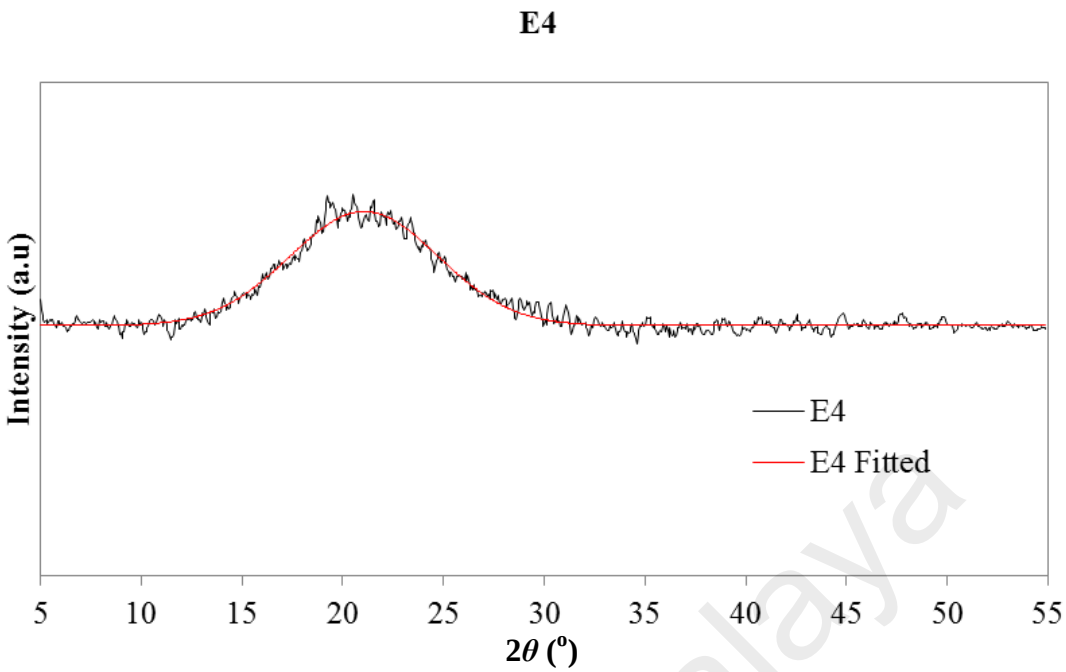

Figure 5.13, continued.

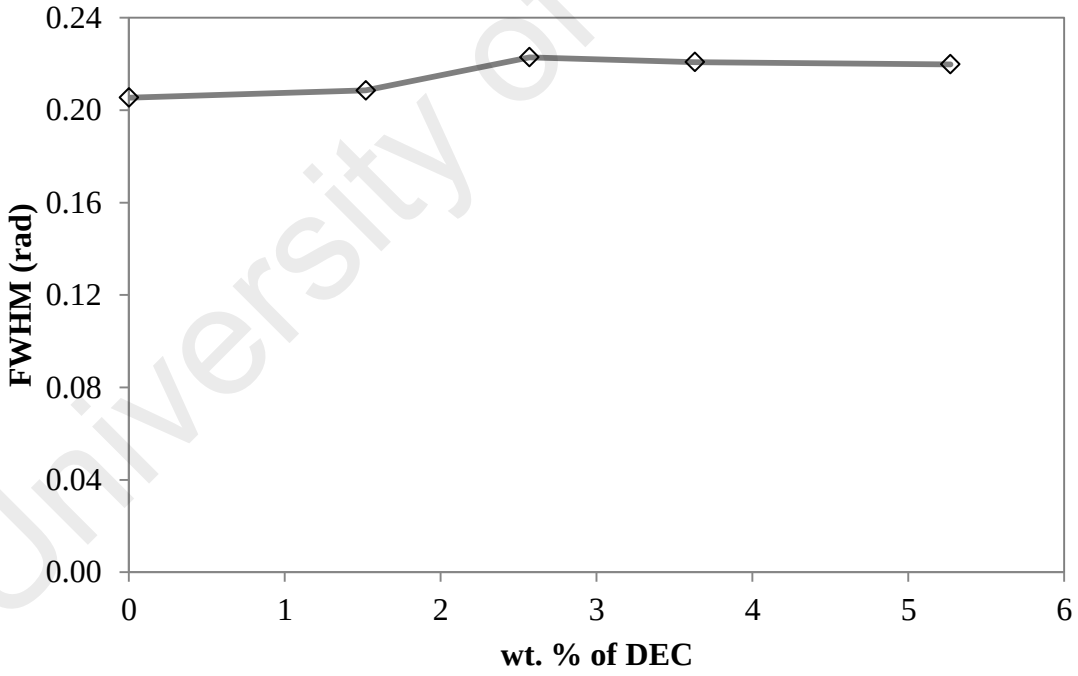

Figure 5.14: FWHM for each PVA-DMSO-EC-PC-KI-TPAI gel polymer electrolytes with variation of DEC

Table 5.4: 2θ and FWHM for PVA-DMSO-EC-PC-KI-TPAI gel electrolytes contain different amount of DEC

Electrolyte	2θ (^{o})	FWHM (rad)
C2	20.36	0.21
E1	21.60	0.21
E2	20.95	0.22
E3	21.61	0.22
E4	21.21	0.22

5.4.2. PVA-EC-PC-DMSO-KI-TBAI-DEC system

Figure 5.15 shows the XRD patterns of PVA-EC-PC-DMSO-KI-TBAI-DEC gel polymer electrolytes with various amount of DEC. All XRD peaks exhibits a broad peak at $2\theta \sim 20^o$ indicates that the gel polymer electrolytes are amorphous. The FWHM value of the PVA-EC-PC-DMSO-KI-TBAI-DEC gel polymer electrolytes has been obtained and shown in Figure 5.16 and Table 5.5. It can be observed that the amorphous nature of gel polymer electrolytes remain unchanged with the amount of DEC. This can be known from the similar value of FWHM.

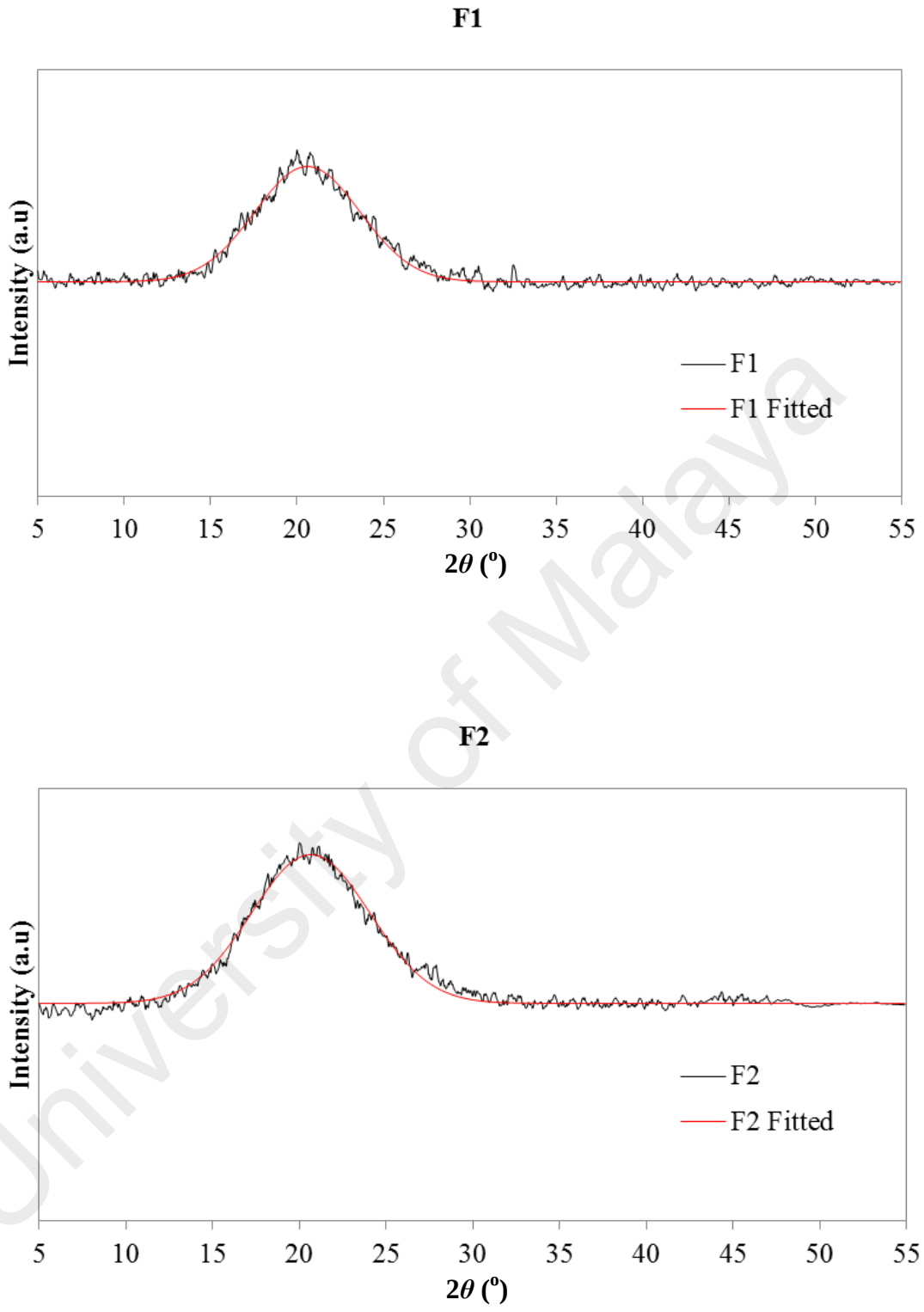

Figure 5.15: All XRD curves with fitted lines for PVA-EC-PC-DMSO-KI-TBAI-DEC gel polymer electrolytes

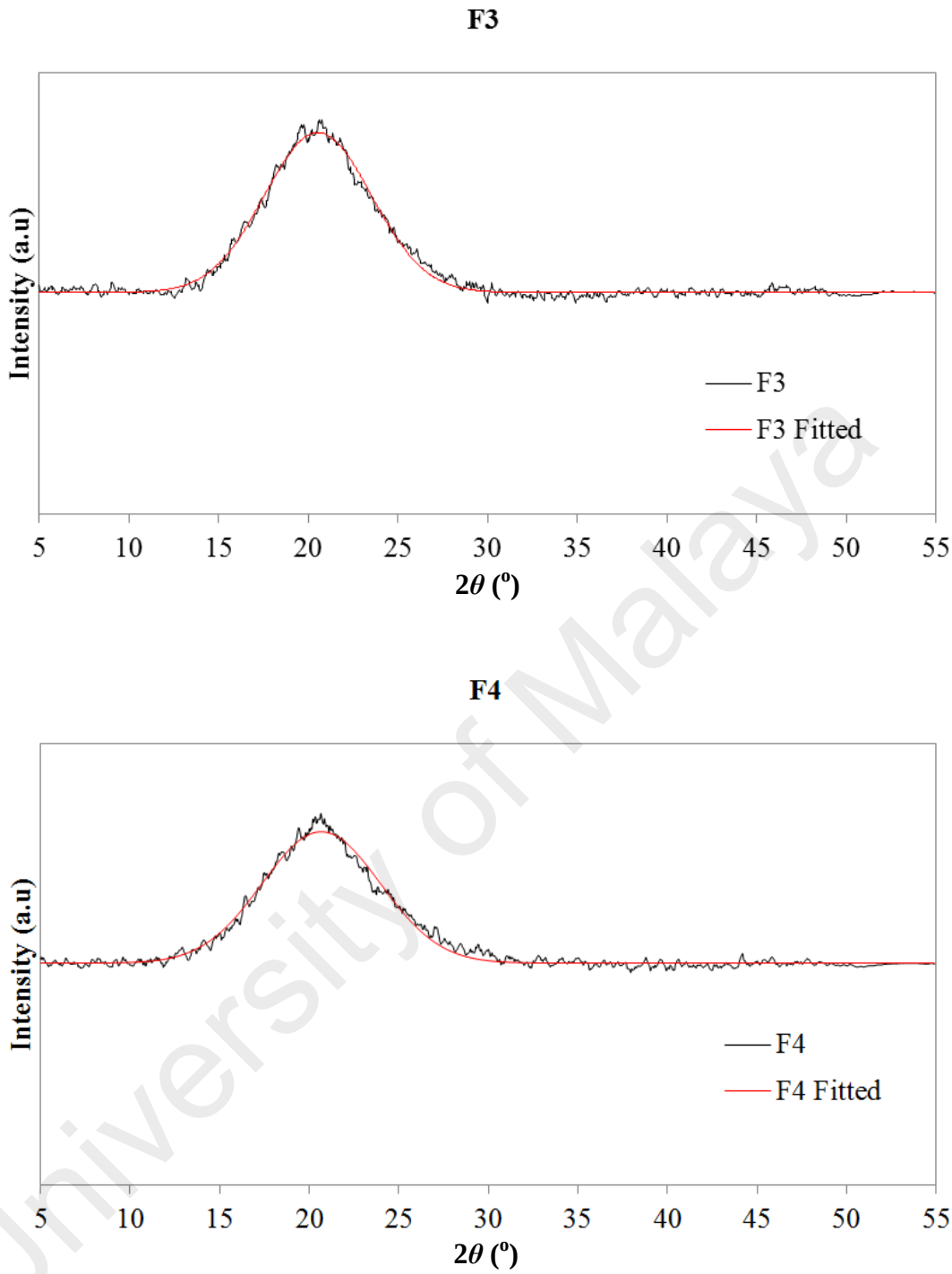

Figure 5.15, continued.

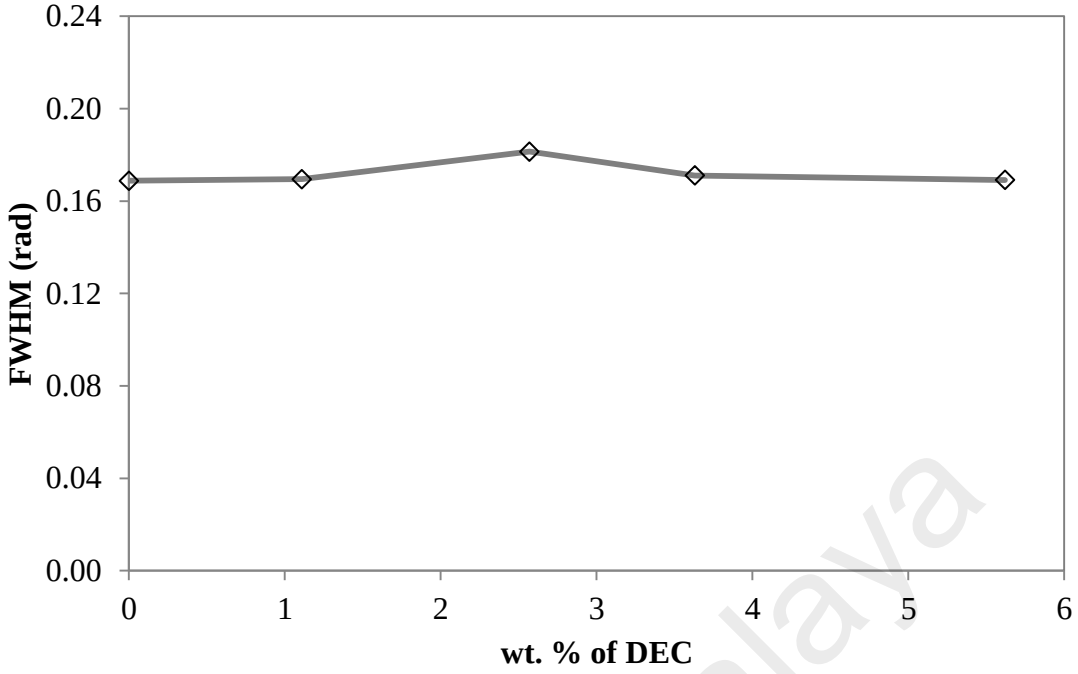

Figure 5.16: FWHM for PVA-DMSO-EC-PC-KI-TBAI gel polymer electrolytes with variation of DEC

Table 5.5: 2θ and FWHM for PVA-DMSO-EC-PC-KI-TBAI gel polymer electrolytes with different amount of DEC

Electrolyte	**2θ (^{o})**	**FWHM (rad)**
D3	20.90	0.169
F1	20.63	0.170
F2	20.93	0.181
F3	20.82	0.171
F4	20.81	0.169

5.5. Summary

In this chapter, the entire XRD patterns for each gel electrolyte system have been shown properly. XRD pattern shows that the gel polymer electrolytes are amorphous in nature. The appearance peaks of TMAI salt in PVA-EC-PC-DMSO-KI-TMAI gel polymer electrolyte system indicates that the TMAI salt is not dissolved properly. Meanwhile, TPAI and TBAI salts are completely dissolved in both PVA-EC-PC-DMSO-KI-TPAI and PVA-EC-PC-DMSO-KI-TBAI gel polymer electrolyte systems.

CHAPTER 6: ELECTROCHEMICAL IMPEDANCE SPECTROSCOPY (EIS)

6.1. Introduction

Electrochemical impedance spectroscopy (EIS) is an important technique to measure the impedance of the gel polymer electrolytes. From the impedance data, the conductivity value of each sample can be calculated. The effect of salt concentration (KI), mixed cations (KI-TMAI, KI-TPAI, and KI-TBAI) and plasticizer (DEC) will be shown in this chapter.

6.2. Conductivity studies

6.2.1. PVA-EC-PC-DMSO-KI system

Figure 6.1 depicts the Cole-Cole plots for PVA-EC-PC-DMSO-KI gel polymer electrolytes at room temperature (RT). Bulk resistance, R_b is obtained by extrapolating the spike with the *x*-axis (Z_r). As can be seen from the figure, all the Cole-Cole plots are in spike form which indicates that electrode polarization is dominant. Thus, its physical model can be described as resistor connected with constant phase element (CPE) (Govindaraj *et. al.*, 1995) as shown in equations (6.1) and (6.2).

$$Z' = R_b + \frac{\cos\left(\frac{\pi p}{2}\right)}{k^{-1}\omega^n} \tag{6.1}$$

$$Z'' = \frac{\sin\left(\frac{\pi p}{2}\right)}{k^{-1}\omega^n} \tag{6.2}$$

where *p* is a fraction of right angle as shown in Figure 6.1 (A1). k^{-1} corresponds to value of capacitance of CPE.

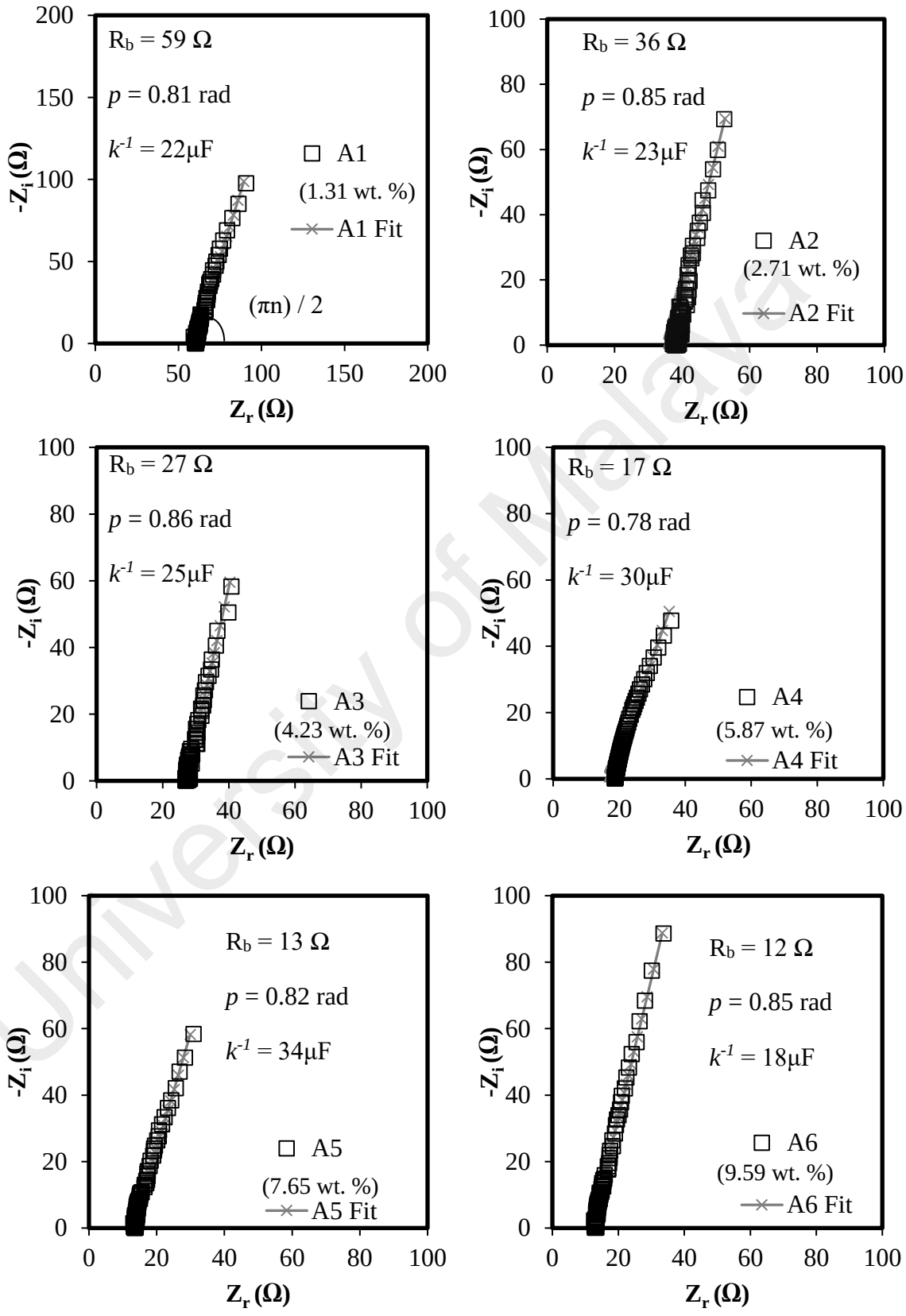

Figure 6.1: Cole-Cole plots for PVA-EC-PC-DMSO-KI gel polymer electrolytes

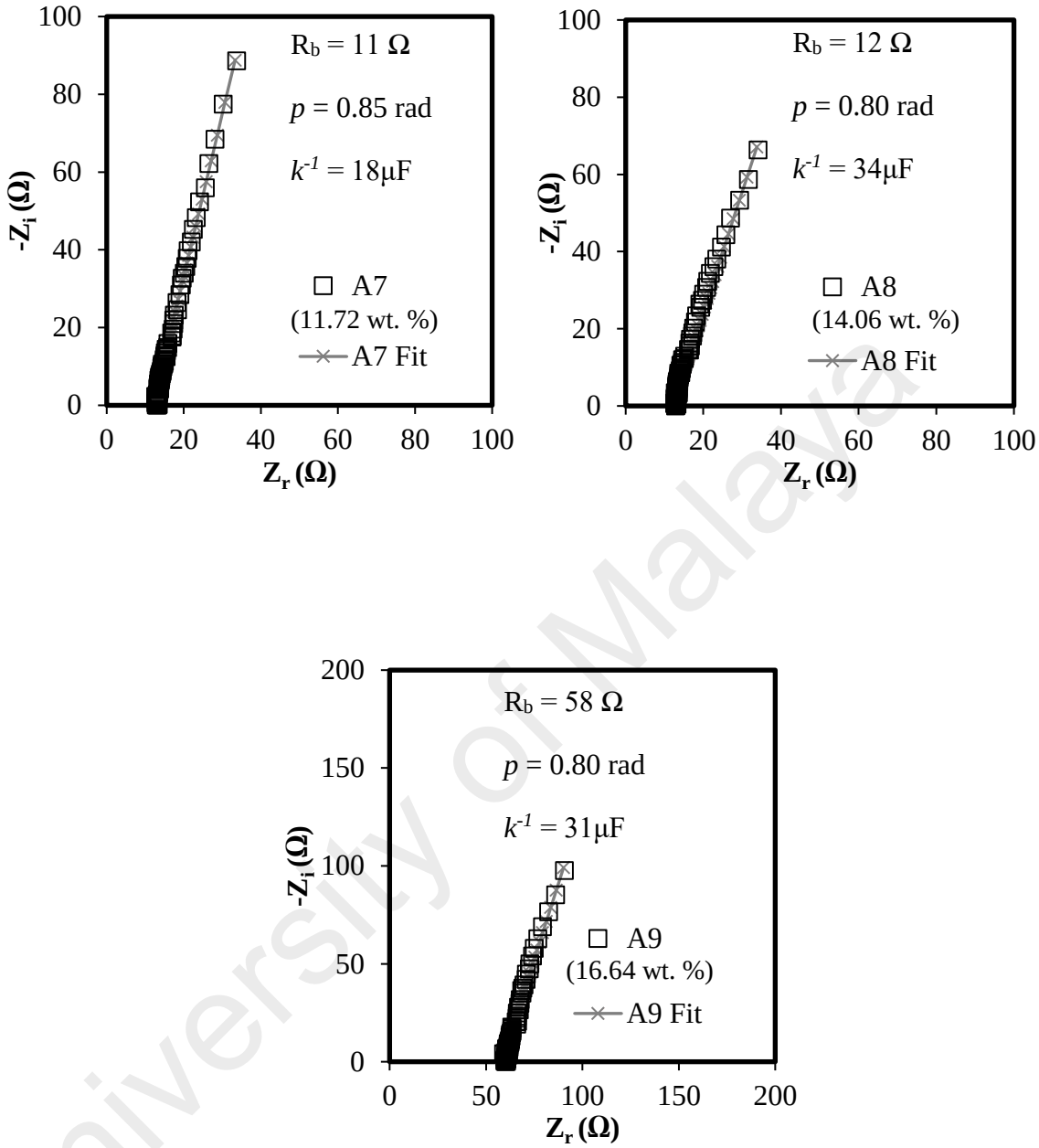

Figure 6.1, continued.

As the weight percentage of KI salt increases, the R_b shows decreasing trend for samples A1 to A7. However, the value of R_b increased for samples A8 and A9. Figure 6.2 (a) displays the graph of conductivity *vs* wt. % of KI. The plotted graph shows that the room temperature ionic conductivity increases from 2.35 ± 0.28 mS cm^{-1} for 1.31 wt. % of KI (A1) to the maximum conductivity of 12.48 ± 0.42 mS cm^{-1} for 11.72 wt.

% of KI (A7). However, after the optimum conductivity of sample A7, the conductivity is observed to decrease for samples A8 (10.90 ± 0.28 mS cm^{-1}) and A9 (10.70 ± 0.14 mS cm^{-1}).

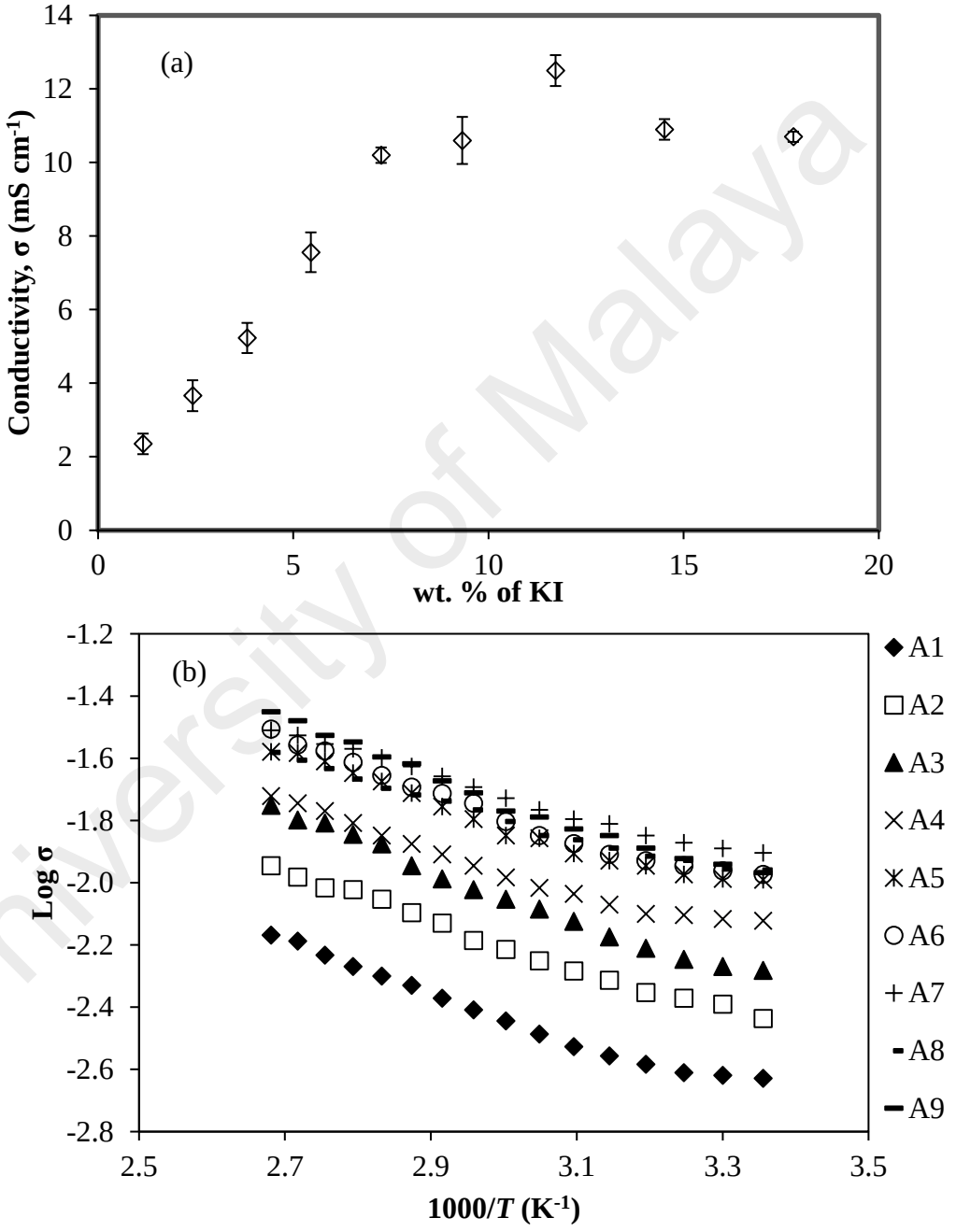

Figure 6.2:(a) Conductivity *vs* wt. % of KI and (b) Log conductivity *vs* 1000/*T* for PVA-EC-PC-DMSO-KI gel polymer electrolytes

The relationship between the conductivity and temperature are plotted in Figure 6.2 (b). Each gel polymer electrolyte for the single iodide system shows that the conductivity increased with increasing temperature. All the graph in Figure 6.2 (b) also show that a linear variations ($R^2 \approx 1$) and therefore can be assuming that the conductivity-temperature dependence follows Arrhenius relation.

Activation energy, E_a is defined as the minimum energy required for chemical reaction begins. In the conductivity studies, the entire conductivity plot is obey Arrhenius relation:

$$\sigma = \sigma_o e^{\left(-\frac{E_a}{k_b T}\right)} \tag{6.3}$$

where σ_o is the pre-exponential factor, k_b is Boltzmann constant and T is absolute temperature in Kelvin. E_a is obtained from the slope of log σ vs 1000/T graph. Here, the value of E_a has been calculated in Table 6.1.

From the table, it can be observed that E_a value for both samples A1 and A2 is 0.15 eV. The value seems slightly decreased to 0.13 eV (A7) and rise again up to 0.16 eV (A8 and A9). The smallest E_a value exhibits the highest conducting gel polymer electrolyte (A7). This indicates that the movement of ions is easier in A7 gel polymer electrolyte compared to others in the same system.

Table 6.1: σ_{RT} and activation energy for gel polymer electrolytes with different amount of KI

Sample	wt. % of KI salt	σ_{RT} (mS cm^{-1})	E_a (eV)
A1	1.15	2.35 ± 0.28	0.15
A2	2.42	3.66 ± 0.42	0.15
A3	3.82	5.23 ± 0.41	0.14
A4	5.45	7.56 ± 0.54	0.14
A5	7.25	10.20 ± 0.21	0.14
A6	9.33	10.60 ± 0.64	0.14
A7	11.72	12.50 ± 0.75	0.13
A8	14.51	10.90 ± 0.28	0.16
A9	17.81	10.70 ± 0.14	0.16

Figure 6.3 shows the dielectric constant, ε_r vs wt. % of KI. The ε_r value has been calculated from Equation (3.14) at frequency 100 kHz and 50 kHz. It can be observed that the trend of ε_r is similar to the ionic conductivity (Figure 6.2 (a)). From Equations (3.11) to (3.13), the diffusion coefficient (D), number density (n) and mobility (μ) of charge carrier have been calculated and listed in Table 6.2.

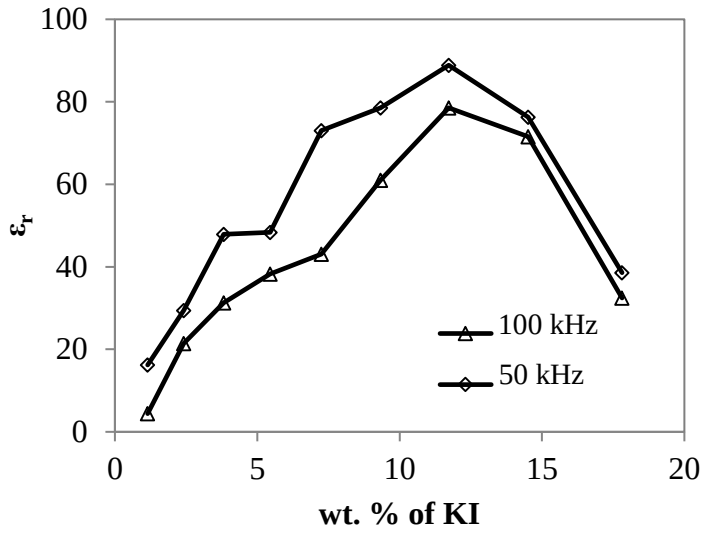

Figure 6.3: ε_r vs wt. % of KI salt for PVA-EC-PC-DMSO-KI gel polymer electrolytes

Table 6.2: Values of *D*, *n*, μ for PVA-EC-PC-DMSO-KI gel polymer electrolytes at different frequencies (100 kHz and 50 kHz)

Frequency at 100 kHz			
	***D* (x 10^{-4} cm^2 s^{-1})**	***n* (x 10^{18} cm^{-3})**	**μ (x 10^{-2} cm^2 V^{-1} s^{-1})**
A1	0.08±0.02	1.18±0.08	0.03±0.01
A2	1.73±0.64	2.39±0.19	0.67±0.02
A3	3.11±0.76	3.69±0.22	1.21±0.57
A4	3.24±0.35	3.74±0.18	1.23±0.31
A5	3.19±0.44	5.13±0.36	1.24±0.45
A6	22.9±3.10	7.43±0.64	8.90±0.32
A7	37.9±9.20	8.29±0.88	14.8±0.17
A8	8.81±0.18	6.38±0.71	3.43±0.64

Table 6.2, continued.

A9	2.18±0.59	5.17±0.26	1.85±0.14
Frequency at 50 kHz			
	D **(x 10^{-4} cm^2 s^{-1})**	***n*** **(x 10^{18} cm^{-3})**	***μ*** **(x 10^{-2} cm^2 V^{-1} s^{-1})**
A1	1.13±0.21	1.32±0.26	0.44±0.09
A2	3.25±0.45	1.80±0.42	1.27±0.65
A3	5.31±0.61	1.95±0.31	2.15±0.47
A4	5.17±0.37	2.35±0.18	2.82±0.12
A5	9.81±0.51	3.78±0.51	3.58±0.75
A6	36.8±1.70	4.48±0.35	4.48±0.68
A7	48.5±1.20	5.13±0.69	18.9±2.90
A8	10.0±2.40	1.74±0.21	3.91±0.54
A9	3.08±0.57	1.57±0.17	1.19±0.94

6.2.2. PVA-EC-PC-DMSO-KI-TMAI system

Figure 6.4 depicts the RT Cole-Cole plots for PVA-EC-PC-DMSO-KI-TMAI gel electrolytes. As the weight percentage of TMAI salt increases, the R_b shows increasing trend.

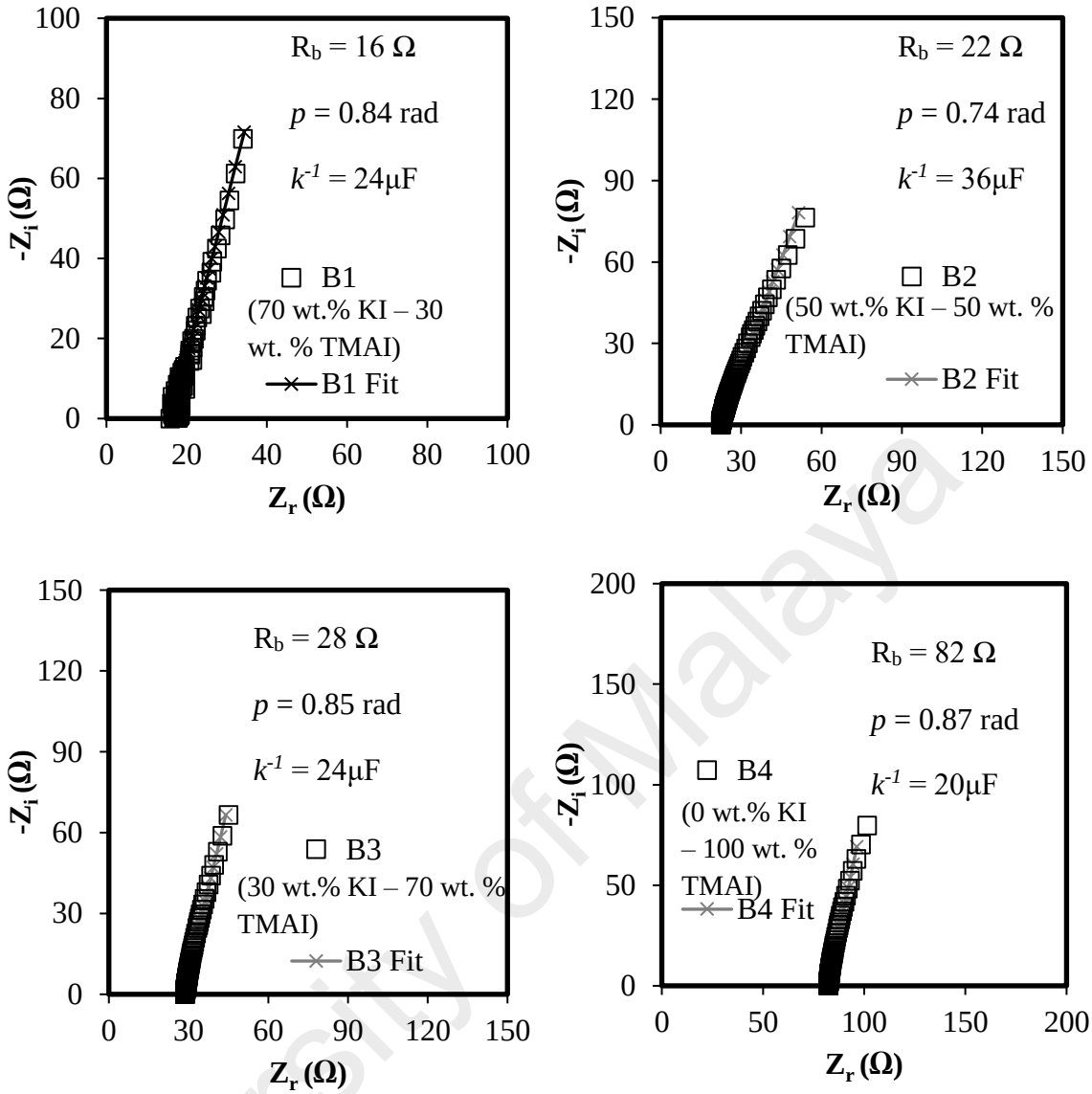

Figure 6.4: Cole-Cole plots for PVA-EC-PC-DMSO-KI-TMAI gel polymer electrolytes

Figure 6.5 (a) shows the graph of RT ionic conductivity *vs* wt. % of KI-TMAI. It can be observed that the conductivity gradually decreases when part of KI salt is replaced by TMAI salt (B1 to B4). B4 (100 wt. % of TMAI) gel polymer electrolyte shows the lowest value of conductivity which is 1.72 ± 0.16 mS cm^{-1}. This value is seven times lower compared to the A7 (100 wt. % of KI) gel polymer electrolyte.

Figure 6.5 (b) shows the relationship between the conductivity and temperature for PVA-EC-PC-DMSO-KI-TMAI gel polymer electrolytes system. It can be observed that

the temperature dependent on conductivity of this gel polymer electrolyte system is follows the Arrhenius behavior ($R^2 \approx 1$).

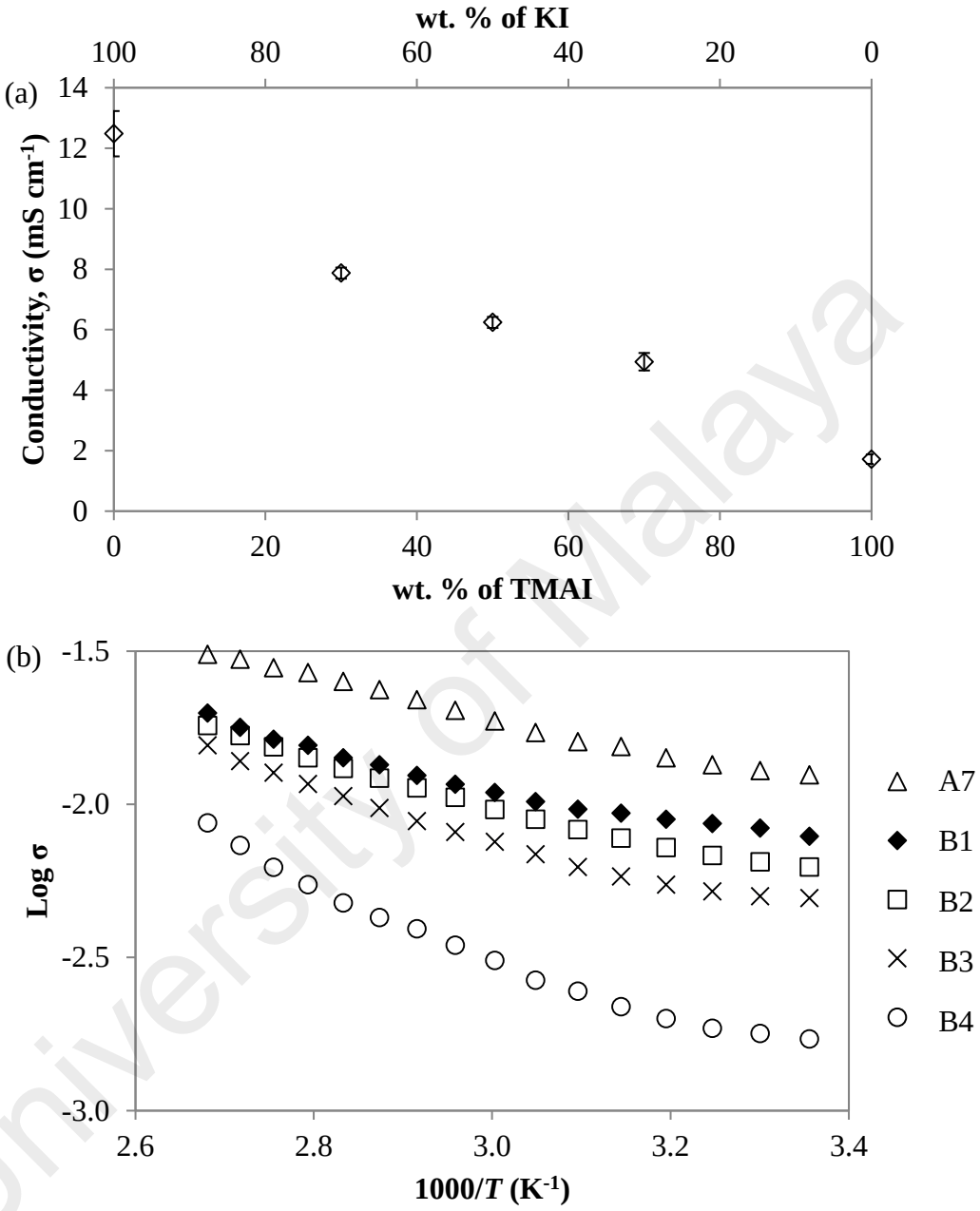

Figure 6.5:(a) Conductivity *vs* wt. % of KI-TMAI and (b) Log conductivity *vs* 1000/*T* for PVA-EC-PC-DMSO-KI-TMAI gel polymer electrolytes

The E_a and conductivity values for gel polymer electrolytes with different amount of KI-TMAI salt have been listed in Table 6.3. The E_a value shows increment when more KI salt is replaced by TMAI salt. The lowest conductivity value of gel polymer electrolyte exhibits the highest value of E_a (B4).

Table 6.3: σ_{RT} and activation energy for gel polymer electrolytes with different amount of KI-TMAI

Sample	KI-TMAI	σ_{RT} (mS cm^{-1})	E_a (eV)
A7	100-0	12.48 ± 0.75	0.13
B1	70-30	7.87 ± 0.18	0.14
B2	50-50	6.24 ± 0.18	0.14
B3	30-70	4.94 ± 0.29	0.15
B4	0-100	1.72 ± 0.16	0.20

Figure 6.6 shows the graph ε_r *vs* wt. % of KI-TMAI salt for PVA-EC-PC-DMSO-KI-TMAI system at frequency 100 kHz and 50 kHz. It can be observed that the trend of ε_r is similar to the ionic conductivity (Figure 6.5(a)). Table 6.4 list the *D, n* and μ value of PVA-EC-PC-DMSO-KI-TMAI gel polymer electrolytes system at 100 kHz and 50 kHz.

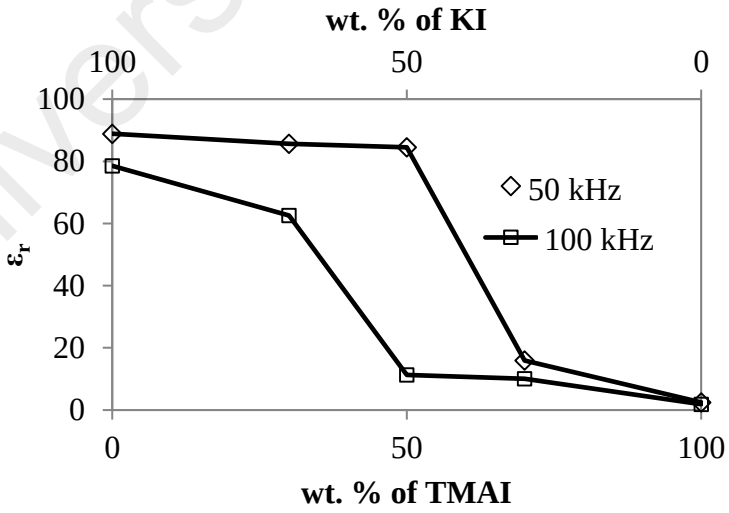

Figure 6.6: ε_r vs wt. % of TMAI salt for PVA-EC-PC-DMSO-KI-TMAI gel polymer electrolytes

Table 6.4: Value of *D, n, μ* for PVA-EC-PC-DMSO-KI-TMAI gel polymer electrolytes at different frequencies (100 kHz and 50 kHz)

Frequency at 100 kHz			
Sample	***D* (x 10^{-4} cm^2 s^{-1})**	***n* (x 10^{18} cm^{-3})**	***μ* (x 10^{-2} cm^2 V^{-1} s^{-1})**
A7	37.9±9.20	8.29±0.88	14.8±6.72
B1	14.7±3.22	0.86±0.02	5.73±0.14
B2	0.43±0.14	24.8±4.23	0.16±0.08
B3	0.24±0.11	35.4±5.35	0.09±0.01
B4	0.006±0.003	451±13	0.002±0.008
Frequency at 50 kHz			
Sample	***D* (x 10^{-4} cm^2 s^{-1})**	***n* (x 10^{18} cm^{-3})**	***μ* (x 10^{-2} cm^2 V^{-1} s^{-1})**
A7	48.5±1.25	5.13±0.69	18.9±2.9
B1	27.6±2.65	0.46±0.08	10.8±1.3
B2	22.7±7.41	4.40±0.25	8.85±0.79
B3	0.56±0.06	14.11±4.43	0.22±0.03
B4	0.01±0.01	261±19	0.004±0.003

6.2.3. PVA-EC-PC-DMSO-KI-TPAI system

Figure 6.7 depicts the RT Cole-Cole plots for PVA-EC-PC-DMSO-KI-TPAI gel electrolytes. As the weight percentage of TPAI salt increases, R_b shows increasing trend.

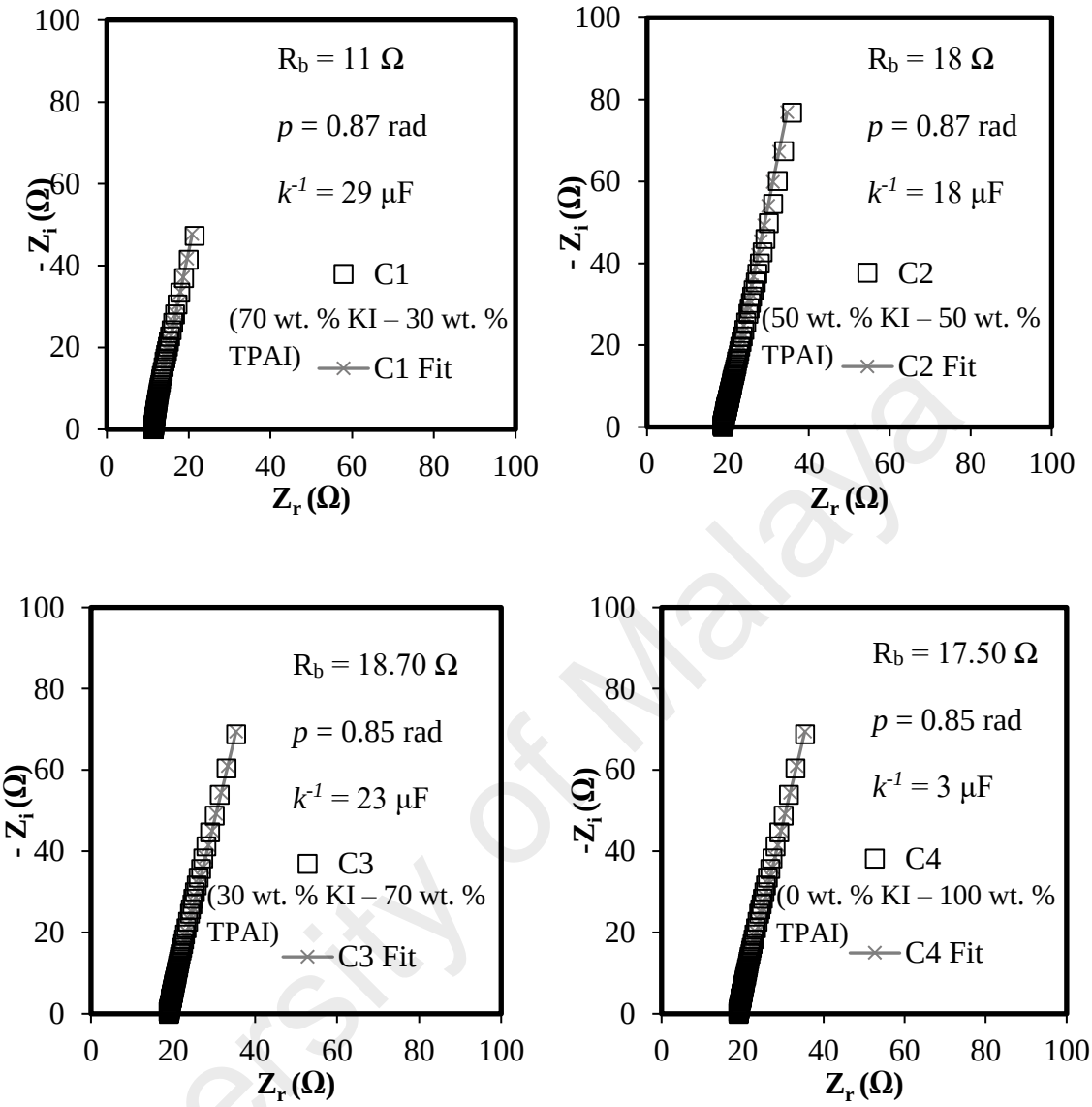

Figure 6.7: Cole-Cole plots for PVA-EC-PC-DMSO-KI-TPAI gel polymer electrolytes

Figure 6.8 (a) shows the graph of RT ionic conductivity *vs* wt. % of KI-TPAI. It can be observed that the conductivity gradually decreases when part of KI salt has been replaced by TPAI salt (C1 to C4). C4 (100 wt. % of TPAI) gel polymer electrolyte shows the lowest value of conductivity which is 6.24 ± 0.64 mS cm^{-1}. This value is two times lower compared to the A7 (100 wt. % of KI) gel polymer electrolyte.

Figure 6.8 (b) shows the relationship between the conductivity and temperature for PVA-EC-PC-DMSO-KI-TPAI gel polymer electrolytes system. It can be observed that

the conductivity temperature relationship of this gel polymer electrolyte system follows the Arrhenius behavior ($R^2 \approx 1$).

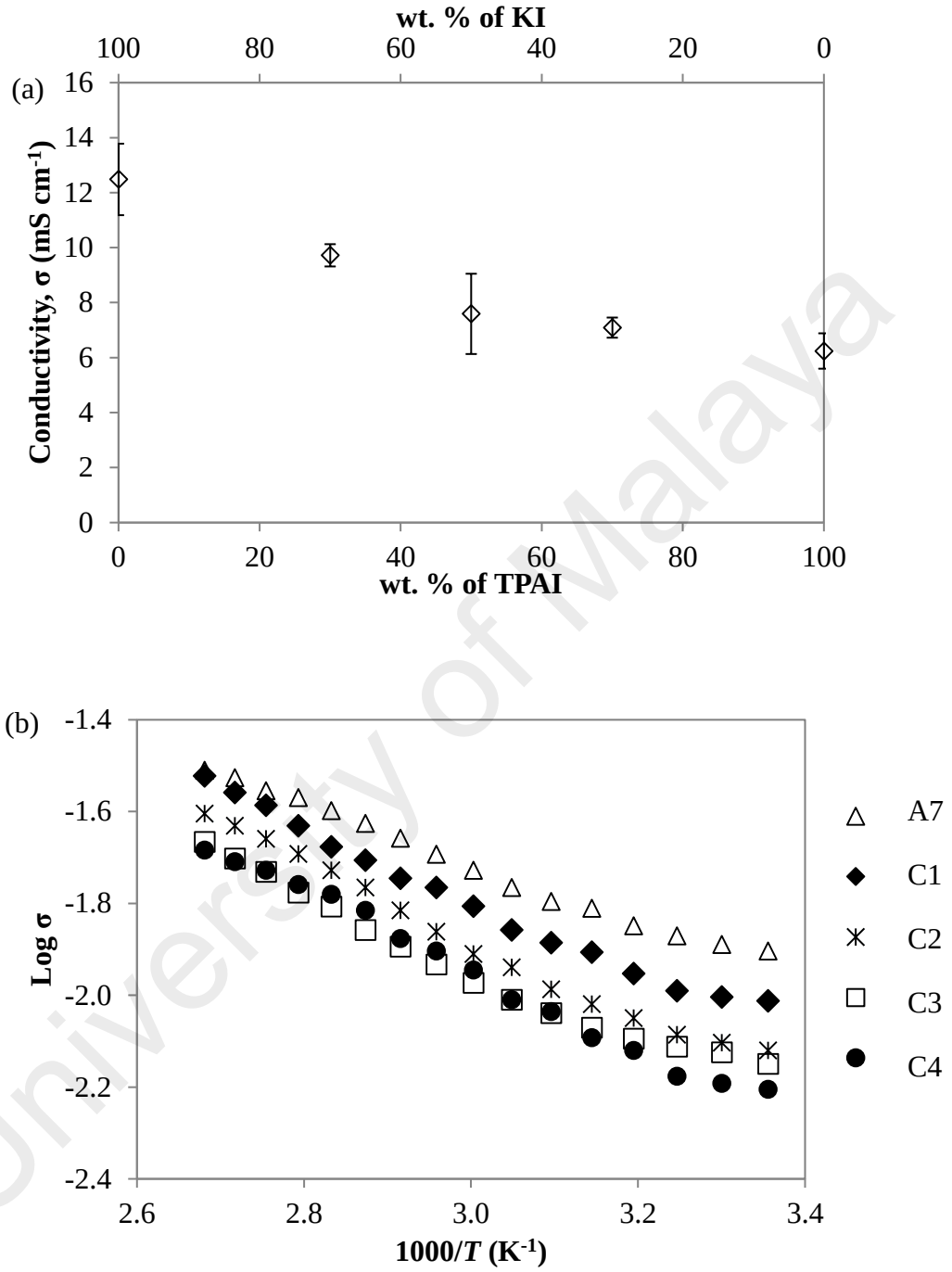

Figure 6.8:(a) Conductivity *vs* wt. % and (b) log conductivity *vs* 1000/*T* for PVA-EC-PC-DMSO-KI-TPAI gel polymer electrolytes

The E_a and conductivity values for gel polymer electrolytes with different amount of KI-TPAI salt have been listed in Table 6.5. The E_a value shows increment when more KI salt is replaced by TPAI salt. The lowest conductivity value of gel polymer electrolyte exhibits the highest value of E_a (C4).

Table 6.5: σ_{RT} and activation energy for gel polymer electrolytes with different amount of KI-TPAI

Sample	KI-TPAI	σ_{RT} (mS cm^{-1})	E_a (eV)
A7	100-0	12.48 ± 0.75	0.13
C1	70-30	9.72 ± 0.41	0.14
C2	50-50	7.59 ± 1.46	0.14
C3	30-70	7.09 ± 0.37	0.14
C4	0-100	6.24 ± 0.64	0.17

Figure 6.9 shows the graph ε_r *vs* wt. % of KI-TPAI salt for PVA-EC-PC-DMSO-KI-TPAI system at frequency 100 kHz and 50 kHz. It can be observed that the trend of ε_r is similar to the ionic conductivity (Figure 6.8(a)). Table 6.6 list the *D*, *n* and μ value for PVA-EC-PC-DMSO-KI-TPAI gel polymer electrolytes system at 100 kHz and 50 kHz.

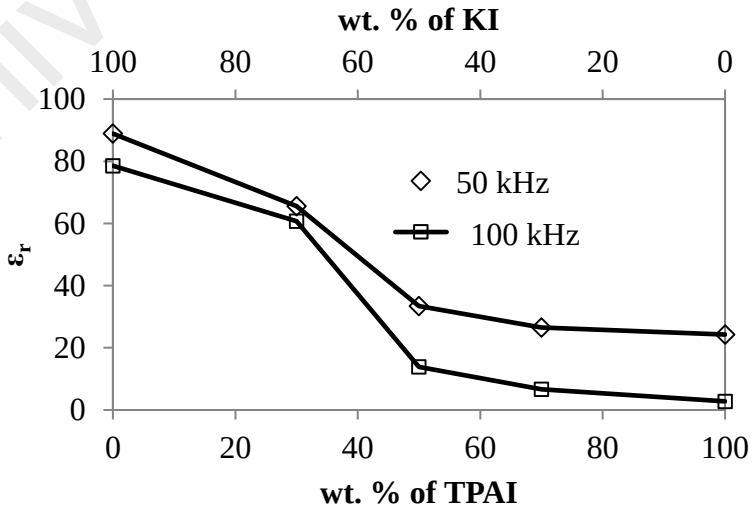

Figure 6.9: ε_r vs wt. % of TPAI salt for PVA-EC-PC-DMSO-KI-TPAI gel polymer electrolytes

Table 6.6: Value of *D*, *n*, μ for PVA-EC-PC-DMSO-KI-TPAI gel polymer electrolytes at different frequencies (100 kHz and 50 kHz)

Frequency at 100 kHz			
Sample	***D*** **(x 10^{-4} cm^2 s^{-1})**	***n*** **(x 10^{18} cm^{-3})**	μ**(x 10^{-2} cm^2 V^{-1} s^{-1})**
A7	37.9±9.20	8.29±0.88	14.8±0.17
C1	13.9±6.20	1.12±0.02	5.40±0.34
C2	0.61±0.07	19.9±2.2	0.24±0.61
C3	0.09±0.03	117±35	0.03±0.07
C4	0.03±0.02	752±81	0.005±0.009
Frequency at 50 kHz			
Sample	***D*** **(x 10^{-4} cm^2 s^{-1})**	***n*** **(x 10^{18} cm^{-3})**	μ **(x 10^{-2} cm^2 V^{-1} s^{-1})**
A7	48.5±1.20	5.13±0.69	18.9±2.90
C1	16.1±2.80	0.97±0.03	6.28±0.19
C2	3.56±0.41	3.42±0.07	1.39±0.16
C3	1.56±0.11	7.29±0.83	0.61±0.09
C4	1.01±0.35	9.86±0.25	0.39±0.04

6.2.4. PVA-EC-PC-DMSO-KI-TBAI system

Figure 6.10 depicts the RT Cole-Cole plots for PVA-EC-PC-DMSO-KI-TBAI gel electrolytes. As the weight percentage of TBAI salt increases, R_b shows increasing trend.

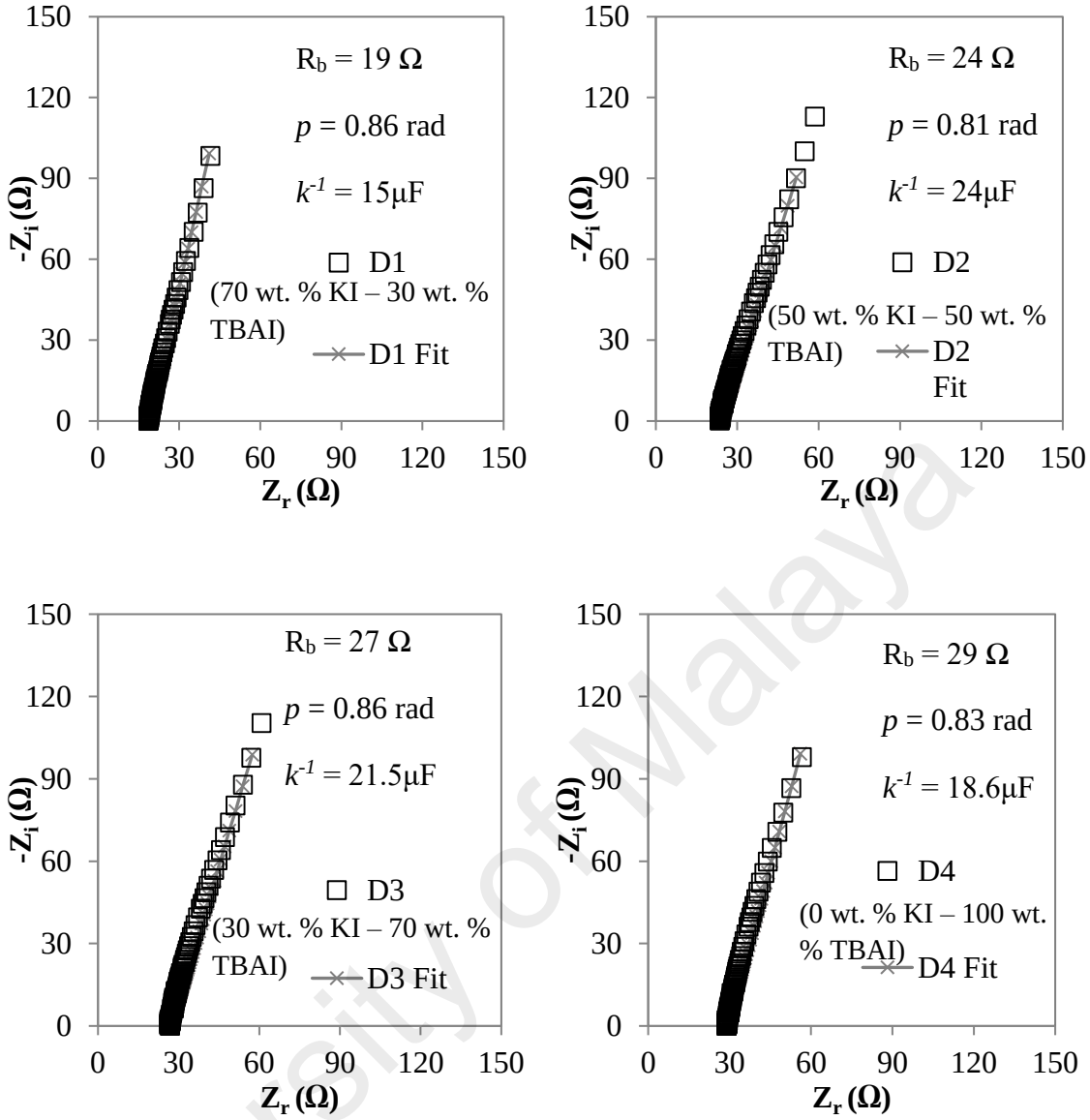

Figure 6.10: Cole-Cole plots for PVA-EC-PC-DMSO-KI-TBAI gel polymer electrolytes

Figure 6.11 (a) shows the graph of RT ionic conductivity *vs* wt. % of KI-TBAI. It can be observed that the conductivity is gradually decreasing when part of KI salt is replaced by TBAI salt (D1 to D4). D4 (100 wt. % of TBAI) gel polymer electrolyte shows the lowest conductivity value which of 4.68 ± 0.20 mS cm^{-1}. This value is three times lower compared to the A7 (100 wt. % of KI) gel polymer electrolyte.

Figure 6.11 (b) shows the relationship between the conductivity and temperatures for PVA-EC-PC-DMSO-KI-TBAI gel polymer electrolytes system. It can be observed that

the temperature dependence conductivity of this gel polymer electrolyte system follows the Arrhenius behavior ($R^2 \approx 1$).

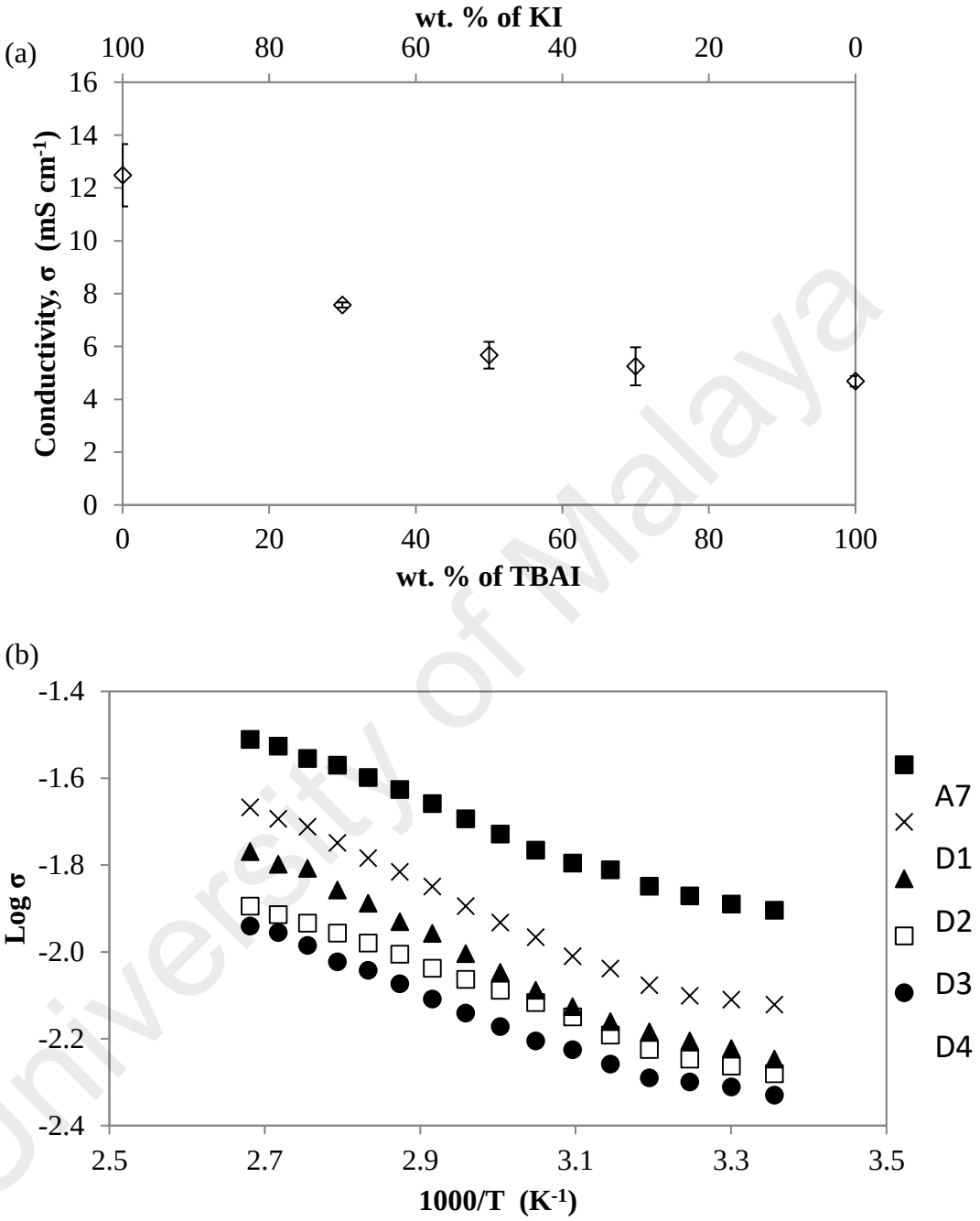

Figure 6.11:(a) Conductivity *vs* wt. % of KI-TBAI and (b) Log conductivity *vs* 1000/*T* for PVA-EC-PC-DMSO-KI-TBAI gel polymer electrolytes

The E_a and conductivity values for gel polymer electrolytes with different amount of KI-TBAI salt have been listed in Table 6.7. It can be observed that the E_a value is slightly increased when small part of KI salt has been replaced by TBAI salt (D1). The value remain unchanged (0.14 eV) until the whole KI salt is replaced by TBAI (D4).

Table 6.7: σ_{RT} and activation energy for gel polymer electrolytes with different amount of KI-TBAI

Sample	KI-TBAI	σ_{RT} (mS cm^{-1})	E_a (eV)
A7	100-0	12.48 ± 0.75	0.13
D1	70-30	7.57 ± 0.10	0.14
D2	50-50	5.67 ± 0.51	0.14
D3	30-70	5.25 ± 0.72	0.14
D4	0-100	4.68 ± 0.20	0.14

Figure 6.12 shows the graph ε_r *vs* wt. % of KI-TBAI salt for PVA-EC-PC-DMSO-KI-TBAI system at frequency 100 kHz and 50 kHz. It can be observed that the trend of ε_r is similar to the ionic conductivity (Figure 6.11(a)). Table 6.8 list the *D*, *n* and μ value for PVA-EC-PC-DMSO-KI-TBAI gel polymer electrolytes system.

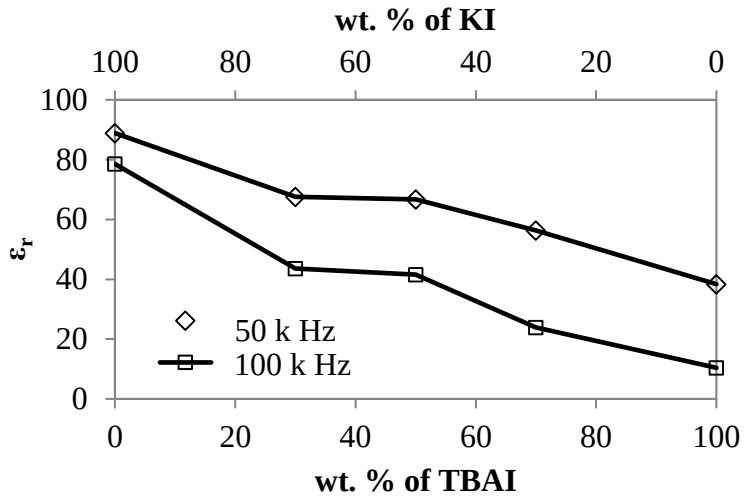

Figure 6.12: ε_r vs wt. % of TBAI salt for PVA-EC-PC-DMSO-KI-TBAI gel polymer electrolytes

Table 6.8: Values of *D, n, μ* for PVA-EC-PC-DMSO-KI-TBAI gel polymer electrolytes at different frequencies (100 kHz and 50 kHz)

Frequency at 100 kHz			
Sample	***D* (x 10^{-4} cm^2 s^{-1})**	***n* (x 10^{18} cm^{-3})**	***μ* (x 10^{-2} cm^2 V^{-1} s^{-1})**
A7	37.9±9.2	8.29±0.88	14.8±0.17
D1	7.15±0.31	1.69±0.42	2.79±0.45
D2	5.50±0.43	1.62±0.61	2.14±0.92
D3	1.27±0.28	6.65±0.82	0.49±0.05
D4	0.19±0.02	40.3±27	0.073±0.021
Frequency at 50 kHz			
Sample	***D* (x 10^{-4} cm^2 s^{-1})**	***n* (x 10^{18} cm^{-3})**	***μ* (x 10^{-2} cm^2 V^{-1} s^{-1})**
A7	48.5±1.2	5.13±0.69	18.9±2.9
D1	17.2±3.1	0.71±0.38	6.69±0.26

Table 6.8, continued.

D2	14.2±4.3	0.74±0.17	5.52±0.18
D3	7.02±0.16	1.20±0.36	2.73±0.20
D4	2.53±0.15	2.96±0.72	0.99±0.51

6.2.5. PVA-EC-PC-DMSO-KI-TPAI-DEC system

Figure 6.13 depicts the RT Cole-Cole plots for PVA-EC-PC-DMSO-KI-TPAI-DEC gel polymer electrolytes. As the weight percentage of DEC increases, the R_b value shows decreasing trend initially for E1 and E2 GPEs. Then, R_b increases as can be observed in Sample E3 and E4.

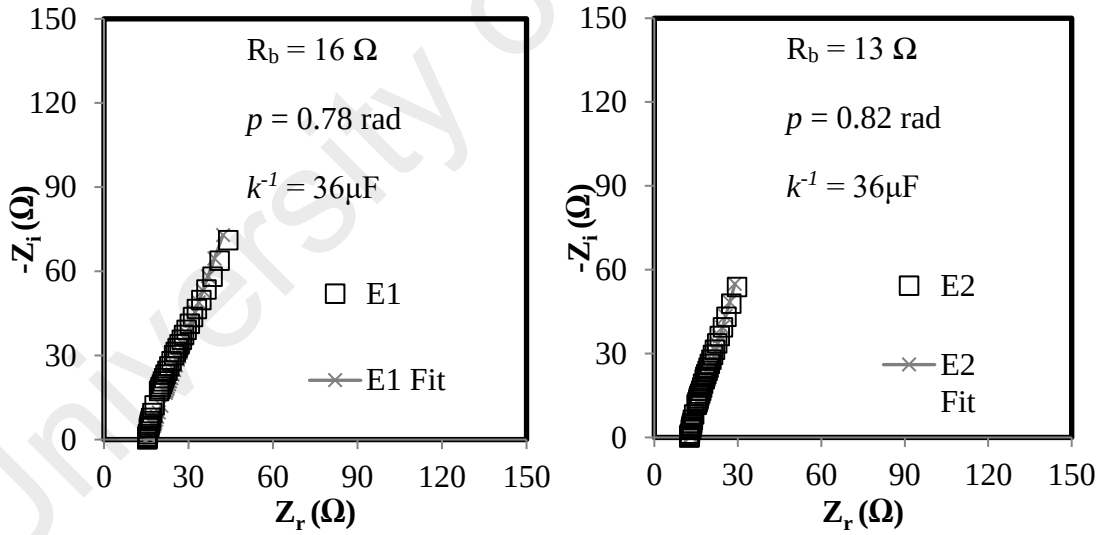

Figure 6.13: Cole-Cole plots for PVA-EC-PC-DMSO-KI-TPAI-DEC gel polymer electrolytes

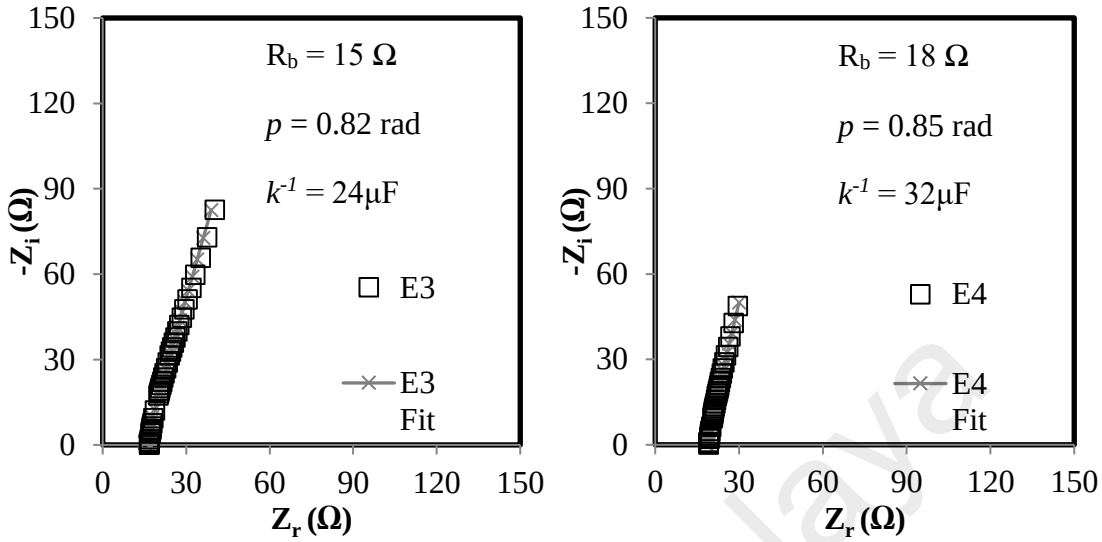

Figure 6.13, continued.

Figure 6.14 (a) shows the graph of RT ionic conductivity *vs* wt. % of DEC. It can be observed that the conductivity gradually increases when DEC was added in the PVA-DMSO-EC-PC-KI-TPAI system. E2 (2.57 wt. % DEC) gel polymer electrolyte show the highest conductivity value which is 11.20 ± 0.19 mS cm^{-1} while E4 (5.27 wt. % DEC) gel polymer electrolyte shows the lowest conductivity value of 6.75 ± 0.44 mS cm^{-1}.

Figure 6.14 (b) shows the relationship between the conductivity and temperature for PVA-EC-PC-DMSO-KI-TPAI-DEC gel polymer electrolytes system. It can be observed that the temperature dependence conductivity of this gel polymer electrolyte system follows the Arrhenius behavior ($R^2 \approx 1$).

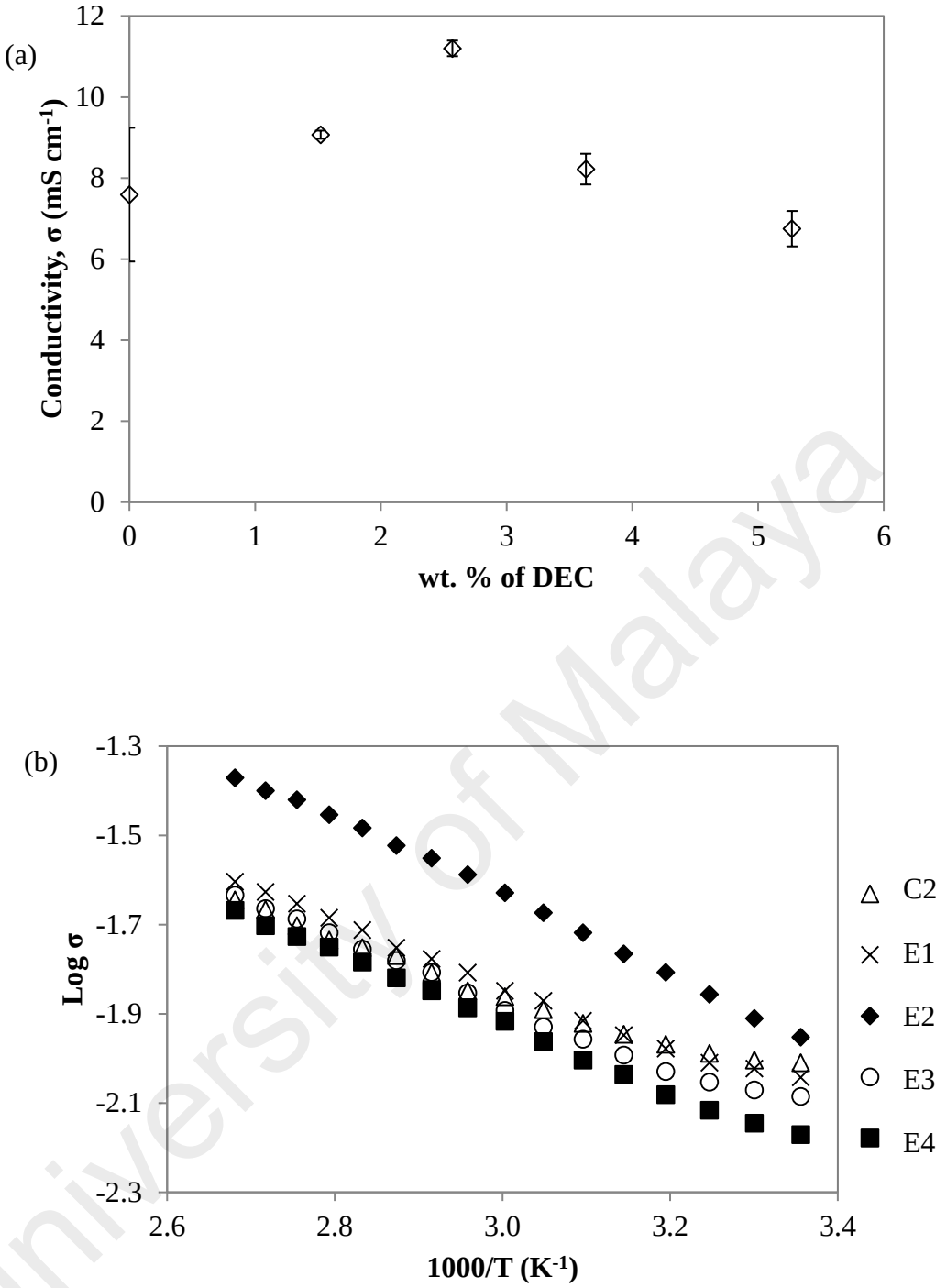

Figure 6.14:(a) Conductivity *vs* wt. % of DEC and (b) Log conductivity *vs* 1000/T for PVA-EC-PC-DMSO-KI-TPAI-DEC gel polymer electrolytes

The E_a and conductivity values for gel polymer electrolytes with different amount of DEC have been listed in Table 6.9. The highest conducting gel polymer electrolyte (E2) exhibits the lowest value of E_a (0.09 eV).

Table 6.9: σ_{RT} and activation energy for gel polymer electrolytes with different amount of DEC

Sample	σ_{RT} (mS cm^{-1})	E_a (eV)
C2	7.59 ± 1.46	0.11
E1	9.07 ± 0.10	0.10
E2	11.20 ± 0.19	0.09
E3	8.22 ± 0.38	0.14
E4	6.75 ± 0.44	0.15

Figure 6.15 shows the graph ε_r *vs* wt. % of DEC for PVA-EC-PC-DMSO-KI-TPAI-DEC system at frequency 100 kHz and 50 kHz. It can be observed that the trend of ε_r is similar to the ionic conductivity (Figure 6.14(a)). Table 6.10 list the *D, n* and μ value for PVA-EC-PC-DMSO-KI-TPAI-DEC gel polymer electrolytes system at 100 kHz and 50 kHz.

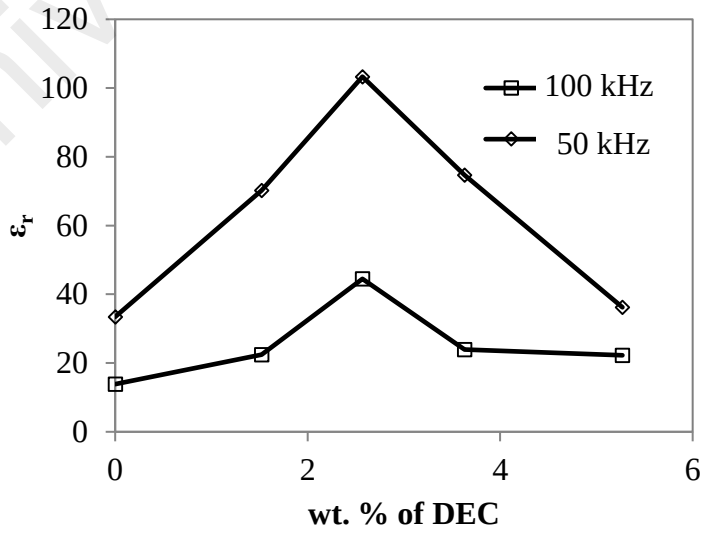

Figure 6.15: ε_r vs wt. % of DEC for PVA-EC-PC-DMSO-KI-TPAI-DEC gel polymer electrolytes

Table 6.10: Value of *D*, *n*, μ for PVA-EC-PC-DMSO-KI-TPAI-DEC gel polymer electrolytes at different frequencies (100 kHz and 50 kHz)

Frequency at 100 kHz			
Sample	**D (x 10^{-4} cm^2 s^{-1})**	***n* (x 10^{18} cm^{-3})**	**μ (x 10^{-2} cm^2 V^{-1} s^{-1})**
C2	0.61±0.71	19.9±2.2	0.24±0.61
E1	1.49±0.41	9.76±0.46	0.58±0.15
E2	5.02±0.23	3.57±0.41	1.96±0.03
E3	1.68±0.27	7.82±0.22	0.66±0.15
E4	1.57±0.13	6.87±0.17	0.61±0.41
Frequency at 50 kHz			
Sample	***D* (x 10^{-4} cm^2 s^{-1})**	***n* (x 10^{18} cm^{-3})**	**μ (x 10^{-2} cm^2 V^{-1} s^{-1})**
C2	3.56±0.41	3.42±0.07	1.39±0.16
E1	14.5±0.43	1.00±0.18	5.66±0.43
E2	27.1±0.13	0.66±0.03	10.6±0.26
E3	16.4±0.56	0.81±0.16	6.40±0.30
E4	4.18±0.07	2.59±0.32	1.63±0.21

6.2.6. PVA-EC-PC-DMSO-KI-TBAI-DEC system

Figure 6.16 depicts the RT Cole-Cole plots for PVA-EC-PC-DMSO-KI-TBAI-DEC gel polymer electrolytes. Figure 6.17 (a) shows the graph of RT ionic conductivity *vs* wt. % of DEC. It can be observed that the conductivity gradually increases when DEC

was added in the PVA-DMSO-EC-PC-KI-TBAI system. F2 (2.57 wt. % of DEC) gel polymer electrolyte shows the highest conductivity value of 6.19 ± 0.06 mS cm^{-1} while F4 (5.27 wt. % of DEC) gel polymer electrolyte shows the lowest value of conductivity which is 5.81 ± 0.06 mS cm^{-1}.

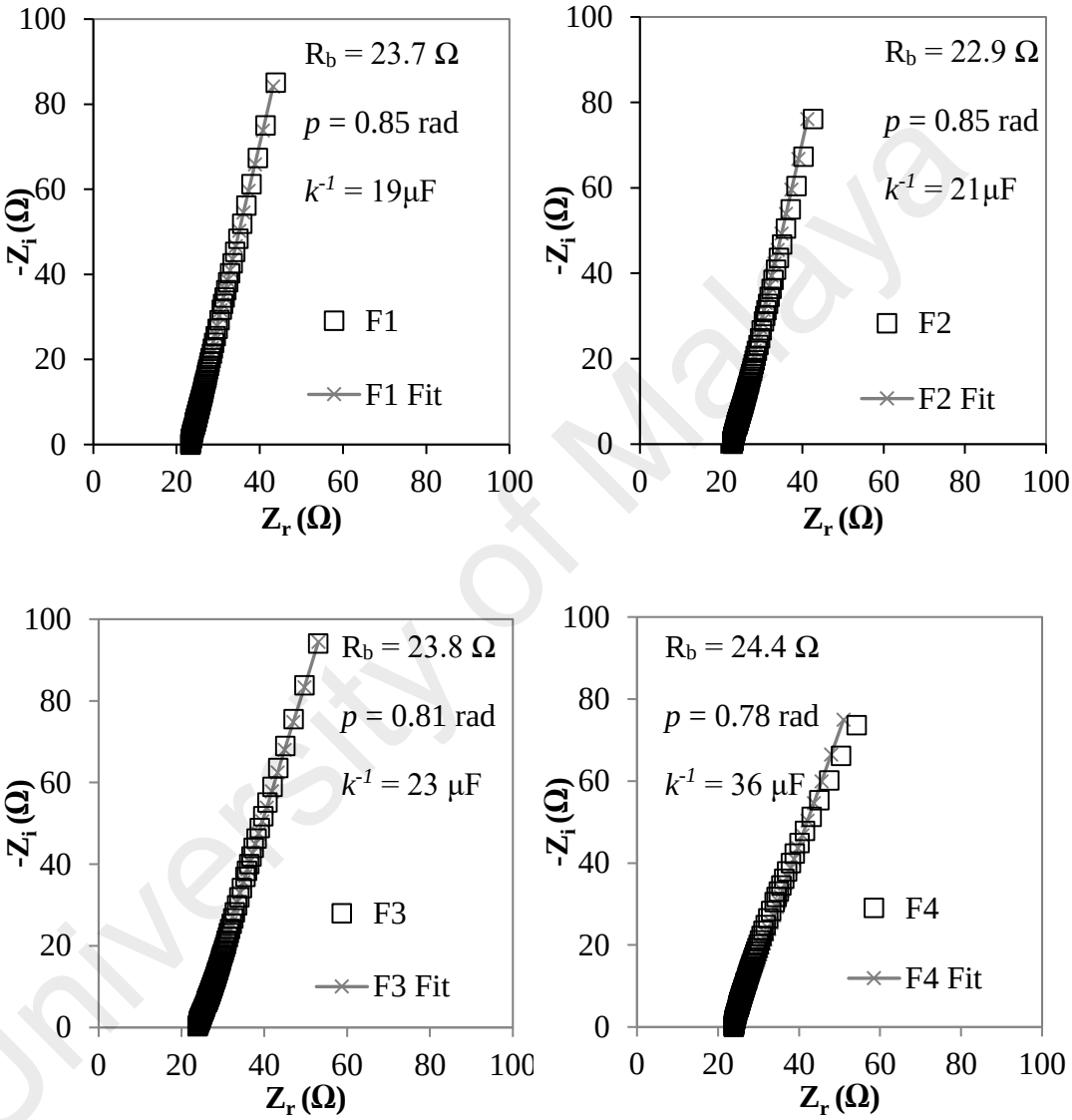

Figure 6.16: Cole-Cole plots for PVA-EC-PC-DMSO-KI-TBAI-DEC gel polymer electrolytes

Figure 6.17 (b) shows the relationship between the conductivity and temperature for PVA-EC-PC-DMSO-KI-TBAI-DEC gel polymer electrolytes system. It can be observed that the temperature dependence conductivity of this gel polymer electrolyte system follows the Arrhenius behavior ($R^2 \approx 1$).

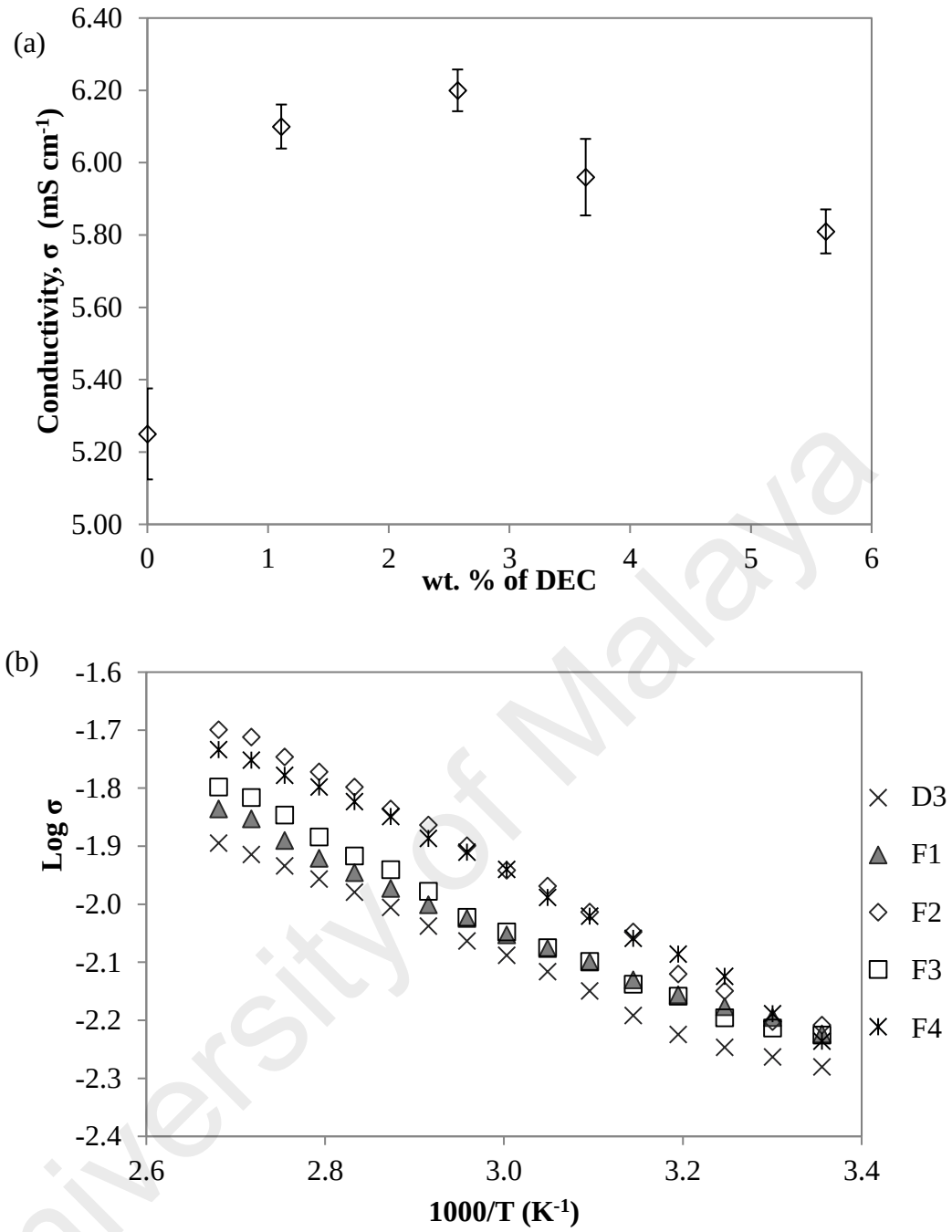

Figure 6.17:(a) Conductivity *vs* wt. % of DEC and (b) Log conductivity *vs* 1000/T for PVA-EC-PC-DMSO-KI-TBAI-DEC gel polymer electrolytes

The E_a and conductivity values for gel polymer electrolytes with different amount of DEC have been listed in Table 6.11. The highest conductivity gel polymer electrolyte (F2) exhibits the lowest value of E_a (0.10 eV).

Table 6.11: σ_{RT} and activation energy for gel polymer electrolytes with different amount of DEC

Sample	σ_{RT} (mS cm^{-1})	E_a (eV)
D3	5.25 ± 0.72	0.14
F1	5.98 ± 0.06	0.11
F2	6.19 ± 0.06	0.10
F3	5.96 ± 0.11	0.13
F4	5.81 ± 0.06	0.14

Figure 6.18 shows the graph ε_r *vs* wt. % of DEC for PVA-EC-PC-DMSO-KI-TBAI-DEC system at frequency 100 kHz and 50 kHz. It can be observed that the trend of ε_r is similar to the ionic conductivity (Figure 6.17(a)). Table 6.12 list the *D*, *n* and μ value for PVA-EC-PC-DMSO-KI-TBAI-DEC gel polymer electrolytes system at 100 kHz and 50 kHz.

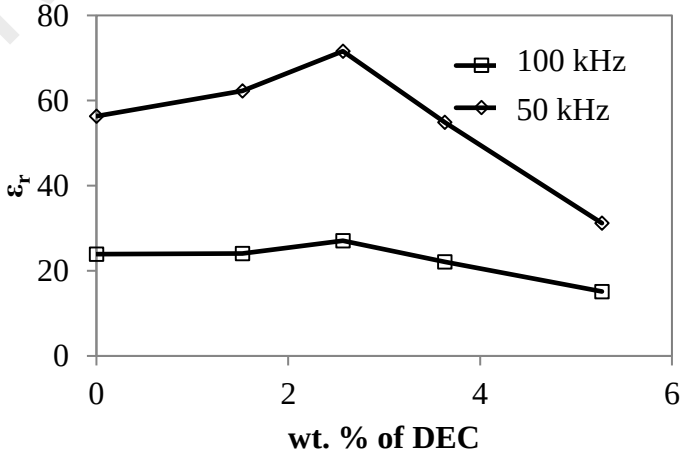

Figure 6.18: ε_r vs wt. % of DEC for PVA-EC-PC-DMSO-KI-TBAI-DEC gel polymer electrolytes

Table 6.12: Value of *D*, *n*, μ for PVA-EC-PC-DMSO-KI-TBAI-DEC gel polymer electrolytes at different frequencies (100 kHz and 50 kHz)

Frequency at 100 kHz			
Sample	***D*** **(x 10^{-4} cm^2 s^{-1})**	***n*** **(x 10^{18} cm^{-3})**	**μ (x 10^{-2} cm^2 V^{-1} s^{-1})**
D3	1.27±0.28	6.65±0.82	0.49±0.05
F1	1.70±0.31	5.62±0.36	0.66±0.06
F2	1.86±0.45	5.33±0.09	0.72±0.24
F3	1.44±0.62	6.66±0.36	0.56±0.18
F4	0.73±0.03	12.8±2.4	0.28±0.31
Frequency at 50 kHz			
Sample	***D*** **(x 10^{-4} cm^2 s^{-1})**	***n*** **(x 10^{18} cm^{-3})**	**μ (x 10^{-2} cm^2 V^{-1} s^{-1})**
D3	7.02±0.16	1.20±0.36	2.73±0.20
F1	11.4±0.35	0.84±0.28	4.45±0.33
F2	13.0±0.19	0.76±0.57	5.06±0.51
F3	8.87±0.26	1.08±0.24	3.46±0.64
F4	3.10±0.47	3.00±0.12	1.20±0.18

6.3. Summary

In this chapter, all the conductivity at room temperature and various temperatures for each system have been displayed. From PVA-EC-PC-DMSO-KI system, the conductivity at room temperature increases with the increasing of KI salt amount. However, PVA-EC-PC-DMSO-KI-TMAI, PVA-EC-PC-DMSO-KI-TPAI and PVA-

EC-PC-DMSO-KI-TBAI systems show decreasing trend for the ambient conductivity. The RT conductivity has been improved with incorporation of DEC plasticizer. The conductivity value increases with the increasing temperature. Activation energy shows a different trend from the conductivity trend where activation energy decreases with the increases in conductivity. All the diffusion coefficient (D), number charge density (n) and mobility (μ) for each electrolyte have been calculated.

CHAPTER 7: DYE-SENSITIZED SOLAR CELL (DSSC)

7.1. Introduction

In this chapter, gel polymer electrolytes with different systems have been used for the DSSC fabrication. The DSSCs configuration was glass /FTO /TiO_2 /Dye /GPE /Pt /FTO /glass. The *J-V* measurements were performed under white light intensity of 100 mW cm^{-2}. The performance parameters such as short circuit current density (J_{sc}), open circuit voltage (V_{oc}), fill factor (*ff*) and efficiency have been obtained.

7.2. Dye-sensitized solar cell for PVA-EC-PC-DMSO-KI system

Figure 7.1 shows the *J-V* curves for DSSCs utilizing PVA-EC-PC-DMSO-KI gel polymer electrolytes system (A1 to A9).

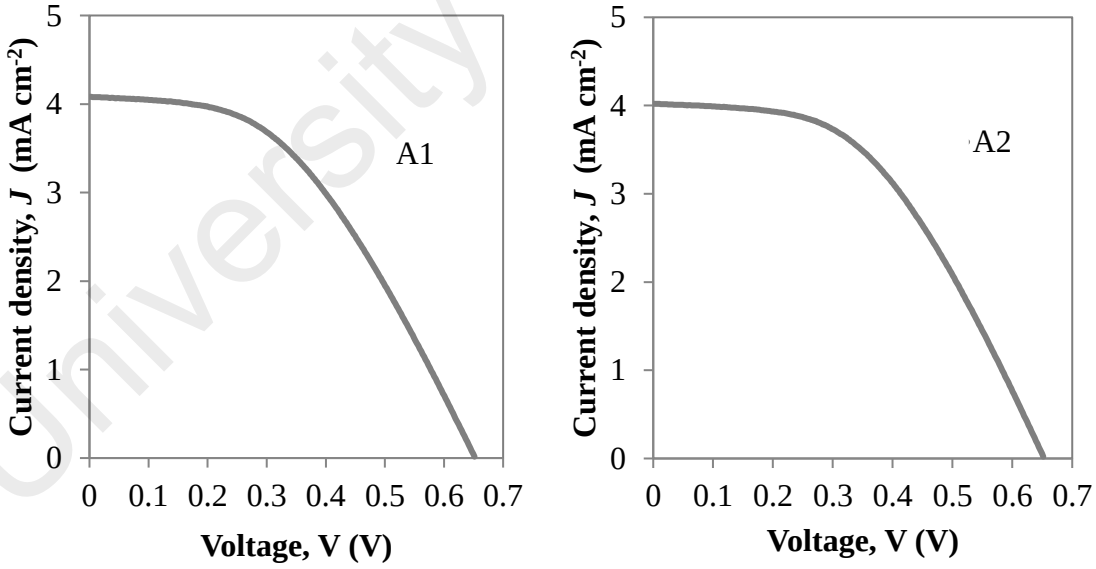

Figure 7.1: *J-V* curves for dye-sensitized solar cell (DSSC) (KI salt)

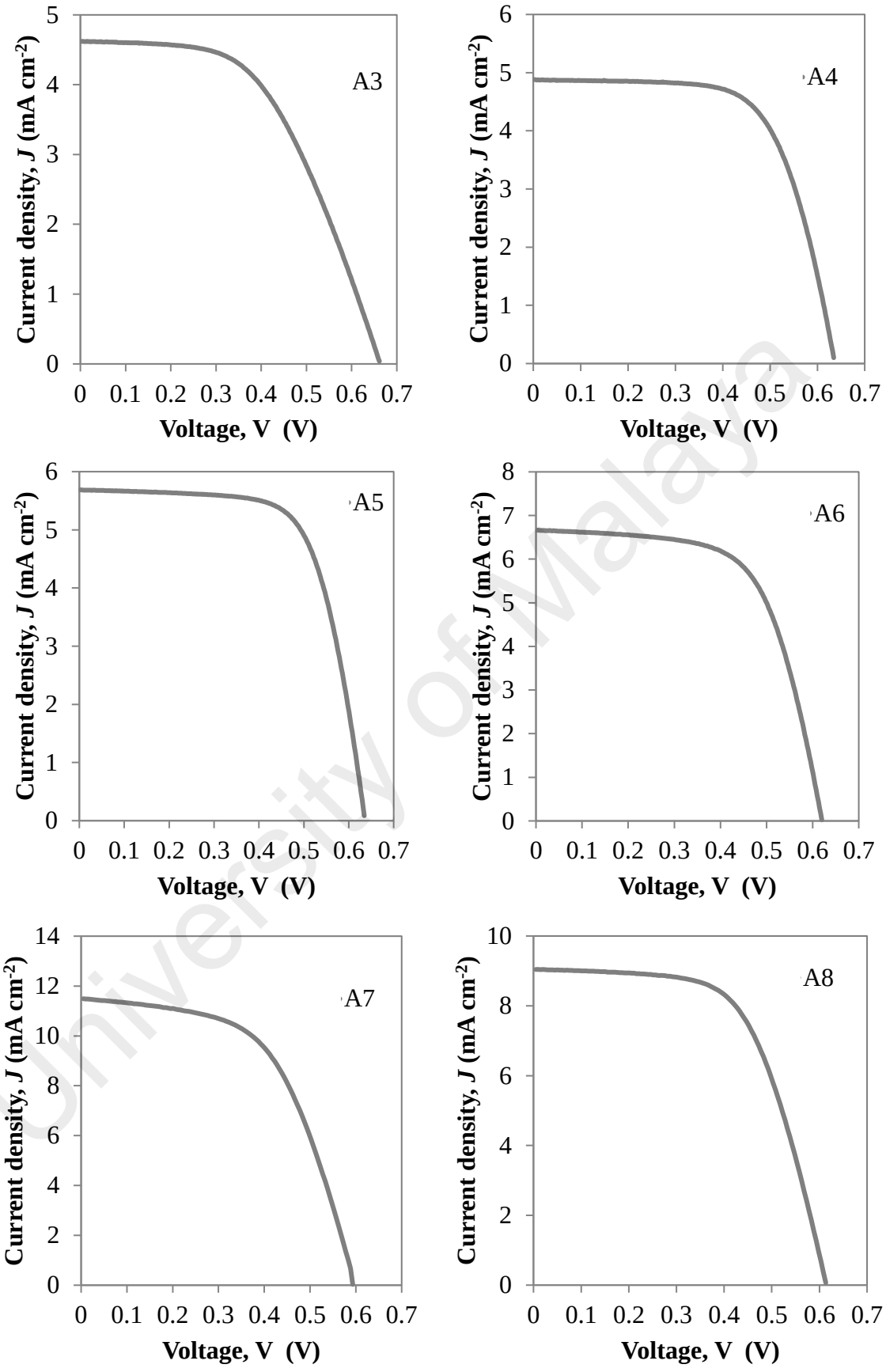

Figure 7.1, continued.

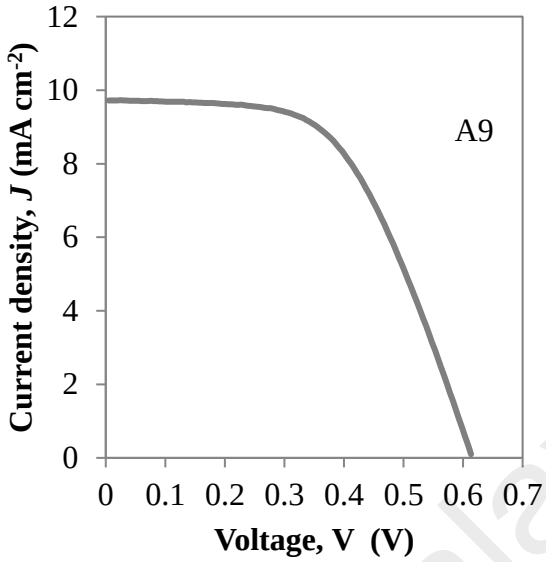

Figure 7.1, continued.

Table 7.1 lists the main parameters of DSSC obtained from the *J-V* curves in Figure 7.1. The J_{sc} value is almost same for DSSC, having A1 and A2 gel polymer electrolytes. The small value of J_{sc} which is 4.08 mA cm^{-2} for DK1 cell and 4.02 mA cm^{-2} for DK2 cell are due to the gel polymer electrolytes used containing small amount of KI. Small amount of KI exhibits low ionic conductivity value (Table 6.1) which leads to small J_{sc} value. The J_{sc} value is gradually increased for DSSCs having A3 to A7 electrolytes. The value increased up to 11.49 mA cm^{-2} for DK7 cell. Comparing DK7 cell with DK1 and DK2 cells, DK7 cell exhibits almost three times higher J_{sc} value. The J_{sc} value decreases to 9.04 mA cm^{-2} and 9.72 mA cm^{-2} for DK8 and DK9 cells respectively. The V_{oc} value is almost unchanged for DK1 cell to DK5 cell which is around 0.65 V. The value slightly decreased to 0.59 V for DK7 cell.

Table 7.1: Parameter of DSSC using gel electrolytes contain different of wt. % of KI

DSSC	Sample	J_{sc} (mA cm^{-2})	V_{oc} (V)	*ff*	Efficiency (%)
DK1	A1	4.08	0.64	0.46	1.20
DK2	A2	4.02	0.65	0.48	1.25
DK3	A3	4.62	0.65	0.53	1.59
DK4	A4	4.88	0.64	0.67	2.09
DK5	A5	5.69	0.64	0.68	2.48
DK6	A6	6.67	0.62	0.63	2.61
DK7	A7	11.49	0.59	0.56	3.80
DK8	A8	9.04	0.61	0.62	3.42
DK9	A9	9.72	0.61	0.56	3.32

The efficiency of DSSCs seems to follow the trends of ionic conductivity. Figure 7.2 shows the plotted graph of efficiency versus KI concentration. The efficiency increased up to 3.80 % for DSSC having A7 gel polymer electrolyte (DK7 cell) before decreased to 3.32 % for DK9 cell.

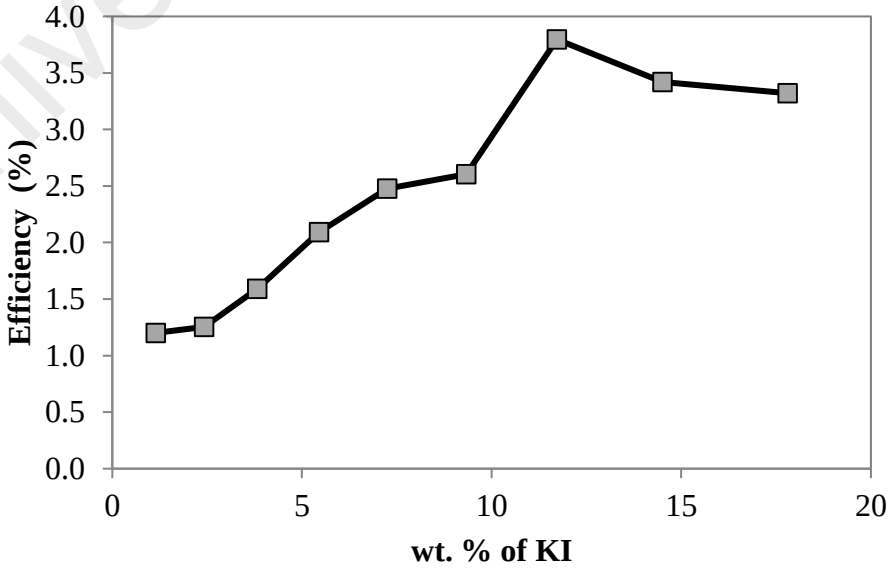

Figure 7.2: Efficiency vs wt. % of KI

7.3. DSSC for PVA-EC-PC-DMSO-KI-TMAI gel electrolytes

Figure 7.3 shows the *J-V* curves for DSSC utilizing PVA-EC-PC-DMSO-KI-TMAI gel polymer electrolytes systems (B1 to B4).

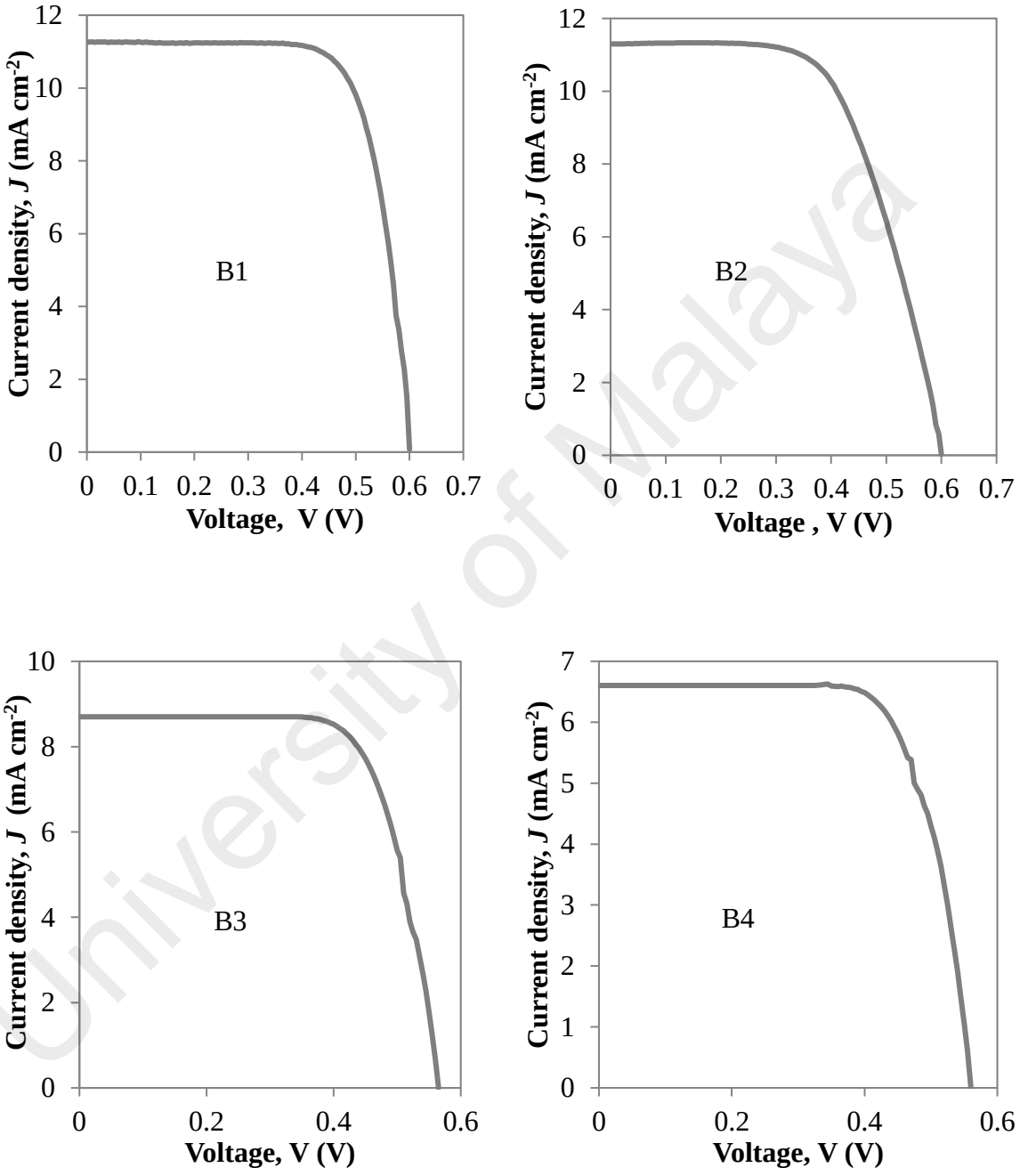

Figure 7.3: *J-V* curves for dye-sensitized solar cell (DSSC) (KI-TMAI salts)

The parameters obtained from the *J-V* curve in Figure 7.3 are listed in Table 7.2. It can be observed that the highest J_{sc} value obtained is 11.30 mA cm^{-2} for DSSC having B1 gel polymer electrolyte (DKM1 cell). However, the decrement in J_{sc} was observed for DKM2, DKM3 and DKM4 cell. From Table 7.2, it can be observed that the open circuit voltage, V_{oc} for all DSSC having gel polymer electrolyte containing KI-TMAI salts exhibits the values ranging between 0.56 V and 0.60 V. The fill factor (*ff)* is observed in the range of 0.61 to 0.79.

The highest efficiency of 5.02 % was observed for DSSC having B1 gel polymer electrolyte (DKM1 cell). The efficiency decreases when gel polymer electrolyte containing higher amount of TMAI were used in DSSC (DKM2, DKM3 and DKM4)

Table 7.2: Parameters of DSSCs using gel electrolytes contain different amount of KI-TMAI

DSSC	Samples	J_{sc} (mA cm^{-2})	V_{oc} (V)	Fill factor (*ff)*	Efficiency, η (%)
DKM1	B1	11.30	0.60	0.74	5.02
DKM2	B2	11.20	0.60	0.61	4.10
DKM3	B3	8.70	0.57	0.74	3.67
DKM4	B4	6.60	0.56	0.79	2.92

7.4. DSSC for PVA-EC-PC-DMSO-KI-TPAI gel electrolytes

Figure 7.4 shows the *J-V* curves for DSSC utilizing PVA-EC-PC-DMSO-KI-TPAI gel polymer electrolytes systems (C1 to C4).

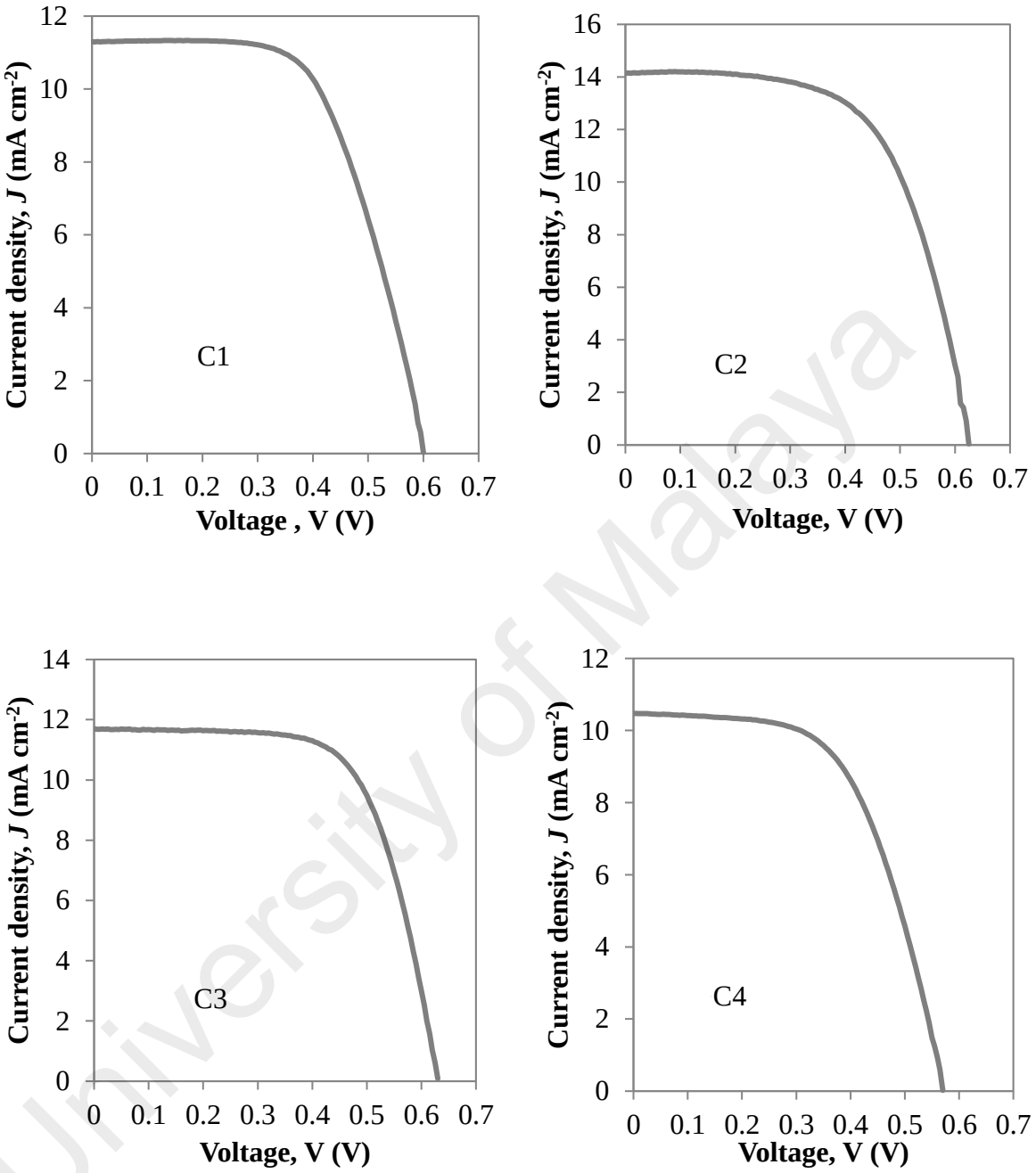

Figure 7.4: *J-V* curves for dye-sensitized solar cell (DSSC) (KI-TPAI salts)

The parameters obtained from the *J-V* curve in Figure 7.4 are listed in Table 7.3. It can be observed that the highest J_{sc} value obtained is 14.10 mA cm^{-2} for DSSC having C2 gel polymer electrolyte (DKP2 cell). However, the decrement in J_{sc} was observed for DKP3 and DKP4 cell.

From Table 7.3, it can be observed that the open circuit voltage, V_{oc} for all DSSC having gel polymer electrolyte containing KI-TPAI salts exhibits the values ranging between 0.57 V and 0.63 V. The fill factor (*ff)* is observed in the range of 0.58 to 0.66.

The highest efficiency of 5.51 % was observed for DSSC having C2 gel polymer electrolyte (DKP2 cell). The efficiency decreases when gel polymer electrolyte containing higher amount of TPAI were used in DSSC (DKP3 and DKP4)

Table 7.3: Parameter of DSSC using gel electrolytes contain different amount of KI-TPAI

DSSC	Samples	J_{sc} (mA cm^{-2})	V_{oc} (V)	Fill factor (*ff)*	Efficiency, η (%)
DKP1	C1	11.20	0.60	0.61	4.10
DKP2	C2	14.10	0.63	0.62	5.51
DKP3	C3	11.69	0.63	0.66	4.86
DKP4	C4	10.47	0.57	0.58	3.46

7.5. DSSC for PVA-EC-PC-DMSO-KI-TBAI gel electrolytes

Figure 7.5 shows the *J-V* curves for DSSC utilizing PVA-EC-PC-DMSO-KI-TBAI gel polymer electrolytes systems (D1 to D4).

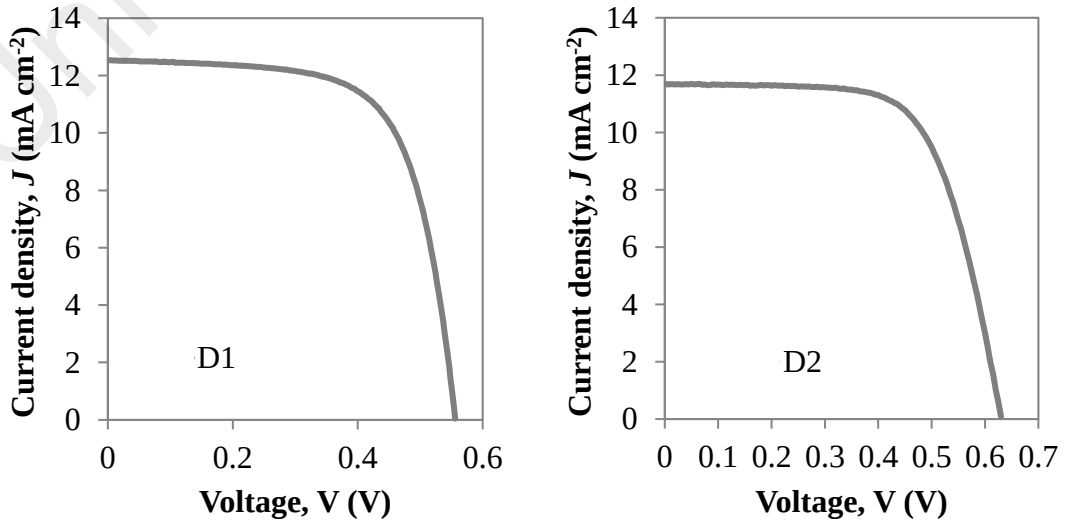

Figure 7.5: *J-V* curves for dye-sensitized solar cell (DSSC) (KI-TBAI salts)

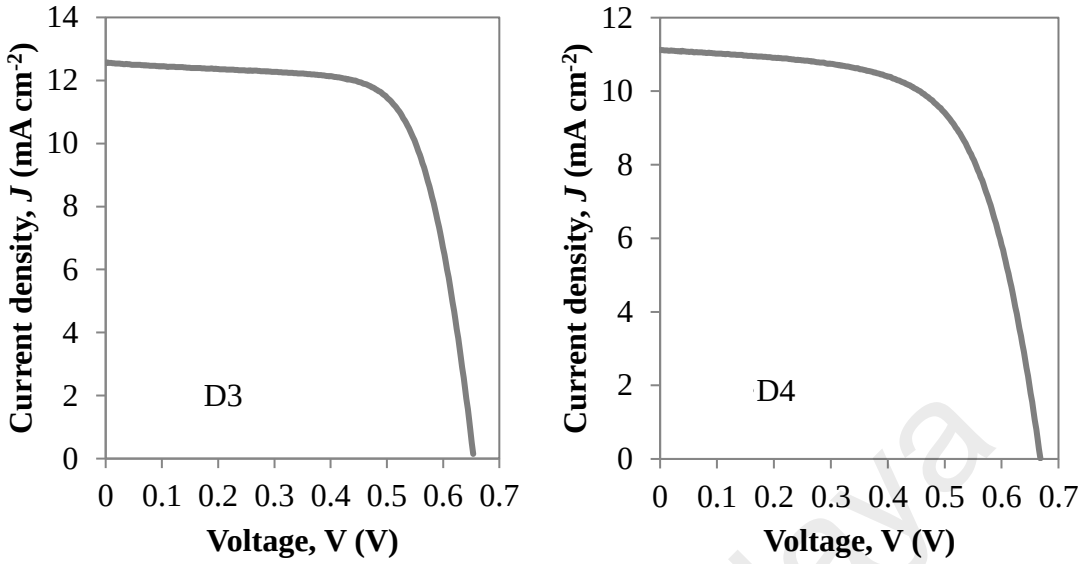

Figure 7.5, continued.

The parameters obtained from the *J-V* curve in Figure 7.5 are listed in Table 7.4. It can be observed that the highest J_{sc} value obtained is 12.56 mA cm^{-2} for DSSC having D3 gel polymer electrolyte (DKB3 cell). However, the decrement in J_{sc} was observed for DKB4 cell. From Table 7.4, it can be observed that the open circuit voltage, V_{oc} for all DSSC having gel polymer electrolyte containing KI-TBAI salts exhibits the values ranging between 0.60 V and 0.67 V. The fill factor (*ff)* is observed in the range of 0.61 to 0.71.

The highest efficiency of 5.80 % was observed for DSSC having D3 gel polymer electrolyte (DKB3 cell). The efficiency decreases when gel polymer electrolyte containing higher amount of TBAI were used in DSSC (DKB4)

Table 7.4: Parameter of DSSC using gel electrolytes contain different amount of KI-TBAI

DSSC	Samples	J_{sc} (mA cm^{-2})	V_{oc} (V)	Fill factor (*ff*)	Efficiency, η (%)
DKB1	D1	11.20	0.60	0.61	4.10
DKB2	D2	11.69	0.63	0.66	4.86
DKB3	D3	12.56	0.65	0.71	5.80
DKB4	D4	11.13	0.67	0.63	4.70

7.6. DSSC for PVA-EC-PC-DMSO-KI-TPAI-DEC system

Figure 7.6 shows the *J-V* curves for DSSC utilizing PVA-EC-PC-DMSO-KI-TPAI-DEC gel polymer electrolytes systems (E1 to E4).

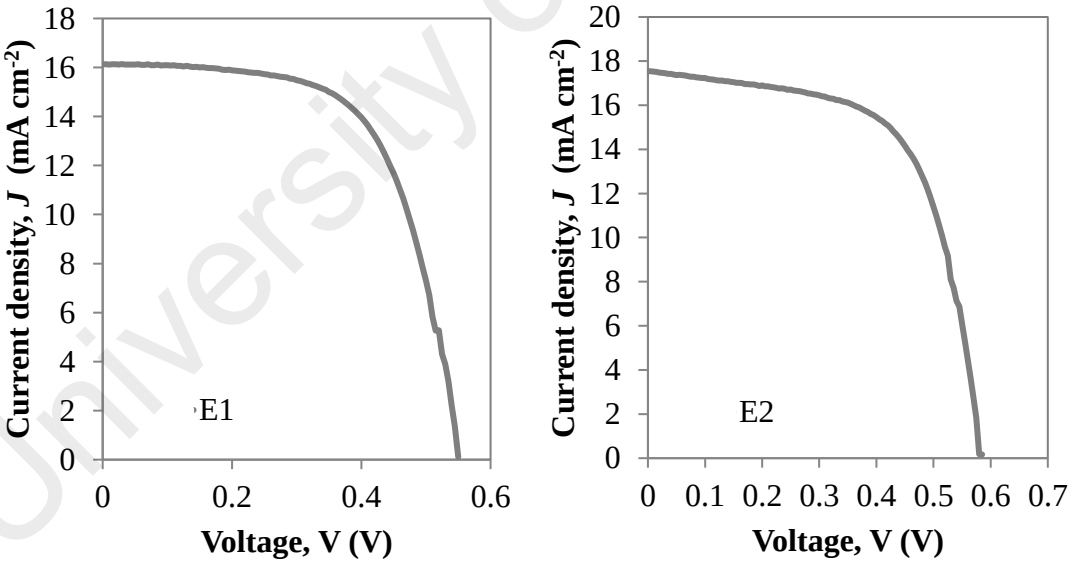

Figure 7.6: *J-V* curves for dye-sensitized solar cell (DSSC) (KI-TPAI-DEC)

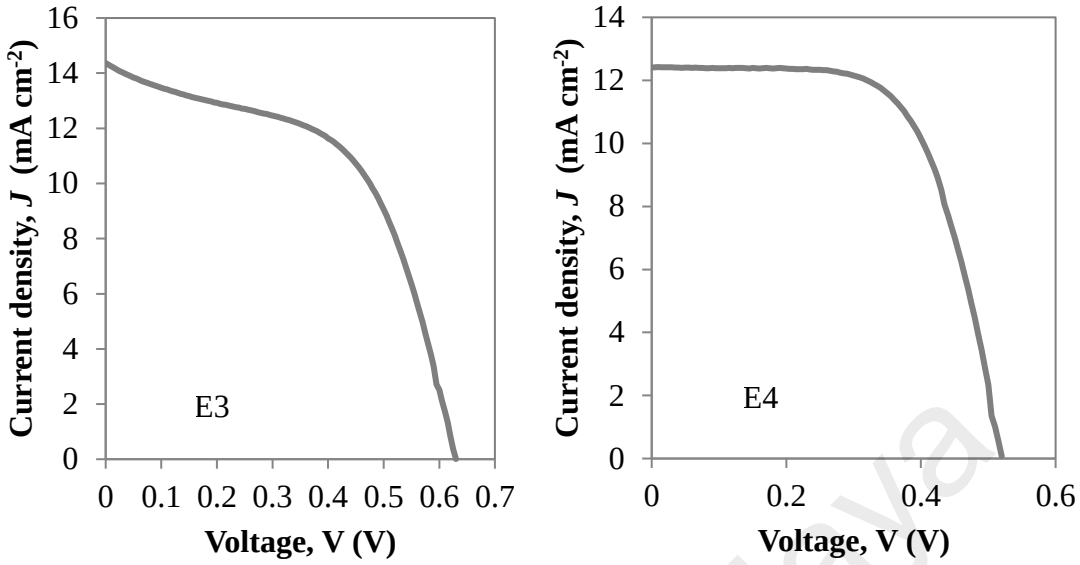

Figure 7.6, continued.

The parameters obtained from the *J-V* curves in Figure 7.6 are listed in Table 7.5. It can be observed that the highest J_{sc} value obtained is 17.58 mA cm^{-2} for DSSC having E2 gel polymer electrolyte (DKPD2 cell). However, the decrement in J_{sc} was observed for DKPD3 and DKPD4 cell. From Table 7.5, it can be observed that the open circuit voltage, V_{oc} for all DSSC having gel polymer electrolyte containing DEC exhibits the values ranging between 0.52 V and 0.63 V. The fill factor (*ff)* is observed in the range of 0.54 to 0.64.

Table 7.5: Parameter of DSSC using gel electrolytes contain different amount of DEC

DSSC	Samples	J_{sc} (mA cm^{-2})	V_{oc} (V)	Fill factor (*ff)*	Efficiency,η (%)
DKPD1	E1	16.13	0.55	0.63	5.59
DKPD2	E2	17.58	0.58	0.63	6.42
DKPD3	E3	14.37	0.63	0.54	4.89
DKPD4	E4	12.42	0.52	0.64	4.13

The highest efficiency of 6.42 % was observed for DSSC having E2 gel polymer electrolyte (DKPD2 cell). The efficiency decreases when gel polymer electrolyte containing higher amount of DEC were used in DSSC (DKPD3 and DKPD4)

7.7. DSSC for PVA-EC-PC-DMSO-KI-TBAI-DEC system

Figure 7.7 shows the *J-V* curves for DSSC utilizing PVA-EC-PC-DMSO-KI-TBAI-DEC gel polymer electrolytes systems (F1 to F4).

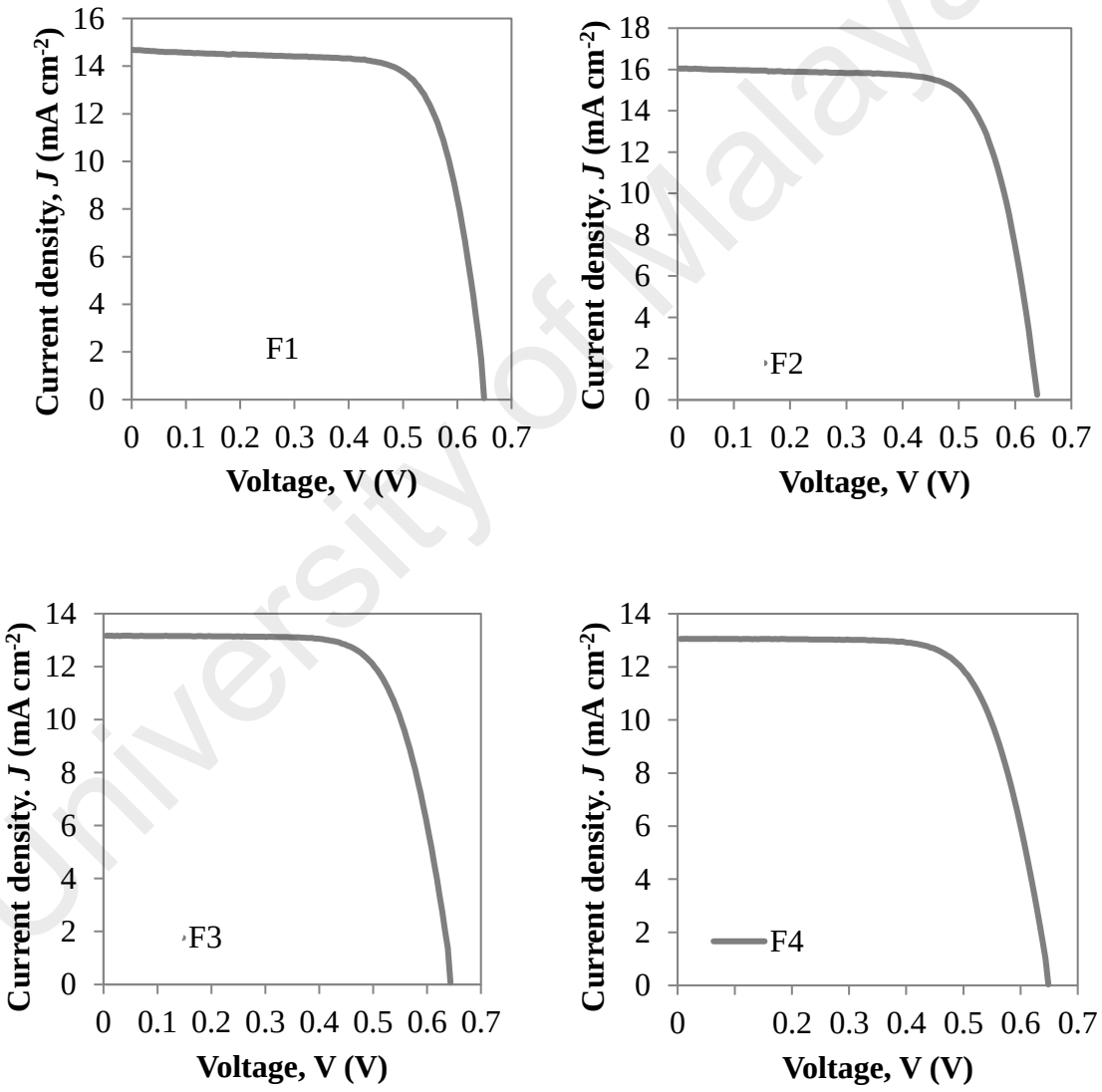

Figure 7.7: *J-V* curves for dye-sensitized solar cell (DSSC) (KI-TBAI-DEC)

Table 7.6: Parameter of DSSC using gel electrolytes contain different amount of DEC

DSSC	Samples	J_{sc} (mA cm^{-2})	V_{oc} (V)	Fill factor (*ff*)	Efficiency, η (%)
DKBD1	F1	14.69	0.65	0.73	6.97
DKBD2	F2	16.05	0.64	0.73	7.50
DKBD3	F3	13.17	0.65	0.71	6.08
DKBD4	F4	13.05	0.65	0.70	5.94

The parameters obtained from the *J-V* curves in Figure 7.7 are listed in Table 7.6. It can be observed that the highest J_{sc} value obtained is 16.05 mA cm^{-2} for DSSC having F2 gel polymer electrolyte (DKBD2 cell). However, the decrement in J_{sc} was observed for DKBD3 and DKBD4 cell. From Table 7.6, it can be observed that the open circuit voltage, V_{oc} for all DSSC having gel polymer electrolyte containing DEC exhibits the values ranging between 0.64 V and 0.65 V. The fill factor (*ff)* is observed in the range of 0.70 to 0.73.

The highest efficiency of 7.50 % was observed for DSSC having F2 gel polymer electrolyte (DKBD2 cell). The efficiency decreases when gel polymer electrolyte containing higher amount of DEC were used in DSSC (DKBD3 and DKBD4)

7.8. Summary

In this chapter, all the *J-V* curves for DSSCs having PVA-EC-PC-DMSO-KI, PVA-EC-PC-DMSO-KI-TMAI, PVA-EC-PC-DMSO-KI-TPAI, PVA-EC-PC-DMSO-KI-TBAI, PVA-EC-PC-DMSO-KI-TPAI-DEC and PVA-EC-PC-DMSO-KI-TBAI-DEC gel polymer electrolytes has been plotted. For DSSCs having PVA-EC-PC-DMSO-KI gel polymer electrolytes system, the efficency increases when the KI salt amount increases. The efficiency is slightly increase with the addition of quarternary ammonium iodide salts and DEC plasticizer into the electrolytes.

CHAPTER 8: DISCUSSION

In 1991, Grätzel and co-researchers has reported a new prospective of solar cell technology using dye-sensitized solar cell with efficiency of ~8 %. Since then, DSSC has been chosen as an alternative for silicon-based solar cells replacement. Dye sensitized solar cell (DSSC) is developing as promising device having some advantages such as (Grätzel 2001):

- Low cost production
- Simple fabrication
- High efficiency.

At the moment, the highest efficiency of DSSC is reported by Kakiage *et al.* (2015). The efficiency was 14 %. The most popular oxide wide bandgap semiconductor used in DSSC was nanocrystalline titania (TiO_2). TiO_2 has developed as versatile oxide ceramic material. Various applications of TiO_2 such as lithium-ion batteries, solar cell and photo-catalysis have been reported (Xu *et al.*, 2007; Park *et al.*, 2011; Ochiai & Fujishima, 2012). TiO_2 nanoparticles have been choosen in this work due to some good properties which have been discussed in Chapter 2. In this work, the double TiO_2 layer has been applied on the FTO glass. The first layer, which is P90-TiO_2 has small particle size (15 nm) are coated on the top of conductive side FTO glass. Then for the second layer, P25-TiO_2 which is has larger particle size (25 nm) has been coated on the top of P90-TiO_2 first layer. The double layers of TiO_2 are influence higher DSSC efficiency by improving light harvesting properties (Im *et al.*, 2011). Each TiO_2 layers has own purpose such as P90-TiO_2 layer has large surface area. In this case, large surface area means by high dye adsorption for TiO_2 nanoparticle (Zhang & Cao, 2011). A dense P90-TiO_2 layer is able to suppress the electron recombination at the

photoanode/electrolyte interface. In addition, P90-TiO_2 layer also has less contact resistance which results in high open circuit voltage, V_{oc}. P25-TiO_2 layer improve the durable light scattering ability and also improve the optical absorption path (Ferber and Luther 1998). This P25-TiO_2 layer also can increase the short-circuit current density, J_{sc} (Jeng *et al*., 2013).

There are some aspects that are critical for electrolytes in the DSSC fabrication such as good contact between TiO_2-dye photoanode and platinum counter electrode, long-term stability, good properties, fast diffusion of charge carrier and not display a significant absorption in the visible range of light (Nogueira *et al*., 2004; Li *et al*., 2006) as discussed in Chapter 2. In this work, gel polymer electrolyte has been choosed in DSSC fabrication which due to some good aspect such as a better contact and high filling property compared to solid polymer electrolyte. Gel polymer electrolyte is also a circumventing approach for the solid and liquid electrolytes problem. In addition, gel-form electrolyte is attending high conductivities where this kind of electrolyte has properties of holding liquid electrolyte by trapping in cages with the polymer host matrices (Wu *et al*., 2006). Polyvinyl alcohol is a synthetic polymer and has outstanding feature with some advantage as discussed in Chapter 2. The chosen of KI salt due to the K^+ cations improve more in open-circuit voltage and fill factor of DSSC performance compare to the other salt such as LiI and NaI (Shi *et al*., 2011). The iodide/triiodide couple has been chosen in this work due to the slow recombination rate with injected electrons in the photoanode (Oskam *et al*., 2001; Lan *et al*., 2006).

Six systems (PVA –DMSO –EC –PC -KI, PVA –DMSO –EC –PC –KI -TMAI, PVA –DMSO –EC –PC –KI -TPAI, PVA –DMSO –EC –PC –KI -TBAI, PVA –DMSO –EC –PC –KI –TPAI -DEC and PVA –DMSO –EC –PC –KI –TBAI -DEC) of gel polymer electrolytes have been prepared in this work. The interactions between polymer, solvent and salts have been investigated via FTIR spectroscopy. The FTIR spectrum of the PVA

powder, DMSO solvent and the gelled PVA-DMSO are shown in Figure 4.1. The O-H stretching of PVA powder is observed at 3316 cm^{-1} (Bhavani *et al*., 2013). Buraidah and Arof (2011) have reported that the hydroxyl band of pure PVA film is observed at 3313 cm^{-1}. The band was shifted to a new location which is 3405 cm^{-1} for PVA-DMSO indicating that the complexation between PVA and DMSO has occured. The S=O band of DMSO has been observed at 1026 cm^{-1} (Nakamoto, 1986). This peak has been shifted to a lower wavenumber at 1017 cm^{-1} for the PVA-DMSO sample. This confirms that the complexation between PVA and DMSO has occurred via sulphur atom (Awadhia & Agrawal, 2007).

The C-O-C stretch of EC and PC can be observed at the region between 1200 to 1150 cm^{-1} (Zhang *et al*., 2013) as shown in Figure 4.3. The C-O-C band was observed at 1156 cm^{-1} for EC and 1180 cm^{-1} for PC. The peak was shifted to 1163 cm^{-1} for DMSO-EC and 1184 cm^{-1} for DMSO-PC. This indicates that there is interaction between DMSO, EC and PC at the C-O-C band. The mixture of DMSO, EC and PC exhibits two peaks (1180 cm^{-1} and 1169 cm^{-1}). In addition, the peaks show at 1767 cm^{-1} and 1794 cm^{-1} for EC and 1782 cm^{-1} for PC are assigned to C=O stretching vibrations (Rajendran, 2004). These peaks have been shifted to 1771 cm^{-1} and 1798 cm^{-1} for DMSO-EC and 1786 cm^{-1} for DMSO-PC which indicates that the interaction between DMSO, EC and PC also occurred at C=O band.

The incorporation of salt into the polymer host revealed that cation of the salt is likely to organize with the polar groups of the polymer and result to complexation. This interaction is more expected to affect the main structure of polymer backbone. The hydroxyl band for PVA-EC-PC-DMSO was observed at 3417 cm^{-1}. The band was shifted when the KI salt was added to the PVA-EC-PC-DMSO. This mean that the K^+ cation is interact with the OH group of PVA. However, the observation of shifted peak do not change much in the double iodide system may be due to the large size of

quaternary ammonium cation. Other than OH group, the interaction of salts with PVA-EC-PC-DMSO can also occurred at C-O-C and C=O bands as shown in Table 4.3, 4.4, 4.5, 4.6, and 4.7.

All XRD diffractograms for PVA-DMSO-EC-PC-KI, PVA-DMSO-EC-PC-KI-TMAI, PVA-DMSO-EC-PC-KI-TPAI, PVA-DMSO-EC-PC-KI-TBAI, PVA-DMSO-EC-PC-KI-TPAI-DEC and PVA-DMSO-EC-PC-KI-TBAI-DEC gel polymer electrolytes have been shown in Chapter 5. The amorphous nature of the samples is favorable for ion movement. All gel polymer electrolytes show the prominent peak at $2\theta = 20^{o}$. The peak position agrees well with the peak exist at $2\theta = 20^{o}$ for pure PVA which is shown in the literature (Krumova *et al*., 2000). All the XRD curves has been deconvoluted using Origin Pro 9 software.

The FWHM value for gel polymer electrolytes is increased with the increasing of KI content. The increase value of FWHM indicates that the gel polymer electrolytes is more amorphous. However, in Table 5.2 and Table 5.3, the FWHM value decreases with the amount of quarternary ammonium salts. When the gel polymer electrolyte contains KI-TPAI and KI-TBAI are added with DEC, the FWHM value increases as shown in Table 5.4 and Table 5.5. The DEC plasticizer enhances the segmental motion and flexibility of polymer backbone. Here the gel polymer electrolytes contain DEC plasticizer are more amorphous (Saikia & Kumar, 2004). The amorphous phase of gel polymer electrolyte is important for obtaining high ionic diffusivity leads to greater ionic conductivity (Muthuvinayagam & Gopinathan, 2015).

The conductivity of gel polymer electrolytes is shown in Chapter 6. In the PVA-EC-PC-DMSO-KI system, the RT ionic conductivity increases with the amount of KI. The highest conductivity of 12.50 mS cm^{-1} was observed for A7 gel polymer electrolyte. The increasing in conductivity is due to the increasing in number density and mobility

of charge carriers as shown in Table 6.2. In addition, mobility increases due to the smaller size K^+ ion with lighter weight effect the ion transport in the electrolyte (Sequeira, *et al*., 1994). The conductivity decreases when the amount of KI is more than 12 % (A8 and A9). This is may be due to the formation of ion pairs an ion aggregates. As can be seen in Table 6.2 the number density and mobility of charge carriers are decrease for A8 and A9 gel polymer electrolytes thereby decrease the conductivity.

The replacement of some part of KI with TMAI decreases the conductivity value as shown in Table 6.3. The decrement in conductivity may be attributed to the decreasing in mobility of charge carriers as shown in Table 6.4. Although the number density is increase with TMAI content (Table 6.4), but due to the bulky size of TMA^+ leads to decrease in mobility and overall conductivity. Larger cations are probable to entangle in the polymer and slow to move in the gel polymer electrolytes. Similar observation for gel polymer electrolytes containing TPAI and TBAI salts. The conductivity decreases as the TPAI and TBAI content increases which are due to the decreasing in mobility of charge carriers as shown in Table 6.6 and Table 6.8. The addition of low molecular weight and high dielectric constant plasticizers in the gel polymer electrolyte has significantly increase the amorphous phase of the polymer. This would affect the flexibility and release of mobile charge carriers due to ion dissolution effect (Pitawala *et al*., 2008). The addition of plasticizer also increases the volume of electrolyte system and decreases the viscosity of the electrolyte so that the ions is becomes more easy to mobile (Rahman *et al*., 2011). In addition, the existing of plasticizer decreases the brittleness of polymer due to the transition of glass transition temperature, T_g of polymer and improve electrical conductivity (Reddy *et al*., 2007). As can be seen in Table 6.9 and Table 6.11, the ionic conductivity of gel polymer electrolytes increases with the additional of DEC plasticizer.

For DSSC having PVA-EC-PC-DMSO-KI gel polymer electrolytes system, the J_{sc} shows an increment value starting from DK2 to DK7 (as shown in Table 7.1). The increase in J_{sc} may be due to the increasing in gel polymer electrolyte conductivity. DSSC having the highest conducting gel polymer electrolyte (A7) exhibits the highest J_{sc} value of 11.49 mA cm^{-2}. It is known that the conductivity increase in PVA-EC-PC-DMSO-KI gel polymer electrolyte system is due to the increase in number density and mobility of charge carriers. Thus, when the number density and mobility of I^-/I_3^- increased, the current flows through the cell become faster. Hence the J_{sc} value will be increased. The effect of conductivity for DSSC performance also has been reported by other researcher (Rahman *et al*., 2004). In addition, when small K^+ cations get adsorbed on the TiO_2 surface, the Fermi level of TiO_2 will be shifted to the positive potential toward the valence band (Arof *et al*., 2014). Hence the electrons injection from the excited dye molecules into the conduction band of TiO_2 will be increased resulting in high J_{sc}. The distance between the Fermi level of TiO_2 and redox potential in the electrolyte become smaller. Thus the V_{oc} value should be decreased. From Table 7.1, it can be observed that the V_{oc} value of DSSCs is almost same for DK1 to DK4 cells which are around 0.65 V. The V_{oc} value decreased to 0.59 V for DK7 cell. Hence, it can be deduced that the effect of K^+ cations can only be observed for DSSC having A6 and A7 gel polymer electrolyte (DK6 and DK7 cells).

The efficiency seem likely to increase marginally start from 1.20 % for DK1 cell up to 3.80 % for DK7 cell. However, the efficiency is decreased to 3.42 % and 3.32 % for DK8 and DK9 cells respectively. It can be observed that the efficiency of DSSCs utilizing PVA-DMSO-EC-PC-KI gel polymer electrolyte follows the trends of ionic conductivity.

Quaternary ammonium iodide salts have been choosen to improve the performance of DSSC. The salt was TMAI, TPAI and TBAI. Generally, the ionic conductivity of gel

polymer electrolyte is contributed by cations and anions. In gel polymer electrolyte containing only KI salt as iodide source, the conductivity is resolute by the association of K^+ cations and I^- anions. However, when part of amount KI salt has been replaced by the TMAI salt the ionic conductivity is contributed by K^+, TMA^+ and I^- ions.

Although the ionic conductivity of gel polymer electrolytes decreases with addition of TMA, TPAI and TBAI salts, the performance of DSSCs are slightly improved as shown in Table 7.2 to Table 7.4. The J_{sc} for gel polymer electrolytes contain dual iodide (KI-TPAI, KI-TBAI) show an increment value compared to gel polymer electrolyte contain only KI salt. The increase in J_{sc} value may be attributed to the increase in number density and mobility of iodide ions. Since the size of cations are large, the major contribution in conductivity is probably iodide ion. The large number of iodide ion helps to increase in the short circuit current density and also the efficiency of DSSC (Arof *et al*., 2014). In addition the larger cations will not easily adhere to TiO_2 surface due to their bulkiness (Bandara *et al*., 2013). The decrease in J_{sc} for DKMI cells may be due to the TMAI is incompletely dissolved in PVA-DMSO-EC-PC-KI-TMAI gel polymer electrolyte.

As can been seen in Table 7.2 to 7.4 the V_{oc} value didn't shows any decrement when TMAI, TPAI and TBAI are added into gel polymer electrolyte. The decreasing value of V_{oc} for DKM3, DKM4 and DKP4 may be due to the increasing in electron recombination process at the photoanode/electrolyte interface. Hence, the performance of DSSC is controlled by the electron injection and regeneration of dyes by iodide ions.

In the PVA-EC-PC-DMSO-KI-TPAI-DEC and PVA-EC-PC-DMSO-KI-TBAI-DEC system, the conductivity show an increase trend where sample C2 and D3 has conductivity of 7.59 mS cm^{-1} and 5.25 mS cm^{-1} are increase up to 11.20 mS cm^{-1} and 6.19 mS cm^{-1} for sample E2 and F2 respectively.

From Table 7.3, it can be observed the highest efficiency of DSSC having PVA-DMSO-EC-PC-KI-TPAI gel polymer electrolytes system was 5.51 % for DKP2 cell. In the PVA-DMSO-EC-PC-KI-TBAI gel polymer electrolytes system, the highest efficiency was 5.8 % for DKB3 cell. The compositions of gel polymer electrolytes in both cells have been added with the DEC plasticizer. It can be observed that the efficiency increase up to 6.42 % for DKPD2 cell and 7.5 % for DKBD2 cell. This is because of DEC plasticizer present where DEC helps ion dissociation and ion mobile in the gel electrolyte. Thus, DEC also enhances conductivity of gel electrolyte and DSSC efficiency surely (Rajendran *et al*., 2004).

CHAPTER 9 : CONCLUSIONS AND SUGGESTION FOR FURTHER WORK

Gel polymer electrolytes such as PVA-EC-PC-DMSO-KI, PVA-EC-PC-DMSO-KI-TMAI, PVA-EC-PC-DMSO-KI-TPAI, PVA-EC-PC-DMSO-KI-TBAI, PVA-EC-PC-DMSO-KI-TPAI-DEC and PVA-EC-PC-DMSO-KI-TBAI-DEC have been successfully prepared. The FTIR spectrum of PVA-DMSO exhibits that the hydroxyl band of PVA which was shifted from 3316 cm^{-1} to a new location which is 3405 cm^{-1}. The S=O band of DMSO was also shifted from 1026 cm^{-1} to 1017 cm^{-1} indicating that the complexation between PVA and DMSO has occurred. The C-O-C peak was observed for EC and PC at 1156 cm^{-1} and 1180 cm^{-1}, respectively. There is no such peak observed in the spectrum of DMSO. This peak was shifted to 1163 cm^{-1} in DMSO-EC spectrum and 1184 cm^{-1} in DMSO-PC spectrum. The incorporation of salt into the gel of PVA-DMSO-EC-PC shows the O-H, C-O-C and C=O bands are shifted to higher or lower wavenumbers indicating there is interaction between the materials.

All gel electrolytes also show that the prominent peak at $2\theta = 20^{o}$. The peak position agrees well with the peak located at $2\theta = 20^{o}$ for pure PVA. The FWHM for each gel polymer electrolytes with different amount of KI salt is increasing with the increase of KI salt amount. Increment in FWHM value implies that the gel polymer electrolytes have become more amorphous. The decrease in FWHM value in the quaternary ammonium salt indicates that the gel polymer electrolytes are less amorphous. The amorphous of gel electrolytes containing KI-TPAI and KI-TBAI have increased with the addition of DEC plasticizer.

The conductivity of gel polymer electrolytes increases with the amount of KI content. The conductivity decreases when part of KI salt was replaced with TMAI, TPAI and TBAI salts. This may be due to the bulky size of TMA^{+}, TPA^{+}, and TBA^{+}

which makes them less mobile in the gel polymer electrolytes. The conductivity increased when DEC was added. The temperature dependent conductivity follows the Arhenius relation. The highest efficiency of DSSC obtained was 7.5 % for DSSC having F2 gel polymer electrolyte.

In order to improve the performance of DSSC in future, some suggestions are forwarded:

- Improve the conductivity of the electrolyte up to 10^{-1} S cm^{-1}.
- Using different techniques of TiO_2 electrode preparation such as printing method.
- Improve the sealing technique of DSSC fabrication. The sealing method and technique should be improved.

REFERENCES

Agarwala, S., Thummalakunta, L. N. S. A., Cook, C. A., Peh, C. K. N., Wong, A. S. W., Ke, L., and Ho, G. W. (2011). Co-existence of LiI and KI in filler-free, quasi-solid-state electrolyte for efficient and stable dye-sensitized solar cell. *Journal of Power Sources, 196*(3), 1651-1656

Agrawal, S., and Shukla, P. (2000). Structural and electrical characterization of polymeric electrolytes: PVA-NH~ 4SCN system. *Indian Journal of Pure and Applied Physics, 38*(1), 53-61.

Ahad, N., Saion, E., and Gharibshahi, E. (2012). Structural, thermal, and electrical properties of PVA-Sodium Salicylate solid composite polymer electrolyte. *Journal of Nanomaterials, 2012*, 8. doi : 10.1155/2012/857569

Ahmad, S., Ab Kadir, M. Z. A., and Shafie, S. (2011). Current perspective of the renewable energy development in Malaysia. *Renewable and Sustainable Energy Reviews, 15*(2), 897-904.

An, H., Xue, B., Li, D., Li, H., Meng, Q., Guo, L., and Chen, L. (2006). Environmentally friendly LiI/ethanol based gel electrolyte for dye-sensitized solar cells. *Electrochemistry Communications, 8*(1), 170-172.

Andersson, A., Johansson, N., Broms, P., Yu, N., Lupo, D., and Salaneck, W. R. (1998). Fluorine tin oxide as an alternative to indium tin oxide in polymer LEDs. *Advanced Materials,* 10(11), 859-863.

Arof, A. K., Aziz, M. F., Noor, M. M., Careem, M. A., Bandara, L. R. A. K., Thotawatthage, C. A., Rupasinghe, W. N. S., and Dissanayake, M. A. K. L. (2014). Efficiency enhancement by mixed cation effect in dye-sensitized solar cells with a PVdF based gel polymer electrolyte. *International Journal of Hydrogen Energy, 39*(6), 2929-2935.

Arof, A. K., Naeem, M., Hameed, F., Jayasundara, W. J. M. J. S. R., Careem, M. A., Teo, L. P., and Buraidah, M. H. (2014). Quasi solid state dye-sensitized solar cells based on polyvinyl alcohol (PVA) electrolytes containing I^-/I_3^- redox couple. *Optical and Quantum Electronics, 46*(1), 143-154.

Attia, G., and El-Kader, M. A. (2013). Structural, optical and thermal characterization of PVA/2HEC polyblend films. *International Journal of Electrochemical Science, 8*, 5672-5687.

Awadhia, A., and Agrawal, S. L. (2007). Structural, thermal and electrical characterizations of PVA:DMSO:NH4SCN gel electrolytes. *Solid State Ionics, 178*(13–14), 951-958.

Awadhia, A., Patel, S., and Agrawal, S. (2006). Dielectric investigations in PVA based gel electrolytes. *Progress in Crystal Growth and Characterization of Materials, 52*(1), 61-68.

Aziz, M. F., Noor, I. M., Sahraoui, B., and Arof, A. K. (2014). Dye-sensitized solar cells with PVA-KI-EC-PC gel electrolytes. *Optical and Quantum Electronics, 46*(1), 133-141.

Bagher, A. M., Vahid, M. M. A., and Mohsen, M. (2015). Types of solar cells and application. *American Journal of Optics and Photonics, 3*(5), 94-113.

Bandara, T. M. W. J., Jayasundara, W. J. M. J. S. R., Dissanayake, M. A. K. L., Furlani, M., Albinsson, I., and Mellander, B. E. (2013). Effect of cation size on the performance of dye sensitized nanocrystalline TiO_2 solar cells based on quasi-solid state PAN electrolytes containing quaternary ammonium iodides. *Electrochimica Acta, 109*, 609-616.

Bandara, T.M.W.J., and Mellander, B.-E. (2011). Evaluation of mobility, diffusion coefficient and density of charge carriers in ionic liquids and novel electrolytes based on a new model for dielectric response, ionic liquids: theory, properties, new approaches, Prof. Alexander Kokorin (Ed.), InTech, DOI: 10.5772/15183.

Bang, S. Y., Ko, M. J., Kim, K., Kim, J. H., Jang, I.-H., and Park, N.-G. (2012). Evaluation of dye aggregation and effect of deoxycholic acid concentration on photovoltaic performance of N749-sensitized solar cell. *Synthetic Metals, 162*(17–18), 1503-1507.

Bassner, S. L., and Klingenberg, E. H. (1998). Using poly (vinyl alcohol) as a binder. *American Ceramic Society Bulletin, 77*(6), 71-75.

Bhavani, S., Pavani, Y., Ravi, M., Kiran Kumar, K., and Narasimha Rao, V. V. R. (2013). Structural and electrical properties of pure and $NiCl_2$ doped PVA polymer electrolytes. *American Journal of Polymer Science, 3*(3), 56-62.

Boschloo, G., and Hagfeldt, A. (2009). Characteristics of the iodide/triiodide redox mediator in dye-sensitized solar cells. *Accounts of Chemical Research, 42*(11), 1819-1826.

Buraidah, M. H., and Arof, A. K. (2011). Characterization of chitosan/PVA blended electrolyte doped with NH_4I. *Journal of Non-Crystalline Solids, 357*(16), 3261-3266.

Buraidah, M. H., Teo, L. P., Majid, S. R., and Arof, A. K. (2009). Ionic conductivity by correlated barrier hopping in NH_4I doped chitosan solid electrolyte. *Physica B: Condensed Matter, 404*(8–11), 1373-1379.

Calogero, G. and Marco, G. D. (2008). Red Sicilian orange and purple eggplant fruits as natural sensitizers for dye-sensitized solar cells. *Solar Energy Materials and Solar Cells, 92*(11), 1341-1346.

Carp, O., Huisman, C. L., and Reller, A. (2004). Photoinduced reactivity of titanium dioxide. *Progress in Solid State Chemistry, 32*(1–2), 33-177.

Chang, H., and Lo, Y.-J. (2010). Pomegranate leaves and mulberry fruit as natural sensitizers for dye-sensitized solar cells. *Solar Energy, 84*(10), 1833-1837.

Chen, J., Peng, T., Fan, K., and Xia, J. (2011). Iodine-free quasi solid-state dye-sensitized solar cells based on ionic liquid and alkali salt. *Journal of Materials Chemistry, 21*(41), 16448-16452.

Ding, M., Xu, K., Zhang, S., Amine, K., Henriksen, G., and Jow, T. (2001). Change of conductivity with salt content, solvent composition, and temperature for electrolytes of $LiPF_6$ in ethylene carbonate-ethyl methyl carbonate. *Journal of the Electrochemical Society, 148*(10), A1196-A1204.

Dissanayake, M. A. K. L., Jayathissa, R., Seneviratne, V. A., Thotawatthage, C. A., Senadeera, G. K. R., and Mellander, B. E. (2014). Polymethylmethacrylate (PMMA) based quasi-solid electrolyte with binary iodide salt for efficiency enhancement in TiO_2 based dye sensitized solar cells. *Solid State Ionics, 265*, 85-91.

Dissanayake, M. A. K. L., Thotawatthage, C. A., Senadeera, G. K. R., Bandara, T. M. W. J., Jayasundera, W. J. M. J. S. R., and Mellander, B. E. (2012). Efficiency enhancement by mixed cation effect in dye-sensitized solar cells with PAN based gel polymer electrolyte. *Journal of Photochemistry and Photobiology A: Chemistry, 246*, 29-35.

Feldman, D. (1988). Polymer electrolyte reviews, J. R. MacCallum and C. A. Vincent, (Eds) Elsevier Applied Science, New York, 1987, pp. 351. *Journal of Polymer Science Part C: Polymer Letters, 26*(8), 371-372.

Ferber, J., and Luther, J. (1998). Computer simulations of light scattering and absorption in dye-sensitized solar cells. *Solar Energy Materials and Solar Cells, 54*(1-4), 265-275.

Godibo, D. J., Anshebo, S. T., and Anshebo, T. Y. (2015). Dye sensitized solar cells using natural pigments from five plants and quasi-solid state electrolyte. *Journal of the Brazilian Chemical Society, 26*(1), 92-101.

Govindaraj, G., Baskaran, N., Shahi, K., and Monoravi, P. (1995). Preparation, conductivity, complex permittivity and electric modulus in $AgI \cdot Ag_2O \cdot SeO_3 \cdot MoO_3$ glasses. *Solid State Ionics, 76*(1), 47-55.

Grätzel, M. (1999). Mesoporous oxide junctions and nanostructured solar cells. *Current Opinion in Colloid & Interface Science, 4*(4), 314-321.

Grätzel, M. (2001). Photoelectrochemical cells. *Nature, 414*(6861), 338-344.

Grätzel, M. (2004). Conversion of sunlight to electric power by nanocrystalline dye-sensitized solar cells. *Journal of Photochemistry and Photobiology A: Chemistry, 164*(1–3), 3-14.

Hara, K., Horiguchi, T., Kinoshita, T., Sayama, K., and Arakawa, H. (2001). Influence of electrolytes on the photovoltaic performance of organic dye-sensitized nanocrystalline TiO_2 solar cells. *Solar Energy Materials and Solar Cells, 70*(2), 151-161.

Hardin, B. E., Snaith, H. J., and Mc Gehee, M. D. (2012). The renaissance of dye-sensitized solar cells. *Nature Photon, 6*(3), 162-169.

Hema, M., Selvasekerapandian, S., Sakunthala, A., Arunkumar, D., and Nithya, H. (2008). Structural, vibrational and electrical characterization of PVA–NH_4Br polymer electrolyte system. *Physica B: Condensed Matter, 403*(17), 2740-2747.

Highlights, P. (2009). Progress in ruthenium complexes for dye sensitised solar cells. *Platinum Metals Review, 53*(4), 216-218.

Hollars, D. R. (2005). Thin-film solar cells, *Google Patents*.

Hollmann, F. W., Mulder, T. J., and Kallan, J. E. (1999). Methodology and assumptions for the population projections of the United States: 1999-2100, US department of

commerce, bureau of the census, population division, population projections branch.

Hu, Y., Tsai, H. L., and Huang, C. L. (2003). Effect of brookite phase on the anatase–rutile transition in titania nanoparticles. *Journal of the European Ceramic Society, 23*(5), 691-696.

Ibrahim, S., Yassin, M. M., Ahmad, R., and Johan, M. R. (2011). Effects of various $LiPF_6$ salt concentrations on PEO-based solid polymer electrolytes. *Ionics, 17*(5), 399-405.

Ileperuma, O. A., Dissanayake, M. A. K. L., and Somasundaram, S. (2002). Dye-sensitised photoelectrochemical solar cells with polyacrylonitrile based solid polymer electrolytes. *Electrochimica Acta, 47*(17), 2801-2807.

Im, J. S., Lee, S. K., and Lee, Y.-S. (2011). Cocktail effect of Fe_2O_3 and TiO_2 semiconductors for a high performance dye-sensitized solar cell. *Applied Surface Science, 257*(6), 2164-2169.

Jasinski, R. and Burrows, B. (1969). Cathodic discharge of nickel sulfide in a propylene carbonate-$LiClO_4$ electrolyte. *Journal of The Electrochemical Society, 116*(4), 422-424.

Jayaweera, E. N., Ranasinghe, C. S. K., Kumara, G. R. A., Wanninayake, W. M. N. M. B., Senarathne, K. G. C., Tennakone, K., Rajapakse, R. M. G., and Ileperuma, O. A. (2015). Novel method to improve performance of dye-sensitized solar cells based on quasi-solid gel-polymer electrolytes. *Electrochimica Acta, 152*, 360-367.

Jeng, M.-J., Wung, Y.-L., Chang, L.-B., and Chow, L. (2013). Particle size effects of TiO_2 layers on the solar efficiency of dye-sensitized solar cells. *International Journal of Photoenergy, 2013*, 9. doi: 10.1155/2013/563897

Jia, Y.-T., Gong, J., Gu, X.-H., Kim, H.-Y., Dong, J., and Shen, X.-Y. (2007). Fabrication and characterization of poly (vinyl alcohol)/chitosan blend nanofibers produced by electrospinning method. *Carbohydrate Polymers, 67*(3), 403-409.

Kadir, M. F. Z., Majid, S. R., and Arof, A. K. (2010). Plasticized chitosan–PVA blend polymer electrolyte based proton battery. *Electrochimica Acta, 55*(4), 1475-1482.

Kakiage, K., Aoyama, Y., Yano, T., Oya, K., Fujisawa, J.-i., and Hanaya, M. (2015). Highly-efficient dye-sensitized solar cells with collaborative sensitization by silyl-anchor and carboxy-anchor dyes. *Chemical Communications, 51*(88), 15894-15897.

Kalaignan, G. P., Kang, M.-S., and Kang, Y. S. (2006). Effects of compositions on properties of PEO–KI–I_2 salts polymer electrolytes for DSSC. *Solid State Ionics, 177*(11–12), 1091-1097.

Katayama, N., Kawamura, T., Baba, Y., and Yamaki, J.-i. (2002). Thermal stability of propylene carbonate and ethylene carbonate – propylene carbonate-based electrolytes for use in Li cells. *Journal of Power Sources, 109*(2), 321-326.

Kato, N., Takeda, Y., Higuchi, K., Takeichi, A., Sudo, E., Tanaka, H., Motohiro, T., Sano, T., and Toyoda, T. (2009). Degradation analysis of dye-sensitized solar cell module after long-term stability test under outdoor working condition. *Solar Energy Materials and Solar Cells, 93*(6–7), 893-897.

Kawashima, T., Ezure, T., Okada, K., Matsui, H., Goto, K., and Tanabe, N. (2004). FTO/ITO double-layered transparent conductive oxide for dye-sensitized solar cells. *Journal of Photochemistry and Photobiology A: Chemistry, 164*(1–3), 199-202.

Kimpa, M. I., Momoh, M., Isah, K. U., Yahya, H. N., and Ndamitso, M. M. (2012). Photoelectric characterization of dye sensitized solar cells using natural dye from pawpaw leaf and flame tree flower as sensitizers. *Materials Sciences and Applications, 3*(5), 281-286.

Kohle, O., Grätzel, M., Meyer, A. F., and Meyer, T. B. (1997). The photovoltaic stability of *bis (isothiocyanato) rlutheniurn (II)-bis-2, 2' bipyridine-4, 4'-dicarboxylic acid* and related sensitizers. *Advanced Materials, 9*(11), 904-906.

Koo, B.-K., Lee, D.-Y., Kim, H.-J., Lee, W.-J., Song, J.-S., and Kim, H.-J. (2006). Seasoning effect of dye-sensitized solar cells with different counter electrodes. *Journal of Electroceramics, 17*(1), 79-82.

Krumova, M., López, D., Benavente, R., Mijangos, C., and Pereña, J. M. (2000). Effect of crosslinking on the mechanical and thermal properties of poly (vinyl alcohol). *Polymer, 41*(26), 9265-9272.

Kumara, G. R. A., Kaneko, S., Okuya, M., Onwona-Agyeman, B., Konno, A., and Tennakone, K. (2006). Shiso leaf pigments for dye-sensitized solid-state solar cell. *Solar Energy Materials and Solar Cells*, *90*(9), 1220-1226.

Lan, Z., Wu, J., Wang, D., Hao, S., Lin, J., and Huang, Y. (2006). Quasi-solid state dye-sensitized solar cells based on gel polymer electrolyte with poly (acrylonitrile-co-styrene) /NaI+I_2. *Solar Energy*, *80*(11), 1483-1488.

Law, C., Pathirana, S. C., Li, X., Anderson, A. Y., Barnes, P. R., Listorti, A. and Ghaddar, T. H. (2010). Water-based electrolytes for dye-sensitized solar cells. *Advanced Materials, 22*(40), 4505-4509.

Lee, J. K. and Yang, M. (2011). Progress in light harvesting and charge injection of dye-sensitized solar cells. *Materials Science and Engineering B: Solid-State Materials for Advanced Technology, 176*(15), 1142-1160.

Li, B., Wang, L., Kang, B., Wang, P., and Qiu, Y. (2006). Review of recent progress in solid-state dye-sensitized solar cells. *Solar Energy Materials and Solar Cells, 90*(5), 549-573.

Liew, C.-W., Ramesh, S., and Arof, A. K. (2014). A novel approach on ionic liquid-based poly(vinyl alcohol) proton conductive polymer electrolytes for fuel cell applications. *International Journal of Hydrogen Energy, 39*(6), 2917-2928.

Liew, C.-W., Ramesh, S., and Arof, A. K. (2015). Characterization of ionic liquid added poly(vinyl alcohol)-based proton conducting polymer electrolytes and electrochemical studies on the supercapacitors. *International Journal of Hydrogen Energy, 40*(1), 852-862.

Lin, H., Li, X., He, X., and Zhao, J. (2015). Application of a novel 3D nano-network structure for Ag-modified TiO_2 film electrode with enhanced electrochemical performance. *Electrochimica Acta, 173*, 242-251.

Longo, C., and De Paoli, M.-A. (2003). Dye-sensitized solar cells: A successful combination of materials. *Journal of the Brazilian Chemical Society*, *14*(6), 889-901.

Luo, J., Wan, Z., Jia, C., Wang, Y., Wu, X., and Yao, X. (2016). Co-sensitization of dithiafulvenyl-phenothiazine based organic dyes with N719 for efficient dye-sensitized solar cells. *Electrochimica Acta, 211*, 364-374.

Mathew, S., Yella, A., Gao, P., Humphry-Baker, R., Curchod, B. F. E., Ashari-Astani, N., Tavernelli, I., Rothlisberger, U., Nazeeruddin, M. K., and Grätzel, M. (2014). Dye-sensitized solar cells with 13% efficiency achieved through the molecular engineering of porphyrin sensitizers. *Nature Chemistry, 6*(3), 242-247.

Maurya, I. C., Neetu, Gupta, A. K., Srivastava, P., and Bahadur, L. (2016). *Callindra haematocephata* and *Peltophorum pterocarpum* flowers as natural sensitizers for TiO_2 thin film based dye-sensitized solar cells. *Optical Materials, 60*, 270-276.

Maurya, I. C., Srivastava, P., and Bahadur, L. (2016). Dye-sensitized solar cell using extract from petals of male flowers *Luffa cylindrica L.* as a natural sensitizer. *Optical Materials, 52*, 150-156.

Mehmood, Umer, Rahman, Saleem-ur, Harrabi, Khalil, Hussein, Ibnelwaleed A., and Reddy, B. V. S. (2014). Recent advances in dye sensitized solar cells. *Advances in Materials Science and Engineering, 2014*, 12. doi: 10.1155/2014/974782

Mekhilef, S., Barimani, M., Safari, A., and Salam, Z. (2014). Malaysia's renewable energy policies and programs with green aspects. *Renewable and Sustainable Energy Reviews, 40*, 497-504.

Meyer, G. J. (1997). Efficient light-to-electrical energy conversion: nanocrystalline TiO_2 films modified with inorganic sensitizers. *Journal of Chemical Education, 74*(6), 652. doi: 10.1021/ed074p652

Miao, R., Luo, Z., Zhong, W., S.-Y. Chen, S.-Y., Jiang, T., Dutta, B., Nasr, Y., Zhang, Y., and Suib, S. L. (2016). Mesoporous TiO_2 modified with carbon quantum dots as a high-performance visible light photocatalyst. *Applied Catalysis B: Environmental, 189*, 26-38.

Mohamed, S. A., Al-Ghamdi, A., Sharma, G. and Mansy, M. El (2014). Effect of ethylene carbonate as a plasticizer on CuI/PVA nanocomposite: Structure, optical and electrical properties. *Journal of Advanced Research, 5*(1), 79-86.

Muthuvinayagam, M., and Gopinathan, C. (2014). Synthesis and characterization of novel proton conducting polymer blend electrolytes. *Polymer-Plastics Technology and Engineering, 53*(13), 1333-1338.

Nakamoto, K. (1986). Infrared and Raman spectra of inorganic and coordination compounds, Wiley Online Library. doi: 10.1002/bbpc.198800131

Nakata, K., and Fujishima, A. (2012). TiO_2 photocatalysis: Design and applications. *Journal of Photochemistry and Photobiology C: Photochemistry Reviews, 13*(3), 169-189.

National Center for Biotechnology Information. PubChem Compound Database; CID=679, 2004-09-16

Nazeeruddin, A., Kay, I., Rodicio, R., Humphry-Baker, E., Müller, P., Liska, N., Vlachopoulos and Grätzel, M. (1993). Conversion of light to electricity by cis-X2bis (2, 2'-bipyridyl-4, 4'-dicarboxylate) ruthenium (II) charge-transfer sensitizers (X= Cl-, Br-, I-, CN-, and SCN-) on nanocrystalline titanium dioxide electrodes. *Journal of the American Chemical Society, 115*(14), 6382-6390.

Nazeeruddin, M. K., De Angelis, F., Fantacci, S., Selloni, A., Viscardi, G., Liska, P., Ito, S., Takeru, B., and Grätzel, M. (2005). Combined experimental and DFT-TDDFT computational study of photoelectrochemical cell ruthenium sensitizers. *Journal of the American Chemical Society*, *127*(48), 16835-16847.

Nogueira, A. F., Longo, C., and De Paoli, M. A. (2004). Polymers in dye sensitized solar cells: overview and perspectives. *Coordination Chemistry Reviews, 248*(13–14), 1455-1468.

Noor, M. M., Buraidah, M. H., Careem, M. A., Majid, S. R., and Arof, A. K. (2014). An optimized poly(vinylidene fluoride-hexafluoropropylene)–NaI gel polymer electrolyte and its application in natural dye sensitized solar cells. *Electrochimica Acta, 121*, 159-167.

Noor, M. M., Buraidah, M. H., Yusuf, S. N. F., Careem, M. A., Majid, S. R., and Arof, A. K. (2011). Performance of dye-sensitized solar cells with (PVDF-HFP)-KI-EC-PC electrolyte and different dye materials. *International Journal of Photoenergy, (2011),* Article ID 960487. doi:10.1155/2011/960487

Ochiai, T., and Fujishima, A. (2012). Photoelectrochemical properties of TiO_2 photocatalyst and its applications for environmental purification. *Journal of Photochemistry and Photobiology C: Photochemistry Reviews, 13*(4), 247-262.

Oh, T. H., Pang, S. Y., and Chua, S. C. (2010). Energy policy and alternative energy in Malaysia: Issues and challenges for sustainable growth. *Renewable and Sustainable Energy Reviews, 14*(4), 1241-1252.

O'Regan, B. and Grätzel, M. (1991). A low-cost, high-efficiency solar cell based on dye-sensitized colloidal TiO_2 films. *Nature, 353*(6346), 737-740.

Oskam, G., Bergeron, B. V., Meyer, G. J., and Searson, P. C. (2001). Pseudohalogens for dye-sensitized TiO_2 photoelectrochemical cells. *The Journal of Physical Chemistry B, 105*(29), 6867-6873.

Osman, Z., and Arof, A. K. (2003). FTIR studies of chitosan acetate based polymer electrolytes. *Electrochimica Acta, 48*(8), 993-999.

Özkan, M., Hashmi, S. G., Halme, J. K., Alp, S., Teemu, P., Jouni, and Lund, P. D. (2017). Inkjet-printed platinum counter electrodes for dye-sensitized solar cells. *Organic Electronics, 44*,159-167.

Park, H., Kim, W.-R., Jeong, H.-T., Lee, J.-J., Kim, H.-G., and Choi, W.-Y. (2011). Fabrication of dye-sensitized solar cells by transplanting highly ordered TiO_2 nanotube arrays. *Solar Energy Materials and Solar Cells, 95*(1), 184-189.

Park, J. H., Yum, J.-H., Kim, S.-Y., Kang, M.-S., Lee, Y.-G., Lee, S.-S., and Kang, Y. S. (2008). Influence of salts on ionic diffusion in oligomer electrolytes and its implication in dye-sensitized solar cells. *Journal of Photochemistry and Photobiology A: Chemistry*, *194*(2–3), 148-151.

Park, N. G., Van De Lagemaat, J., and Frank, A. J. (2000). Comparison of dye-sensitized rutile- and anatase-based TiO_2 solar cells. *Journal of Physical Chemistry B, 104*(38), 8989-8994.

Park, N.-G., Chang, S.-H., van de Lagemaat, J., Kim, K.-J., and Frank, A. J. (2000). Effect of cations on the open-circuit photovoltage and the charge-injection efficiency of dye-sensitized nanocrystalline rutile TiO_2 films. *Bulletin-Korean Chemical Society, 21*(10), 985-988.

Penza, M., and Cassano, G. (2000). Relative humidity sensing by PVA-coated dual resonator SAW oscillator. *Sensors and Actuators B: Chemical*, *68*(1–3), 300-306.

Phinjaturus, K., Maiaugree, W., Suriharn, B., Pimanpaeng, S., Amornkitbamrung, V., and Swatsitang, E. (2016). Dye-sensitized solar cells based on purple corn sensitizers. *Applied Surface Science*, *380*, 101-107.

Pitawala, H. M. J. C., Dissanayake, M. A. K. L., Seneviratne, V. A., Mellander, B. E., and Albinson, I. (2008). Effect of plasticizers (EC or PC) on the ionic conductivity and thermal properties of the $(PEO)_9$ LiTf: Al_2O_3 nanocomposite polymer electrolyte system. *Journal of Solid State Electrochemistry, 12*(7-8), 783-789.

Prajapati, G. K., Roshan, R., and Gupta, P. N. (2010). Effect of plasticizer on ionic transport and dielectric properties of PVA–H_3PO_4 proton conducting polymeric electrolytes. *Journal of Physics and Chemistry of Solids, 71*(12), 1717-1723.

Qiao, Q., Beck, J., Lumpkin, R., Pretko, J., and McLeskey Jr, J. T. (2006). A comparison of fluorine tin oxide and indium tin oxide as the transparent electrode for P3OT/TiO_2 solar cells. *Solar Energy Materials and Solar Cells, 90*(7–8), 1034-1040.

Rahman, M. Y. A., Salleh, M. M., Talib, I. A., and Yahaya, M. (2004). Effect of Ionic conductivity of a PVC–$LiClO_4$ based solid polymeric electrolyte on the performance of solar cells of ITO/TiO_2/PVC–$LiClO_4$/graphite. *Journal of Power Sources, 133*(2), 293-297.

Rahman, M., Ahmad, A., Lee, T., Farina, Y., and Dahlan, H. (2011). Effect of ethylene carbonate (EC) plasticizer on poly (vinyl chloride)-liquid 50% epoxidised natural rubber (LENR50) based polymer electrolyte. *Materials Sciences and Applications, 2*(7), 817.

Rajendran, S., Bama, V. S., and Prabhu, M. R. (2010). Effect of lithium salt concentration in PVAc/PMMA-based gel polymer electrolytes. *Ionics, 16*(1), 27-32.

Rajendran, S., Sivakumar, M., Subadevi, R., and Nirmala, M. (2004). Characterization of PVA–PVdF based solid polymer blend electrolytes. *Physica B: Condensed Matter, 348*(1–4), 73-78.

Reddy, T. J. R., Achari, V. B. S., Sharma, A. K., and Rao, V. V. R. N. (2007). Effect of plasticizer on electrical conductivity and cell parameters of (PVC+$KBrO_3$) polymer electrolyte system. *Ionics, 13*(1), 55-59.

Saikia, D. and Kumar, A. (2004). Ionic conduction in P(VDF-HFP)/PVDF–(PC + DEC)–$LiClO_4$ polymer gel electrolytes. *Electrochimica Acta, 49*(16), 2581-2589.

Senevirathne, A. M. C., Seneviratne, V. A., Ileperuma, O. A., Bandara, H. M. N., and Rajapakse, R. M. G. (2016). International Conference on Materials for Advanced Technologies (ICMAT 2015), Symposium C – Solar PV (Photovoltaics) materials, manufacturing and reliability novel quasi-solid-state electrolyte based on γ-butyrolactone and tetrapropylammonium iodide for dye-sensitized solar cells using fumed silica as the gelling agent. *Procedia Engineering, 139*, 87-92.

Senthilkumar, S. T., Selvan, R. K., Melo, J. S., and Sanjeeviraja, C. (2013). High performance solid-state electric double layer capacitor from redox mediated gel polymer electrolyte and renewable tamarind fruit shell derived porous carbon. *ACS Applied Materials & Interfaces, 5*(21), 10541-10550.

Sequeira, C., A.C., M. Plancha, J.C. and L. Araújo, P.S. (1994). Conductivity studies on solid polymer electrolytes. *Journal Physics IV France, 04*(C1), C1-17-C11-35.

Shi, Y., Wang, Y., Zhang, M., and Dong, X. (2011). Influences of cation charge density on the photovoltaic performance of dye-sensitized solar cells: lithium, sodium, potassium, and dimethylimidazolium. *Physical Chemistry Chemical Physics, 13*(32), 14590-14597.

Sima, C., Grigoriu, C., and Antohe, S. (2010). Comparison of the dye-sensitized solar cells performances based on transparent conductive ITO and FTO. *Thin Solid Films, 519*(2), 595-597.

Singh, K. P., Singh, R. P., and Gupta, P. N. (1995). Polymer based solid state electrochromic display device using PVA complex electrolytes. *Solid State Ionics, 78*(3–4), 223-229.

Sirimanne, P. M., Senevirathna, M. K. I., Premalal, E., Pitigala, P. K. D. D. P., Sivakumar, V., and Tennakone, K. (2006). Utilization of natural pigment extracted from pomegranate fruits as sensitizer in solid-state solar cells. *Journal of Photochemistry and Photobiology A: Chemistry, 177*(2-3), 324-327.

Sloop, S. E., Pugh, J. K., Wang, S., Kerr, J., and Kinoshita, K. (2001). Chemical reactivity of PF_5 and $LiPF_6$ in ethylene carbonate/dimethyl carbonate solutions. *Electrochemical and Solid-State Letters, 4*(4), A42-A44.

Sönmezoğlu, S., Akyürek, C., and Akin, S. (2012). High-efficiency dye-sensitized solar cells using ferrocene-based electrolytes and natural photosensitizers. *Journal of Physics D: Applied Physics, 45*(42), 425101.

Subramania, A., Sundaram, N. K., Kumar, G. V., and Vasudevan, T. (2006). New polymer electrolyte based on (PVA–PAN) blend for Li-ion battery applications. *Ionics, 12*(2), 175-178.

Tobishima, S.-I. and Yamaji, A. (1984). Ethylene carbonate - propylene carbonate mixed electrolytes for lithium batteries. *Electrochimica Acta, 29*(2), 267-271.

Tsai, J.-K., Hsu, W. D., Wu, T.-C., Zhou, J.-S., Li, J.-L., Liao, J.-H., and Meen, T.-H. (2013). Dye-sensitized solar cells with optimal gel electrolyte using the taguchi design method. *International Journal of Photoenergy, 2013*, 5. doi: 10.1155/2013/617126

Wang, J., Shen, L., Li, H., Wang, X., Nie, P., Ding, B., Xu, G., Dou, H., and Zhang, X. (2014). A facile one-pot synthesis of TiO_2/nitrogen-doped reduced graphene oxide

nanocomposite as anode materials for high-rate lithium-ion batteries. *Electrochimica Acta, 133*, 209-216.

Watase, M. and Nishinari, K. (1989). Effects of the degree of saponification and concentration on the thermal and rheological properties of poly(vinyl alcohol)-dimethyl sulfoxide-water gels. *Polymer Journal, 21*(7), 567-575.

Wei, Y.-S., Jin, Q.-Q., and Ren, T.-Z. (2011). Expanded graphite/pencil-lead as counter electrode for dye-sensitized solar cells. *Solid-State Electronics, 63*(1), 76-82.

Wen, C., Ishikawa, K., Kishima, M., and Yamada, K. (2000). Effects of silver particles on the photovoltaic properties of dye-sensitized TiO_2 thin films. *Solar Energy Materials and Solar Cells, 61*(4), 339-351.

Wolfbauer, G., Bond, A. M., Eklund, J. C., and MacFarlane, D. R. (2001). A channel flow cell system specifically designed to test the efficiency of redox shuttles in dye sensitized solar cells. *Solar Energy Materials and Solar Cells, 70*(1), 85-101.

Wongcharee, K., Meeyoo, V., and Chavadej, S. (2007). Dye-sensitized solar cell using natural dyes extracted from rosella and blue pea flowers. *Solar Energy Materials and Solar Cells, 91*(7), 566-571.

Wu, J., Lan, Z., Wang, D., Hao, S., Lin, J., Huang, Y., Yin, S., and Sato, T. (2006). Gel polymer electrolyte based on poly (acrylonitrile-co-styrene) and a novel organic iodide salt for quasi-solid state dye-sensitized solar cell. *Electrochimica Acta, 51*(20), 4243-4249.

Wu, J., Lan, Z., Wang, D., Hao, S., Lin, J., Wei, Y., Yin, S., and Sato, T. (2006). Quasi-solid state dye-sensitized solar cells-based gel polymer electrolytes with poly (acrylamide)–poly(ethylene glycol) composite. *Journal of Photochemistry and Photobiology A: Chemistry, 181*(2–3), 333-337.

Wu, J., Li, P., Hao, S., Yang, H., and Lan, Z. (2007). A polyblend electrolyte (PVP/PEG+KI+I_2) for dye-sensitized nanocrystalline TiO_2 solar cells. *Electrochimica Acta, 52*(17), 5334-5338.

Xu, J., Jia, C., Cao, Bin., and Zhang, W. F. (2007). Electrochemical properties of anatase TiO_2 nanotubes as an anode material for lithium-ion batteries. *Electrochimica Acta, 52*(28), 8044-8047.

Yahya, M., Harun, M., Ali, A., Mohammat, M., Hanafiah, M., Ibrahim, S., Mustaffa, M., Darus, Z., and Latif, F. (2006). XRD and surface morphology studies on chitosan-based film electrolytes. *Journal of Applied Sciences, 6*(15), 3150-3154.

Yamazaki, E., Murayama, M., Nishikawa, N., Hashimoto, N., Shoyama, M. and Kurita, O. (2007). Utilization of natural carotenoids as photosensitizers for dye-sensitized solar cells. *Solar Energy, 81*(4), 512-516.

Yang, H., Huang, M., Wu, J., Lan, Z., Hao, S., and Lin, J. (2008). The polymer gel electrolyte based on poly (methyl methacrylate) and its application in quasi-solid-state dye-sensitized solar cells. *Materials Chemistry and Physics, 110*(1), 38-42.

Yang, Z., Chen, T., He, R., Li, H., Lin, H., Li, L., Zou, G., Jia, Q., and Peng, H. (2013). A novel carbon nanotube/polymer composite film for counter electrodes of dye-sensitized solar cells. *Polymer Chemistry, 4*(5), 1680-1684.

Yao, W., Zhang, Z., Gao, J., Li, J., Xu, J., Wang, Z., and Yang, Y. (2009). Vinyl ethylene sulfite as a new additive in propylene carbonate-based electrolyte for lithium ion batteries. *Energy & Environmental Science, 2*(10), 1102-1108.

Yella, A., Lee, H. W., Tsao, H. N., Yi, C., Chandiran, A. K., Nazeeruddin, M. K., Diau, E. W. G., Yeh, C. Y., Zakeeruddin, S. M., and Grätzel, M. (2011). Porphyrin-sensitized solar cells with cobalt (II/III)-based redox electrolyte exceed 12 percent efficiency. *Science, 334*(6056), 629-634.

Zhang, B., Zhou, Y., Li, X., Ren, X., Nian, H., Shen, Y., and Yun, Q. (2013). Ion-molecule interaction in solutions of lithium tetrafluoroborate in propylene carbonate: an FTIR vibrational spectroscopic study. *International Journal Electrochemical Science, 8*, 12735-12740.

Zhang, Q., and Cao, G. (2011). Nanostructured photoelectrodes for dye-sensitized solar cells. *Nano Today, 6*(1), 91-109.

Zhou, H., Wu, L., Gao, Y., and Ma, T. (2011). Dye-sensitized solar cells using 20 natural dyes as sensitizers. *Journal of Photochemistry and Photobiology A: Chemistry, 219*(2–3), 188-194.

LIST OF PUBLICATIONS

1. **Aziz, M. F.**, Noor, I. M., Sahraoui, B., and Arof, A. K. (2014). Dye-sensitized solar cells with PVA-KI-EC-PC gel electrolytes. *Optical and Quantum Electronics, 46*(1), 133-141.
2. **Aziz, M. F.**, Buraidah, M. H., Careem, M. A., and Arof, A. K. (2015). PVA based gel polymer electrolytes with mixed iodide salts (K^+I^- and $Bu_4N^+I^-$) for dye-sensitized solar cell application. *Electrochimica Acta, 182*, 217-223.
3. **Aziz, M. F.**, Noor, I. M., Buraidah, M. H., Careem, M. A., and Arof, A. K. (2013). *PVA-based gel polymer electrolytes doped with $(CH_3)_4NI$/KI for application in dye-sensitized solar cells.* Paper presented at the International Conference on Transparent Optical Networks.
4. **Aziz, M. F.**, Buraidah, M. H., and Arof, A. K. (2013). *Dye-sensitized solar cells using binary iodide-PVA gel electrolyte.* Paper presented at the International Conference on Transparent Optical Networks.

Other collaboration

1. Kufian, M. Z., **Aziz, M. F.**, Shukur, M. F., Rahim, A. S., Ariffin, N. E., Shuhaimi, N. E. A., and Arof, A. K. (2012). PMMA-LiBOB gel electrolyte for application in lithium ion batteries. *Solid State Ionics, 208*, 36-42.
2. Yusuf, S. N. F., **Aziz, M. F.**, Hassan, H. C., Bandara, T. M. W. J., Mellander, B. E., Careem, M. A., and Arof, A. K. (2014). Phthaloylchitosan-based gel polymer electrolytes for efficient dye-sensitized solar cells. *Journal of Chemistry, 2014*.
3. Arof, A. K., **Aziz, M. F.**, Noor, M. M., Careem, M. A., Bandara, L. R. A. K., Thotawatthage, C. A., and Dissanayake, M. A. K. L. (2014). Efficiency enhancement by mixed cation effect in dye-sensitized solar cells with PVdF based gel polymer electrolyte. *International Journal of Hydrogen Energy, 39*(6), 2929-2935.